THE PETROLOGY OF THE BASALTS OF THE DORDABIS FORMATION, IN THE VICINITY OF DORDABIS IN CENTRAL S.W.A./NAMIBIA

by

Ian Eric Williams-Jones, B.Sc. (Hons)

Thesis presented for the degree of Master of Science
in the Department of Geology, Rhodes University,
Grahamstown.

September, 1984

DECLARATION

All work in this thesis is the original work of the author except where specific acknowledgement is made to the work of others.

SIGNED: I E Williams-Jones

I E Williams-Jones
Department of Geology
Rhodes University
GRAHAMSTOWN

September, 1984

ABSTRACT

The late Proterozoic volcanic and sedimentary sequence in the Dordabis area SWA/Namibia has been named the Dordabis Formation and subdivided, on the basis of field, petrological and petrographic evidence, into the Opdam and Bitterwater Members.

Relict phases including augite and minor plagioclase only occur in the Bitterwater metalavas, as recrystallisation is complete in the Opdam metalavas. The composition of the relict feldspars ranges from labradorite in the ophitic basalts to oligoclase in the blastoporphyritic metalavas. The feldspars in the Opdam member are albitic in composition (An content 0,0 to 1,7). Epidote compositions are typical of those occurring in metabasic rocks. Samples with high-iron whole-rock compositions are accompanied by high concentrations of Fe^{3+} in concomitant epidotes.

Sixty three samples were analysed using X-ray fluorescence spectrometry to determine concentrations of major and 16 trace elements. Although greenschist facies metamorphism, metasomatism and shearing have produced scatter in the more mobile element concentrations, variation trends in other elements closely resemble modelled low-pressure fractional crystallisation trends. The Dordabis metalavas are petrologically classified as sub-alkaline, tholeiitic continental basalts. Low K/Rb ratios and low ratios of less incompatible to more incompatible elements probably reflect a source that has either been metasomatically enriched or that has undergone little previous partial melting. Overlapping whole-rock variation trends indicate that the generally more evolved Opdam and primitive tholeiitic Bitterwater lavas are cogenetic.

A comparison of the Dordabis Formation with the Sinclair Sequence and the Koras Group shows that their ages, petrology, petrography, associated sedimentary suites and depositional environments are similar. It is concluded that they may possibly be coeval equivalents.

CONTENTS

1. INTRODUCTION

1.1 General

The study area is situated in the Dordabis district approximately 90km south-east of Windhoek, in South West Africa (SWA)/Namibia (Fig. 1). The relief in the area is marked by isolated north-east trending ridges and hills that consist of volcanic and sedimentary rocks. These rocks are part of a late Proterozoic sequence that forms the southern margin of the Damara Sequence in the Dordabis area (Fig. 1).

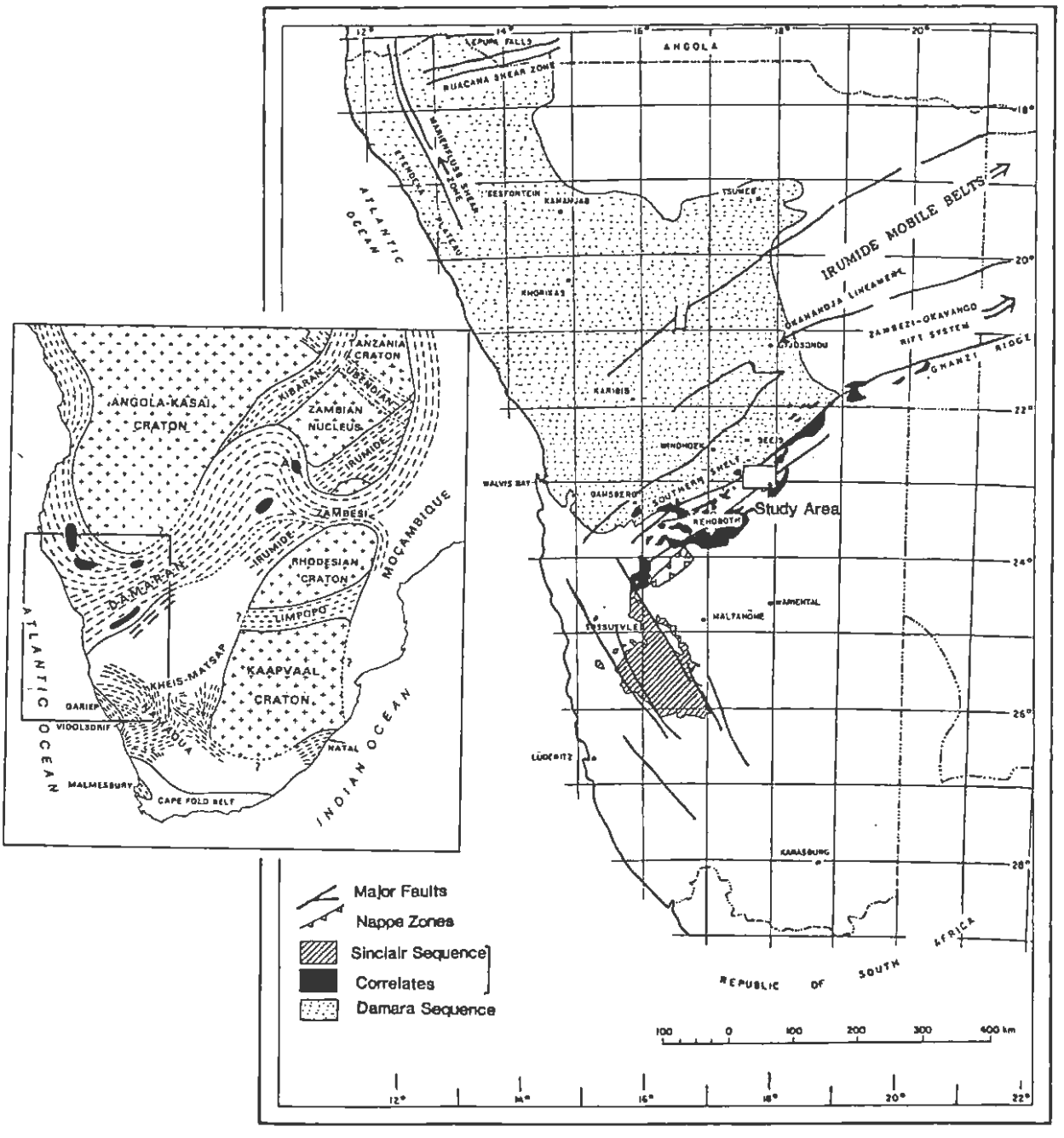

Figure 1 Regional geotectonic sketch map of the Damara Sequence, the Sinclair Sequence and its correlates, showing the location of the present study area (after Hunter and Pretorius, 1981; Mason, 1981; S.A.C.S., 1980). The reference map shows the distribution of cratons and mobile belts in central and southern Africa.

The rock sequences investigated in this study form part of the Irumide belt of volcanism and sedimentation, the exposures of which are generally poor and isolated. This dissertation is primarily concerned with the detailed geochemistry of the lavas in this area.

1.2 Regional Geotectonic Setting and Geological History

The structural framework of central and southern Africa is characterised by a number of ancient cratonic provinces separated by generally younger mobile belts (Fig. 1). The cratonic provinces consist of granitoid gneisses and greenstone belts. The intervening mobile belts mark zones of crustal weakness and sites of volcanic activity, sedimentation, deformation and metamorphism.

In northern SWA/Namibia the Angola-Kasai craton (3500Ma, Cahen et al., 1976) is covered mainly by younger Tertiary and Quaternary deposits. The western and southern boundaries of this craton are defined by the Damara metamorphic belt which is located along long-standing zones of crustal weakness (Fig. 1). This north-east trending zone of weakness has been very important in SWA/Namibian geological history, because in pre-Damaran times it also controlled the location and evolution of the Irumide sequences.

The Irumide cycle of sporadic volcanism, sedimentation and granite emplacement in SWA/Namibia, north-western Botswana and southern Malawi occurred between 1400Ma and 900Ma ago (Mason, 1981). In SWA/Namibia the activity was localised mainly in fault-bounded basins along the north-east trending zone of weakness (see "Correlates" in Figure 1) and also along the north to north-west trending zone of weakness containing the Sinclair Sequence. Watters (1974) termed this volcano-plutonic belt the Rehoboth Magmatic Arc, and suggested that it represents a pre-Damaran arc complex above a subduction zone. Much debate exists about the validity of this model. Martin and Porada (1977) have argued against the plate tectonic model and instead they postulated a rift-related model. It is now generally agreed that at least the early stages of the Irumide cycle were ensialic (Martin and Porada, 1977; Kröner, 1977; Mason, 1981; Tankard et al., 1982). Mason (1981) suggested that the Irumide cycle marks a long period of sporadic tectonic unrest with rifting, associated volcanic activity and the development of restricted intermontane yoked basins which accommodated thick, but localised piles

of clastic sediments, volcanic rocks and lacustrine deposits. The volcanic sequence studied in this project was probably deposited in one of these yoked basins.

The late Precambrian Damaran sequence was deposited on a foundation of granitoid basement gneisses, granites and infolded supra-crustal formations of pre-Irumide and Irumide age (Mason, 1981). The Pan-African Damaran orogeny (550 ± 100Ma) has affected these older rocks, especially along the southern margin of the Damara Belt. Here metamorphism and south-east directed thrusting have resulted in north-east trending folds, and tectono-metamorphic overprinting of older rocks. The effects can be seen in the Dordabis area, which is characterised by north-east trending upright folds and faults, and greenschist facies metamorphism.

South of the Damara belt, Nama sediments were laid down on the stable continental platform. Throughout the Phanerozoic this platform remained stable but was covered by volcanic rocks and sediments of the Karoo Supergroup and the Tertiary to Quaternary Kalahari beds.

1.3 Previous Geological Work in the Dordabis Area

The sediments and volcanics in the Dordabis area were first mapped, described and named the Dordabis Series by Gevers (1934). He subdivided this complex series into an Upper Group consisting of dense and compact, well-bedded quartzites, feldspathic sandstones and massive conglomeratic arkoses, and a Lower Group consisting of deep-red to chocolate-coloured quartzites and sandstones, sedimentary breccias and conglomerates (Table 1). Gevers (op. cit.) further considered that the Lower Group of the Dordabis Series had been intruded by numerous, mostly parallel sills and lenses of post-Nama pre-Karoo eruptive diabase.

Schalk (1961), on remapping this area, found that Gevers' (op. cit.) Upper Group was equivalent to the Nosib Group of the Damara System, and was separated from the Lower Group by a major unconformity. He therefore renamed the Upper Group the Kamtsas Series of the Damara System, and the Lower Group and other rocks not mapped by Gevers, the Dordabis System. This redefined Dordabis System was further subdivided into the Opdam, Skumok and Doornpoort Formations. Schalk's (op. cit.) Opdam Formation consists of quartzites with interbedded amygdaloidal mafic lavas, breccias, slate, phyllite and a basal conglomerate. His Skumok Formation

TABLE 1: A comparison of the stratigraphic columns for the Dordabis area proposed by various authors.

Gevers (1934)			SCHALK (1961)		SCHALK (1972/73)		S.A.C.S. (1980)		PRESENT AUTHOR		
Nama System	Dordabis Series	Omitara Quartzite	Nosib Group		Nosib Group		Nosib Group		Nosib Group	Kuduberg Formation (Kasch, 1981)	
		Upper Group		Kamtsas Series		Kamtsas Series		Kamtsas Formation		Kamtsas Formation	
		Lower Group (Intruded by post-Nama, pre-Karoo eruptive diabase)	Pre-Damara Dordabis System	Doornpoort Formation		Doornpoort Formation	Sinclair Equivalents	Doornpoort Formation	Sinclair Sequence Equivalents	Doornpoort Formation	
				Skumok Formation				Nückopf Formation		Nückopf Formation	
				Opdam Formation		Opdam Formation	Rehoboth Sequence	Marienhof Formation		Dordabis Formation	Bitterwater Member
					Rehoboth Sequence	Marienhof Formation					Opdam Member
									Rehoboth Sequence	Marienhof Formation	

lies unconformably on top of the Opdam Formation and consists mainly of rhyolite, felsite, ignimbrite, quartz porphyry sills, quartzite, mafic lava, slate and sedimentary breccias, whereas his Doornpoort Formation is disconformably separated from the Skumok Formation and consists of conglomerates, quartzites, slate and sedimentary breccias interbedded with rhyolite flows near the base.

During 1972/73 Schalk (pers. comm.) surveyed the area around and further to the west of Rehoboth and established the presence of another succession, the Marienhof Formation. This formation contains abundant basic and intermediate lavas which Schalk thought closely resembled those of the Dordabis System. However, they are accompanied by an altogether different sedimentary suite consisting of grey to white glassy quartzite, very thick greyish phyllite, some conglomerate, rhyolitic porphyry and pyroclastic rocks. Schalk believed that the lower portion of the Opdam Formation belonged to the Marienhof Formation rather than to the Dordabis System. On the 1:1 000 000 Geological Map of South West Africa/Namibia (1980) and in S.A.C.S. (1980) the Opdam Formation is included in the Marienhof Formation.

1.4 Aims of the Study

Previous geological work indicates that perception of the stratigraphy of this area, and especially that of the Opdam Formation is confused. No petrological work and little detailed petrography has previously been

done on the lavas in this area. These factors led to the motivation of this project, the aims of which can be summarised by the following points:

1) To characterise and classify the volcanic rocks of the Opdam Formation around Dordabis using both petrography and precise whole-rock major and trace element analyses.

2) To note chemical variations within the lavas and to account for them.

3) To determine whether the volcanics under study correlate with any other volcanics in the Rehoboth Magmatic Arc, specifically the basic volcanics of the Barby Formation of the Sinclair Group.

1.5 Field Work

Field work was carried out during February and March 1983 with the aid of 1:36 000 aerial photographs on which the geology had been mapped by K. Schalk between 1958 and 1960. Suitable representative sections through the sequence were located, logged in detail and the lavas extensively sampled (Plan 1 and 2). This included both sampling vertically through a flow and through a sequence of flows in order to determine interflow and intraflow compositional variations. Flow differentiation and contacts were difficult to discern in the field because many flow features had been destroyed by metamorphism and/or shearing. In certain areas, especially in the lower more sheared parts of the sequence, many flows were too weathered to merit sampling. Of the 160 samples collected from the sequence, 63 were carefully selected for detailed chemical analysis (see section 5.2.2).

2. GENERAL STRATIGRAPHY OF THE DORDABIS FORMATION

2.1 Introduction

The history of stratigraphic subdivision of the rock sequence in the Dordabis area has been discussed in the introduction and is summarised in Table 1. Schalk's (1961) Opdam Formation has been subdivided into two members based on petrological, petrographic and field evidence. As the type section for one of these members is situated on the farm Opdam, further confusion is minimised by renaming Schalk's (op. cit.) Opdam Formation the Dordabis Formation. The Dordabis Formation has been subdivided into the Opdam and Bitterwater Members which are named after the farms on which their type sections are located. Only brief descriptions of the members are given in this section, as they are discussed in depth in following chapters.

2.2 The Opdam Member

The Opdam Member comprises volcanic and clastic sedimentary rocks and is unconformably separated from the underlying Marienhof Formation by a major shear zone. Shearing is not confined to the base of the member and is evident in a number of lava flows. The more sheared lavas grade from chlorite schists to phyllites and in some parts have been intruded by younger quartz veins. The basal conglomerate, at the type section of this member, on the farm Opdam is up to 30m thick and has an argillaceous phyllitic to schistose matrix and strained pebbles, suggesting that it also has been extensively sheared (Fig. 2). Exposed thicknesses of the Opdam Member range from about 500m on the farms Ibenstein and Autabib to a maximum thickness of 800 to 1000m on the farms Opdam and Dubis.

Overlying the basal conglomerate, basaltic lava flows and flow breccias are interbedded with pink to brown quartzites which exhibit a sugary appearance in places. The volcanic breccias usually occur above the lava flows and often grade into the quartzite layers. Occasionally volcanic breccias occur both above and below lava flows. This allows easier recognition of contacts particularly between petrographically similar flows. Schistose textures are common and mineral assemblages indicate greenschist facies metamorphism. Although amygdales are still visible in some flows, metamorphic recrystallisation of the basalts is complete. The quartzites are seldomly thicker than 5m, and their greater competence

Figure 2 Sheared basal conglomerate of the Opdam Member.

compared to the interbedded metalavas has resulted in pinch and swell structures and occasionally boudins developing in more deformed areas.

2.3 The Bitterwater Member

The Bitterwater Member comprises volcanic rocks and clastic sedimentary rocks and overlies the Opdam Member conformably. At the type section on the farms Bitterwater and Grasvlakte this member reaches an estimated thickness of 2500 to 3000m. Although metamorphism is of the greenschist facies, recrystallisation is incomplete in some of the feldspar phyric and ophitic lavas, indicating that lower pressure and temperature conditions reigned in the Bitterwater Member than the Opdam Member. The lavas are generally thicker, less altered and therefore more resistant to weathering than those in the underlying Opdam Member. Laterally persistent flow breccias are similar to those in the Opdam Member although they tend to be wider and more extensively developed, especially where the associated lavas are thicker. The quartzites are generally also similar to those in the Opdam Member, although they also tend to be thicker. A 750m thick sequence of quartzites separates this member from the unconformably overlying Doornpoort Formation. On the farm Dordabis malachite staining suggests that certain lavas may have been hydrothermally enriched in copper-sulphide minerals.

3. PETROGRAPHY

3.1 Introduction

The petrography of the interbedded quartzites, volcanic breccias and volcanics occurring in the Dordabis Formation is described below. The quartzites and flow breccias of the Opdam Member cannot be distinguished petrographically from those of the Bitterwater Member. To prevent duplication of petrographic descriptions of the two members, general descriptions are given of these two rock types as they occur throughout the Dordabis Formation.

3.2 The Dordabis Formation Quartzites

The interflow sediments are classified as immature sublitharenites or protoquartzites according to the scheme of Pettijohn et al. (1972). These protoquartzites exhibit variable degrees of induration, but most are well-indurated. Colours are generally pink, purple and red-brown. The coarser grained arenites tend to be sugary in appearance and due to the larger grain size, these quartzites are less indurated and more porous than the average protoquartzite. Bedding is well preserved, and usually takes the form of horizontal bedding, although planar cross bedding and trough cross bedding are common in the thicker sedimentary horizons (Fig. 3).

Figure 3 Horizontal and planar cross bedded quartzites in the Bitterwater Member on the farm Ibenstein

Quartz is the dominant mineral and makes up between 85% and 95% of the rock. Most quartz grains consist of single crystals, generally with only slightly strained extinction (Fig. 8A). Grain sizes usually vary from 0,1 to 1mm, altnough in the sugary quartzites grain sizes range from 1 to 2mm. Authigenic overgrowth and grain solution is common, and occasionally sutured grains have formed in the more recrystallised parts of the quartzites. Rounded zircon, and opaque ores, probably ilmenite make up 0 to 5% of the sediment. The matrix constitutes 5 to 15% of the sediment and is generally very fine-grained, consisting mainly of quartz, micas, clays, chloritoid and piedmontite. The matrix of certain quartzites in the Opdam Member on the farm Ibenstein is rich in piedmontite (Fig. 8B), imparting a pink colour to the rock especially on weathered surfaces.

Syntaxial cement coats most quartz grains and many interstitial voids are filled. Most grains are moderately to poorly sorted, generally rounded and have medium sphericity.

3.3 The Dordabis Formation Volcanic Breccias

The non-stratified unsorted breccias grade from volcanic clast-supported breccias bordering the lava flows into matrix-supported breccias bordering the quartzites (Fig. 4). The clast-supported breccias are bound together by welding of the fragment edges and minor quartzite cement, while the matrix-supported breccias are bound together by a fine-grained quartzitic groundmass (Fig. 8C).

QUARTZITE

Matrix-supported flow breccia

FLOW BRECCIA

Volcanic clast-supported breccia

LAVA FLOW

Figure 4 Contact relationships between the lava flows, flow breccias and quartzites.

Parsons (1968) proposed a genetic classification of volcanic breccias based on the process of fragmentation. The breccias in question are classified according to Parsons as frictional autoclastic volcanic breccias of the flow breccia type, formed by autobrecciation of lavas. This process involves congealing of the outer surfaces of the unconfined

lava flow, subsequent movement resulting in rupture of the congealed surfaces and various forms of frictional autobrecciation. Sand and volcanic ash are deposited on top of the flows and enter into the spaces between the clasts in the breccia.

The clasts are dense, monolithologic, angular and often scoriaceous (Fig. 5). The fragments from flow-top breccias have the same composition as the underlying lava. A number of the larger flow breccias contained clasts of varying sizes. Large isolated amygdaloidal and scoriaceous lava fragments range in size from 3 to 30cm, while finer volcanic fragments in the groundmass range from 1 to 10mm. These clasts consist mostly of glass (now devitrified), extensively saussuritised plagioclase and epidote, with minor clinozoisite, chlorite and actinolite. Calcite is often an important component of some clasts, especially in the Opdam Member.

Figure 5 Scoriaceous and angular volcanic breccia clasts of varying sizes, set in a fine-grained sedimentary matrix

The matrix of the flow breccias is mainly sedimentary, although the presence of small euhedral feldspar laths in an outcrop on the farm Zeshoek suggests the presence of minor volcanic ash. The matrix material is usually of a similar nature to the overlying quartzites, although it tends to be finer grained. In some matrix-supported breccias, preferential weathering of the volcanic clasts can result in the hard

quartz-rich matrix forming spectacular positive relief features. Figure 6 shows the unweathered surface of such a matrix-supported breccia. The matrix consists mainly of fine-grained (<0,5mm) subangular quartz, with minor actinolite, clinozoisite, feldspars, opaques and chloritoid (Fig. 8D). Calcite and less commonly actinolite can occur as medium to large grains and aggregates of grains (1 to 3mm) in the matrix, especially in the altered flow breccias in Opdam Member.

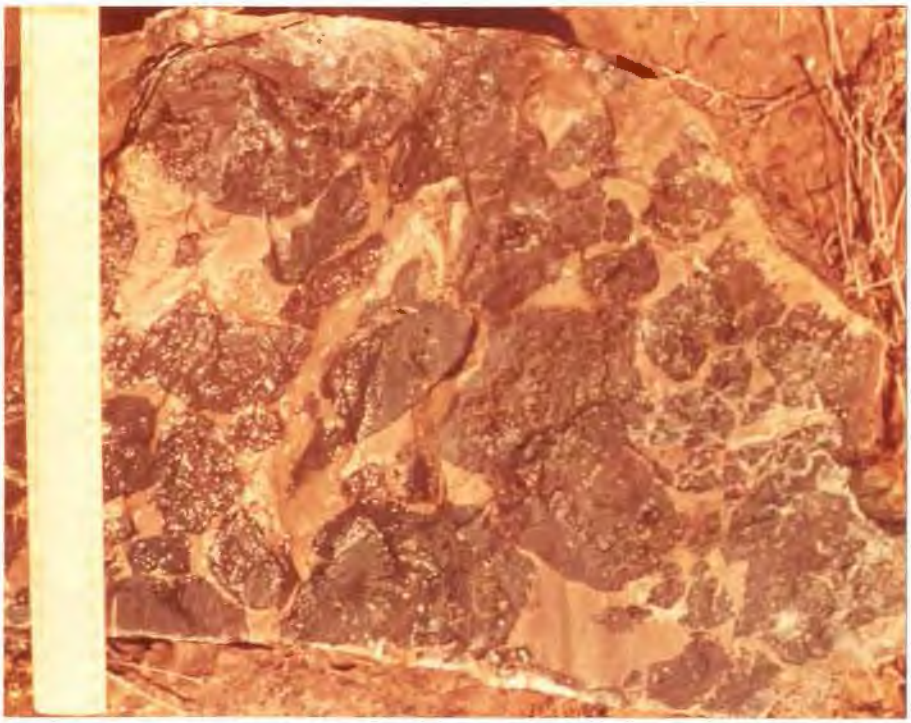

Figure 6 Matrix-supported volcanic breccia on the farm Zeshoek, where volcanic clasts are set in a quartz-rich, red-brown matrix.

3.4 The Opdam Member Lavas

The Opdam Member metalavas were studied and sampled at parallel sections on the farms Opdam and Dubis. These grey-green, aphanitic to fine grained phaneritic metalavas are often sheared to form greenschists or occasionally phyllites. Exceptions do occur near the top of this member on the farm Ibenstein at section B on plates 1 and 2. Here samples IWJ6 and IWJ7 were collected from a medium-grained lava containing albite phenocrysts reaching 3mm in length (Fig. 8E).

The metalavas are totally recrystallised and display typical low-grade greenschist facies metabasic mineral assemblages. Most primary igneous textures have been destroyed. Amygdales are present in a number of the

less sheared lavas and usually contain epidote, quartz, calcite and chlorite. Recrystallised veins transect a number of flows and consist mainly of fine-grained, granoblastic-polygonal quartz and minor albite, although coarser veins of granoblastic-polygonal calcite/magnesite also occur. Epidote and albite porphyroblasts are common throughout this member.

The schistose metalavas can be grouped into two main petrographic types distinguished by the presence or absence of calcite. The calcite usually occurs as 0,5 to 6,0mm poikiloblasts and porphyroblasts that are preferentially weathered in the field to give a brown, pitted outer surface. Rotation structures do occasionally occur, indicating rotation of certain calcite porphyroblasts during growth (Fig. 8F). Subhedral to euhedral ilmenite porphyroblasts (Fig. 8G) are usually finer grained than the calcite porphyroblasts and generally less than 1mm in size. These porphyroblasts are usually set in a fine-grained matrix consisting of 20 to 40% chlorite, 5 to 25% albite, 5 to 20% muscovite, 5 to 15% calcite, 2 to 15% opaque ores and leucoxene, $\pm$ actinolite, $\pm$ quartz, $\pm$ epidote, $\pm$ sphene and $\pm$ clinozoisite. Nematoblastic actinolite can occur in substantial amounts in certain schists, as in sample IWJ149, where it forms 20% of the metalava. The muscovite is usually decussate (Fig. 8G) and was only recognised in lavas containing calcite.

The second petrographic type contains no calcite or muscovite. The metalavas are usually also fine-grained and schistose in nature and consist of 10 to 40% albite, 10 to 35% nematoblastic actinolite, 15 to 30% chlorite, 5 to 20% epidote and 3 to 17% opaque ores and leucoxene, $\pm$ quartz, $\pm$ sphene and $\pm$ clinozoisite.

3.5 The Bitterwater Member Lavas

The Bitterwater Member lavas were studied and sampled on the farms Ibenstein, Autabib, Dordabis, Zeshoek, Grasvlakte and Bitterwater. The metalavas are unsheared and usually phaneritic fine-grained, although a number of medium-grained and aphanitic lavas also occur. Igneous textures are usually preserved, the most recognisable being the blastopoikilophitic and the feldspar blastoporphyritic textures. Recrystallisation is incomplete and relict pyroxenes and, to a lesser extent, plagioclases are common.

The metalavas can be grouped into three main petrographic types: the small-feldspar blastoporphyritic type, the large-feldspar blastoporphyritic type and the blastophitic type.

The small-feldspar blastoporphyritic type is typically green-grey in colour and is abundant, especially in the lower half of this member. The feldspar phenocrysts and, less frequently, smaller opaque oxide phenocrysts (ilmenite) are usually set in an aphanitic groundmass. The porphyritic character is well displayed on weathered surfaces, where pale green to cream feldspar and dark rust-red opaque minerals contrast strongly with a pale green-brown matrix. Plagioclase phenocrysts are usually tabular, subhedral to anhedral and range in size from 0,5 to 4mm. Plagioclase phenocrysts, now largely altered to cryptocrystalline saussurite (Fig. 8H), make up to 40% of the rock. The saussuritisation is so extensive that it prevents the microscopic determination of the feldspar composition. The groundmass usually consists of fine-grained to aphanitic plagioclase, epidote, chlorite, leucoxene, opaque minerals and pyroxene, $\pm$ actinolite, $\pm$ quartz, $\pm$ clinozoisite, $\pm$ sphene and $\pm$ calcite/magnesite.

The large-feldspar blastoporphyritic metalava (Fig. 7) occurs near the top of the formation on the farm Grasvlakte. Saussuritised plagioclase phenocrysts, set in a microcrystalline groundmass very similar to that of the small-feldspar porphyritic type, make up about 50% of the rock (Fig. 8I). These plagioclase phenocrysts are mostly subhedral, tabular and range in size from 2 to 15mm, although the more lath-shaped phenocrysts reach 25 or 30mm in size. The aphanitic groundmass consists of chlorite, saussurite, epidote, ilmenite and leucoxene.

The fine-grained porphyritic rocks have undergone at least two stages of crystallisation. Porphyritic extrusive lavas indicate that phenocrysts have grown prior to, and at a much slower rate, presumably in intratelluric magma chambers, than the matrix minerals. The fine-grained matrices solidified as a result of rapid chilling during the final stages of extrusion.

The blastophitic and blastopoikilophitic metalavas (Fig. 8J) contain pale green anhedral pyroxene oikocrysts set in a purple-grey matrix. The clinopyroxene oikocrysts are partly altered to pale-green actinolite. They range in size from 1 to 10mm and make up 20 to 50% of the metalava.

Figure 7 Weathered surface of a large-feldspar blastoporphyritic lava illustrating cream-coloured subhedral plagioclase set in a brown matrix

The enclosed euhedral feldspar laths as usually less than 0,1mm in size and are saussuritised. The groundmass appears to have been fine-grained to aphanitic before metamorphism and consists of saussurite, opaque ores (ilmenite), leucoxene, epidote and chlorite, ± actinolite, ± clinozoisite ± quartz and ± sphene.

In less altered lavas the groundmass appears to have had an intergranular texture. Amygdales are usually composed of quartz and less commonly of epidote, calcite and chlorite and occur throughout this member (Fig. 8K).

Figure 8

A. Typical immature sublitharenite, where slightly strained quartz grains make up 90 to 95% of the sediment (crossed nicols).

B. Immature sublitharenite, where quartz grains are separated by a matrix rich in piedmontite (P) (uncrossed nicols).

C. Volcanic breccia, where two monolithologic volcanic clasts (Vol. Clast) are separated by a fine-grained sedimentary matrix (crossed nicols).

D. Fine-grained sedimentary matrix within the volcanic breccia. It consists mainly of subangular quartz grains (uncrossed nicols).

E. Medium-grained Opdam Member metalava (sample IWJ6), rich in albite (A) phenocrysts ranging in size from 1 to 3mm, epidote (E) and opaque minerals (O) (crossed nicols).

F. Rotated calcite porphyroblasts in a schistose metalava from the Opdam Member (uncrossed nicols).

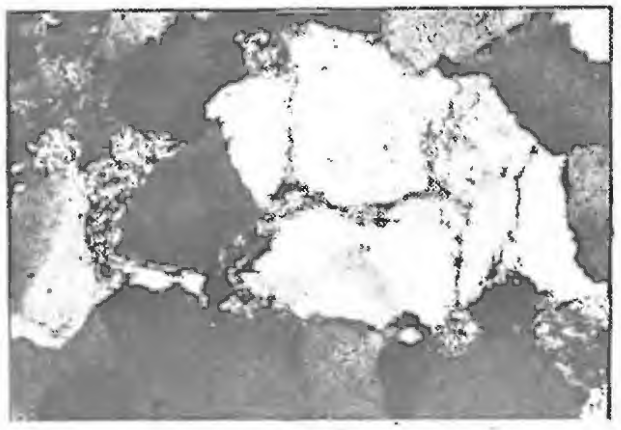

A

1 mm

B

1 mm

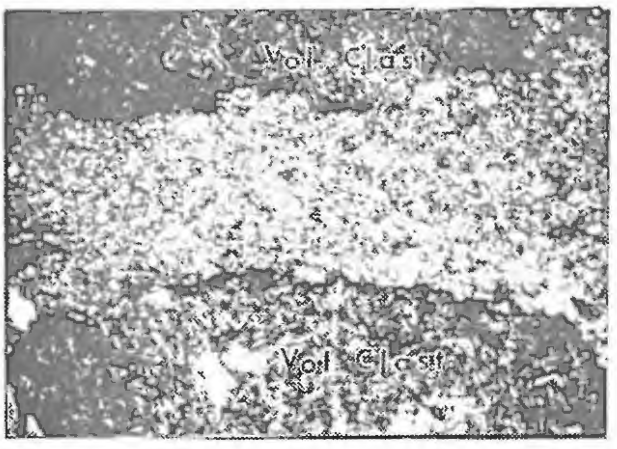

C

1 mm

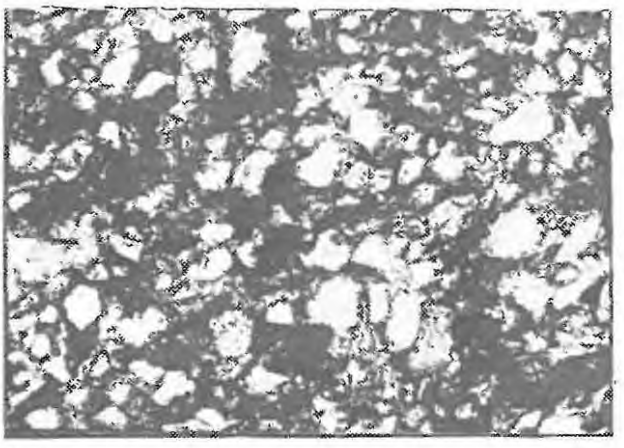

D

1 mm

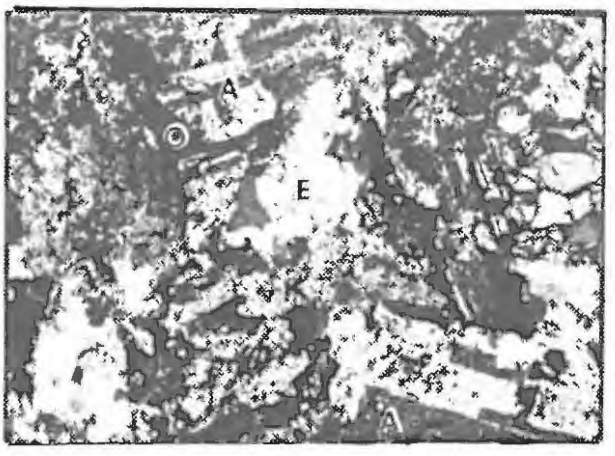

E

1 mm

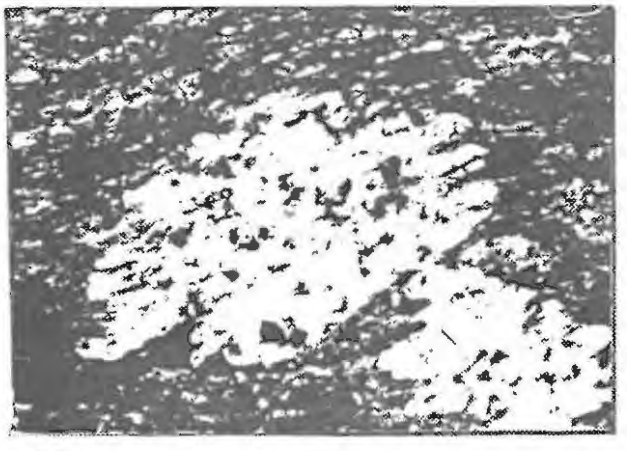

F

1 mm

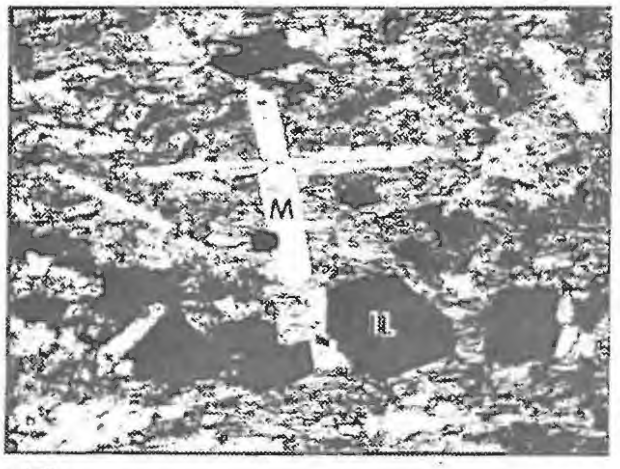

G

1 mm

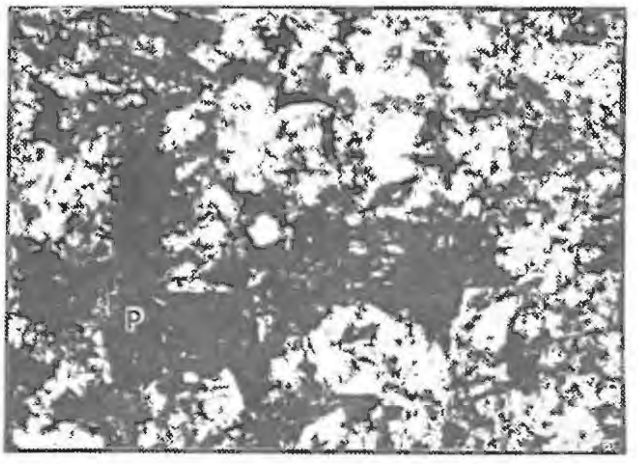

H

1 mm

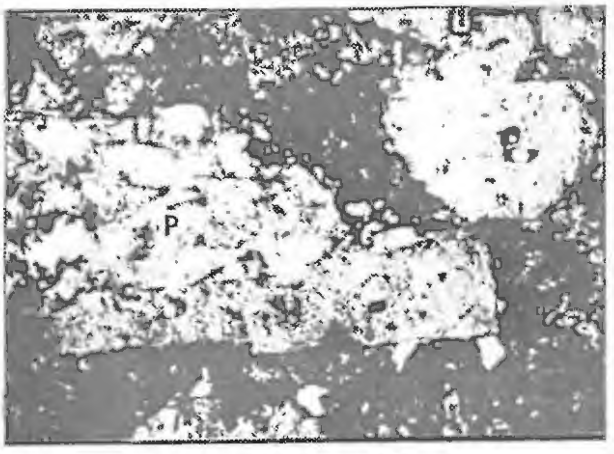

I

1 mm

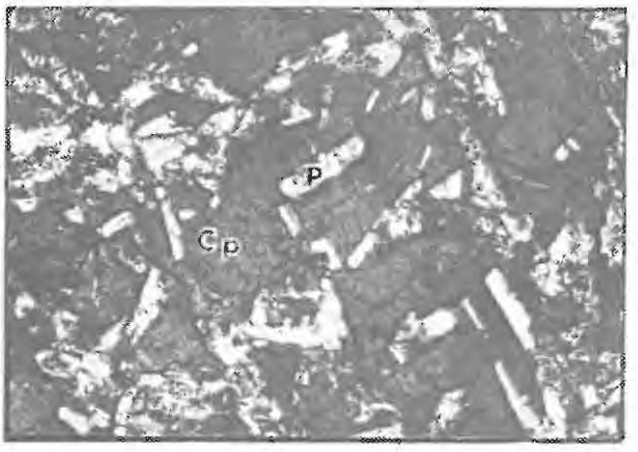

J

1 mm

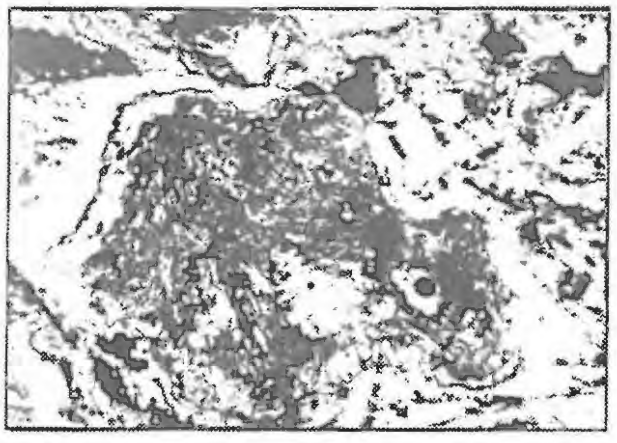

K

1 mm

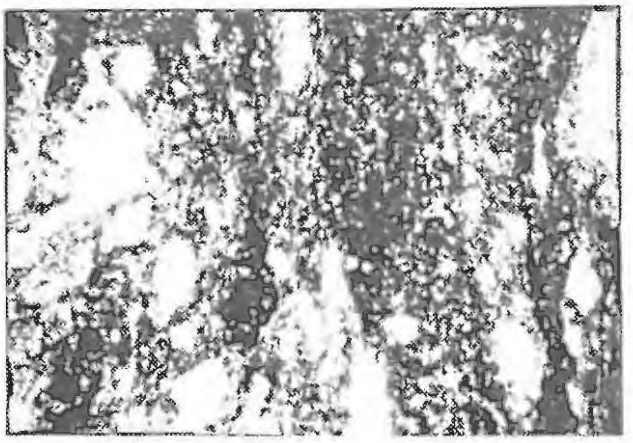

L

1 mm

4. MINERALOGY

4.1 Introduction

The Dordabis Formation metalavas have typical greenschist facies metabasaltic mineral assemblages. Microprobe analyses of the metamorphic phases albite and epidote, and of the relict ophitic pyroxene and minor plagioclase phenocrysts occurring in the Bitterwater Member lavas are presented in this chapter.

The electron microprobe does not allow routine determination of water and the distinction between ferrous and ferric iron. Total iron is calculated as Fe^{2+} for feldspars and pyroxenes and as Fe^{3+} for epidotes. Constantly low oxide totals for hydrous minerals (e.g. epidote) indicate the presence of water.

The symbols in Table 2 are used to identify the Dordabis Formation samples on the various diagrams illustrating mineral compositions. Analytical conditions are tabulated in Appendix 1.

Table 2 Symbols used to represent sampled lavas for which selected microprobe analyses are presented

OPDAM MEMBER	BITTERWATER MEMBER	
⊞ IWJ143	■ IWJ72	● IWJ77
⊕ IWJ156	⊙ IWJ89	▽ IWJ76
⊕ IWJ7	⊠ IWJ78	○ IWJ75
	⊗ IWJ117	▼ IWJ137
	▲ IWJ92	□ IWJ139
	◇ IWJ86	△ IWJ140

4.2 Pyroxenes

The general formula for the pyroxene group proposed by Cameron and Papike (1981) is:

$$XYZ_2O_6$$

where X represents Na, Ca, Mn^{2+}, Fe^{2+}, Mg and Li in the distorted 6-fold to 8-fold coordinated M_2 site; Y represents Mn^{2+}, Fe^{2+}, Mg, Fe^{3+}, Al, Cr and Ti in the octahedral M_1 site; and Z represents Si and Al in the tetrahedral site. Other cations not mentioned above can occur in trace amounts in pyroxenes.

The Dordabis Formation pyroxenes show a typical tholeiitic trend when plotted on the pyroxene quadrilateral, with their iron content increasing as their calcium content decreases (Fig. 9). The pyroxenes are typical augites ranging in composition from $Ca_{36,0}Mg_{41,7}Fe_{10,6}$ to $Ca_{45,6}Mg_{49,3}Fe_{17,3}$. The iron content can vary by up to 6% within individual coarser-grained pyroxene oikocrysts in samples IWJ76, IWJ77 and IWJ137, indicating that the grains are zoned (Fig. 9).

Mineral chemistry can reflect crystallisation conditions. IWJ75 was collected in the upper margin and IWJ76 in the central portion of a 80m thick lava flow. The atomic percentage iron in the pyroxene oikocrysts vary from 13,07 to 15,36% in IWJ75 and from 10,88 to 18,58% in IWJ76 (see Fig. 9). This indicates that the pyroxenes in IWJ76 are the more zoned of the two samples and that it therefore presumably cooled at a slower rate than IWJ75.

Some pyroxenes contain significant amounts of cations other than those presented in the traditional quadrilateral. The cations analysed for, and which substitute for Ca, Mg, Fe and Si include Ti, Al, Mn, Na and Cr. Substituting cations' charges must balance. Cameron and Papike (1981) showed that substituting cations obey the following charge balance equation:

$$^{vi}R^{3+} + 2^{vi}Ti^{4+} = Na + {}^{iv}Al$$

where R^{3+} is $^{iv}Al + {}^{vi}Fe^{3+} + {}^{vi}Cr^{3+}$. This indicates that substitution couples include $^{vi}Al - {}^{iv}Al$, $^{vi}Fe^{3+} - {}^{iv}Al$, $^{vi}Cr^{3+} - {}^{iv}Al$, $^{vi}Ti^{4+} - 2{}^{iv}Al$, $Na - {}^{vi}Al$, $Na - {}^{vi}Fe^{3+}$, $Na - {}^{vi}Cr^{3+}$ and $2Na - {}^{vi}Ti^{4+}$. The cation Mn^{2+} behaves similarly to, and hence substitutes readily for Fe^{2+} in

pyroxenes. This is shown by the positive correlation between MnO and FeO content in Figure 10. MgO/(MgO + FeO) (MMF) values decrease with fractionation. Figures 11 and 12 show that with decreasing MMF ratios, the TiO_2 content of the pyroxenes increases and the Cr_2O_3 content decreases. Cr_2O_3 and TiO_2 have opposite fractionation trends because the $^{vi}Cr^{3+}$-^{iv}Al couple substitute into early-formed pyroxenes at the expense of $^{vi}Ti^{4+}$-$2^{iv}Al$. This can be explained by the fact that the crystal field stabilisation energy of Cr is far greater than that of Ti (Campbell and Borley, 1974).

Cameron and Papike (1981) found that ^{vi}Al - ^{iv}Al and $^{vi}Ti^{4+}$ - ^{iv}Al are generally the most important substitution couples in pyroxenes. Figures 13 and 14, show that within certain samples the Na/Al and to a lesser extent Ti/Al ratios are constant, indicating that the Na-^{iv}Al and $^{vi}Ti^{4+}$-^{iv}Al substitution couples are probably important in the Dordabis pyroxenes. The pyroxenes analysed fall into two groups of Na/Al ratios (Fig. 13). The first larger group has ratios ranging between 1/8 and 1/4, while the second Cr-poor, Na-rich pyroxene group has a ratio of about 5/8. Figure 14 shows that the majority of the pyroxenes have a Ti/Al ratio less than 1/4. The augites from each sample tend to plot in groups with similar Ti/Al ratios. This behaviour can be explained by Gamble and Taylor's (1980) observation that titanium and aluminium contents increase with increasing cooling rate and decrease with decreasing temperature at constant cooling rate. This relationship is observed in an 80m thick lava flow in the Dordabis Formation, where the pyroxenes from the presumably faster-cooling upper margin (sample IWJ75) have a higher titanium and aluminium content than those from the slower-cooling, coarse-grained centre of the flow (sample IWJ76).

Altered basalts, like those in the Dordabis Formation, often contain fresh clinopyroxene crystals set in an altered matrix. A number of workers in this field have recognised significant chemical differences between clinopyroxenes from basalts of different tectonic settings. Although a better characterisation can be achieved using whole-rock chemistry, this difference in pyroxene chemistry can supplement the whole-rock data in constraining tectonic environments of eruption.

Kushiro (1960) and Le Bas (1962) demonstrated that the alkalinity of the parent magma could be identified by using plots of Al_2O_3 versus

SiO_2 in pyroxene. Le Bas (op. cit.) distinguished between non-alkaline, alkaline and peralkaline magma types. Figure 15 indicates that the Dordabis lavas fall in the non-alkaline field on the Al_2O_3 versus SiO_2 plot. Nisbet and Pearce (1977) found that tholeiitic ocean floor basalts, tholeiitic within-plate basalts and volcanic arc basalts all plot in this field. They used discriminant analysis on 329 microprobe analyses of "augitic" clinopyroxene from four known tectonic environments, and were able with varying degrees of success to distinguish between them. Figure 16 shows that the Dordabis lavas fall mainly in the ocean floor basalt and volcanic arc basalt field on the Nisbet and Pearce (op. cit.) discriminant function diagram. However, trace and major whole-rock chemistry, considered in a later section, has indicated that the basalts are most probably continental tholeiitic basalts. This inconsistency can be expected as Nisbet and Pearce (op. cit.) found only 42,3% of within-plate tholeiitic basalts plot in the correct field. It is of interest to note that the pyroxenes of the within-plate Karoo tholeiitic basalts analysed by Mitchell (1980) plot in the same field as the Dordabis lavas.

The above discussion indicates that pyroxene analyses can be confidently used only to distinguish between alkali and tholeiitic magma types. Schweitzer et al. (1979) have emphasised that tholeiitic pyroxenes are generally lower in TiO_2, Na_2O and to a lesser extent Al_2O_3 and Fe_2O_3, while they are higher in Cr_2O_3 and SiO_2 than alkalic basaltic pyroxenes. By comparing the Dordabis Formation pyroxene compositions with analyses of pyroxene from basalts of known alkaline and tholeiitic affinities (analyses 17-1 & 11-1 in Table 3.1) it appears that the Dordabis Formation basalts are tholeiitic in nature.

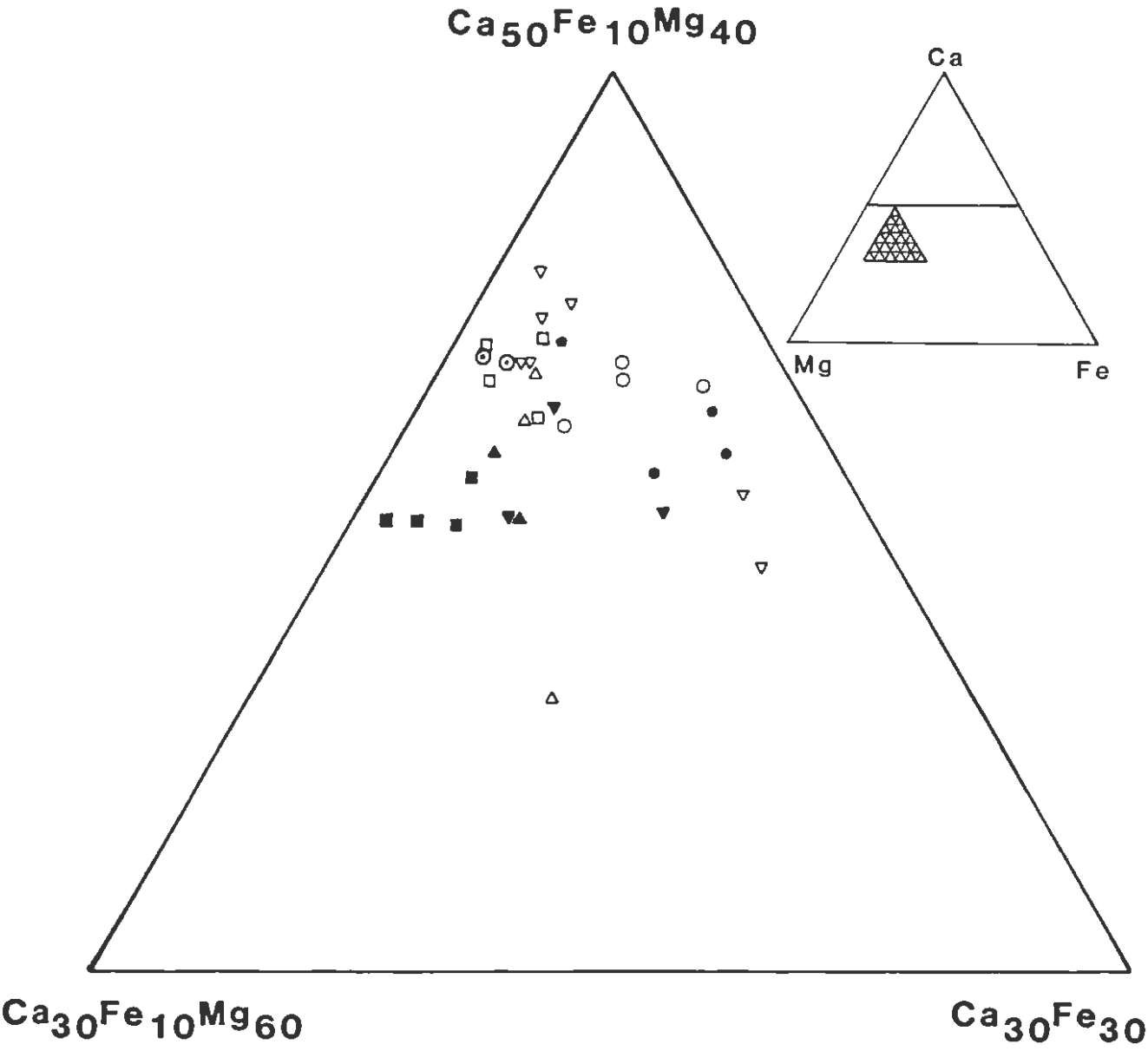

Figure 9 Ca-Mg-Fe plots of the Bitterwater Member clinopyroxenes

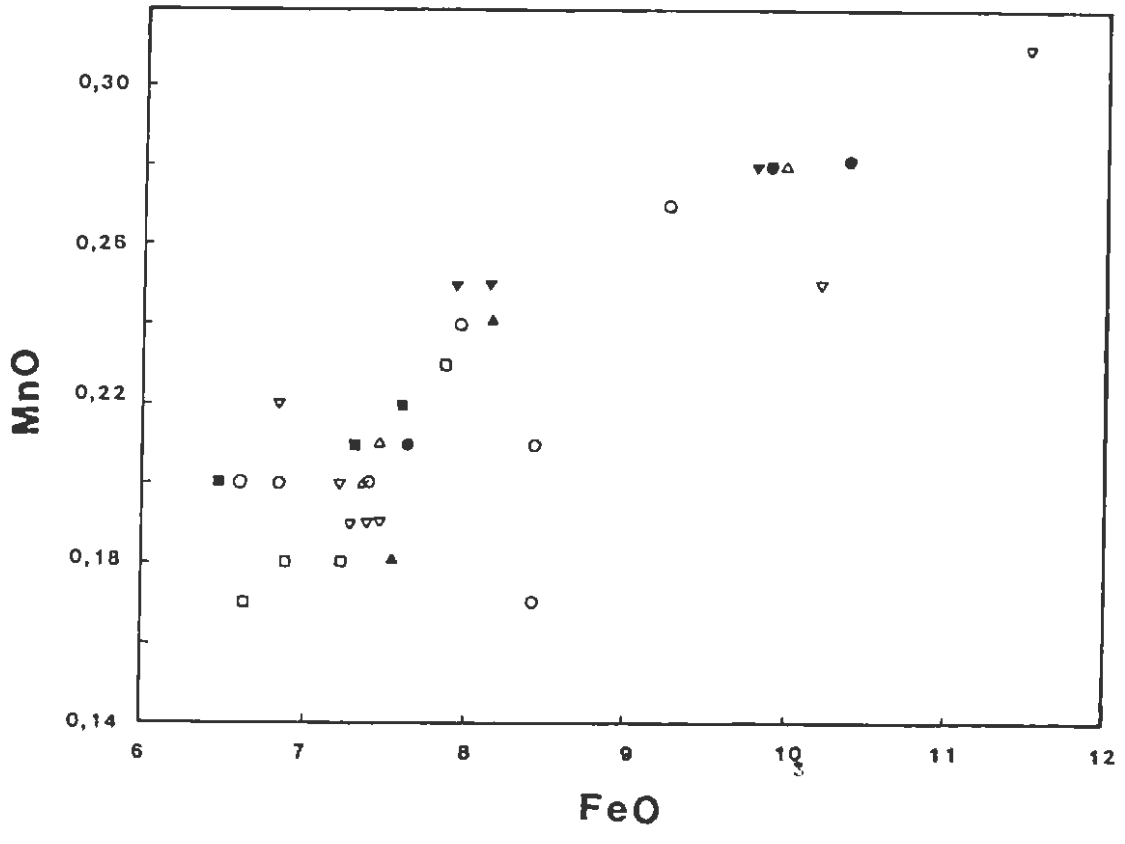

Figure 10 MnO versus FeO variation diagram for the Bitterwater pyroxenes

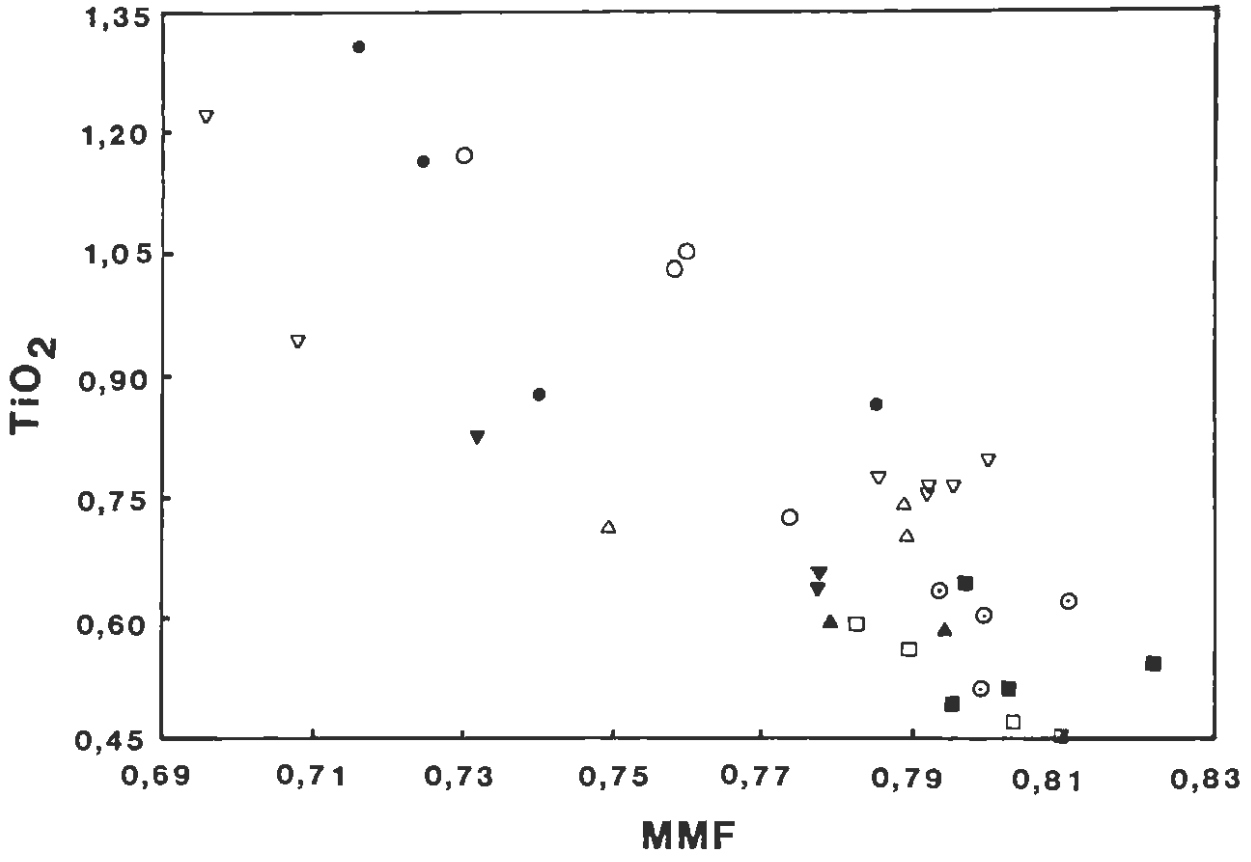

Figure 11 TiO_2 versus MMF variation diagram for the Bitterwater pyroxenes

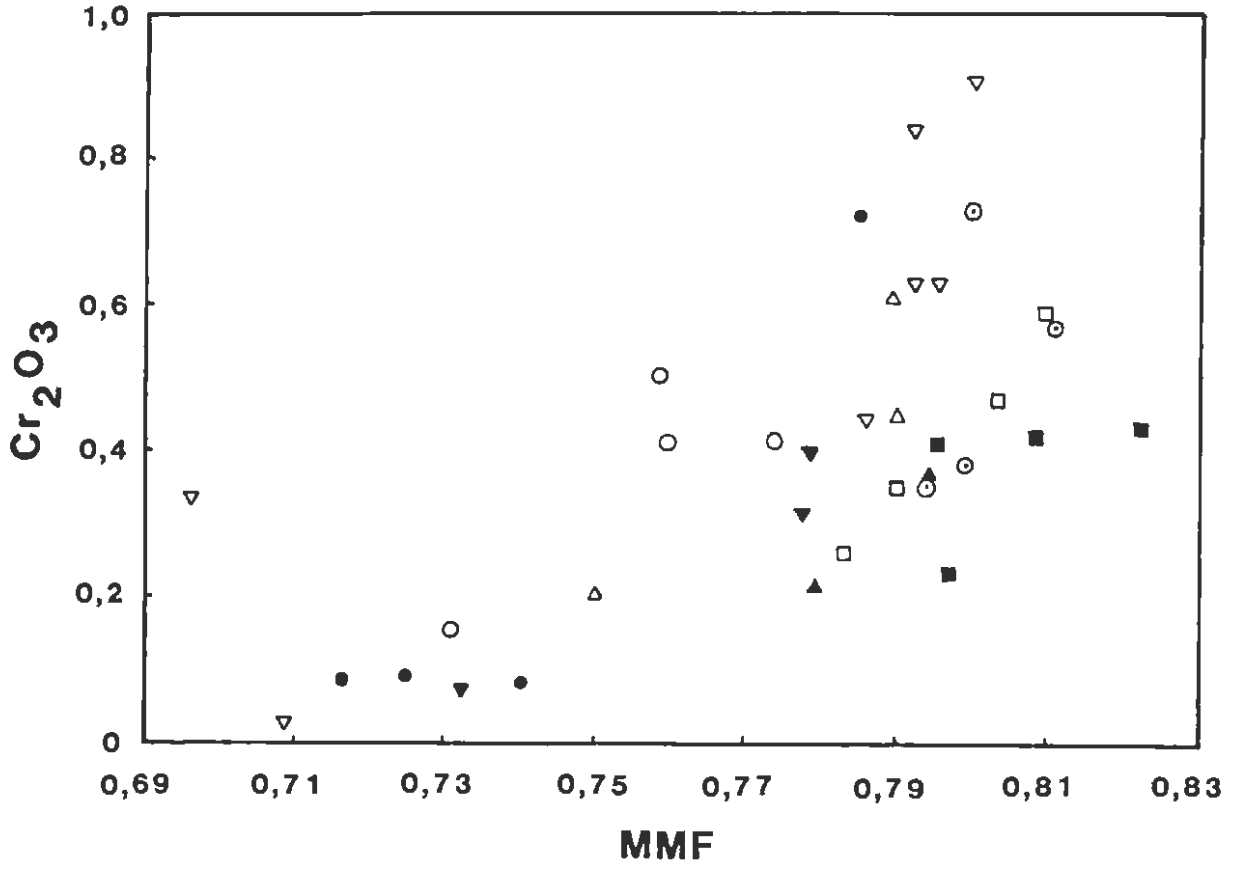

Figure 12 Cr_2O_3 versus MMF variation diagram for the Bitterwater pyroxenes

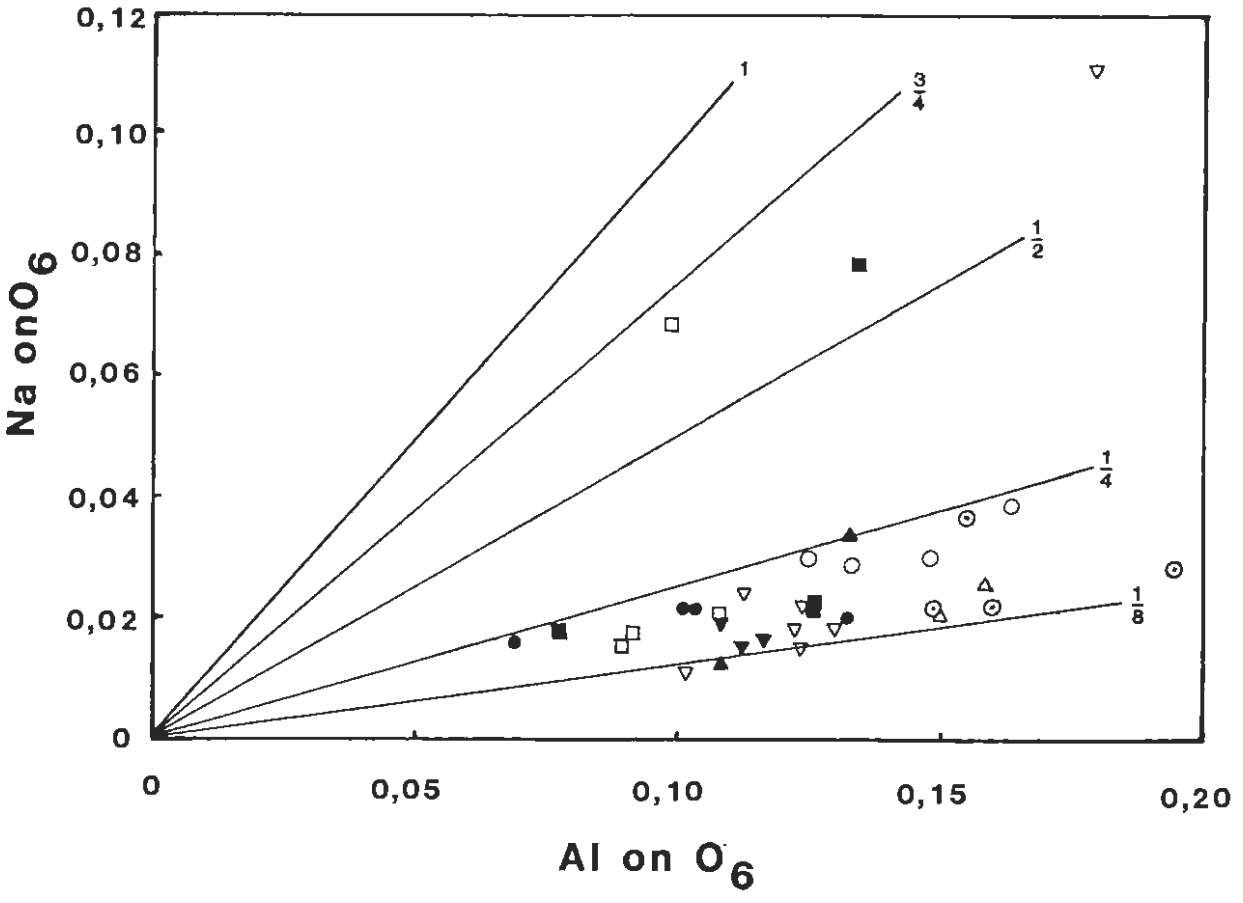

Figure 13 Plot illustrating Na-Al substitution in the Bitterwater pyroxenes

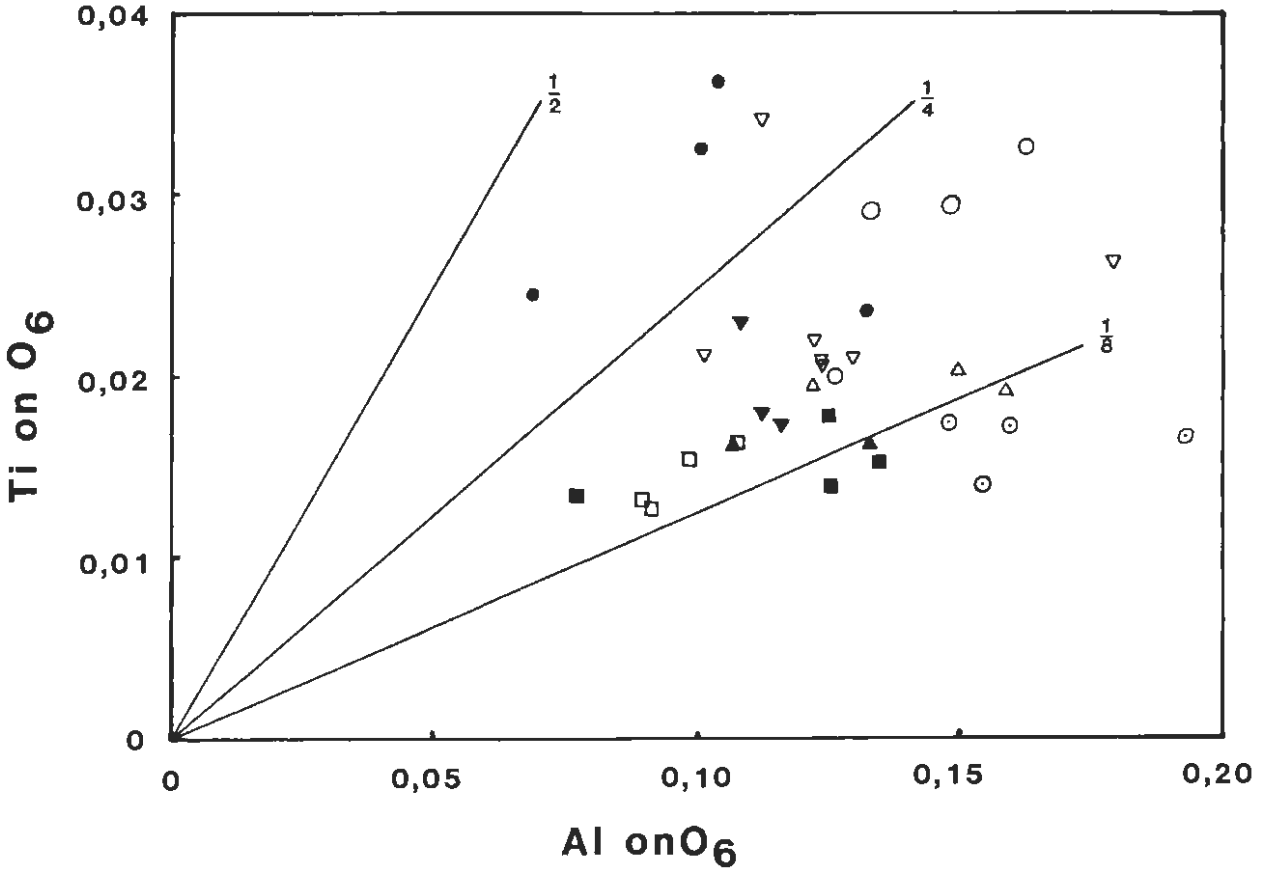

Figure 14 Plot illustrating Ti-Al substitution in the Bitterwater pyroxenes

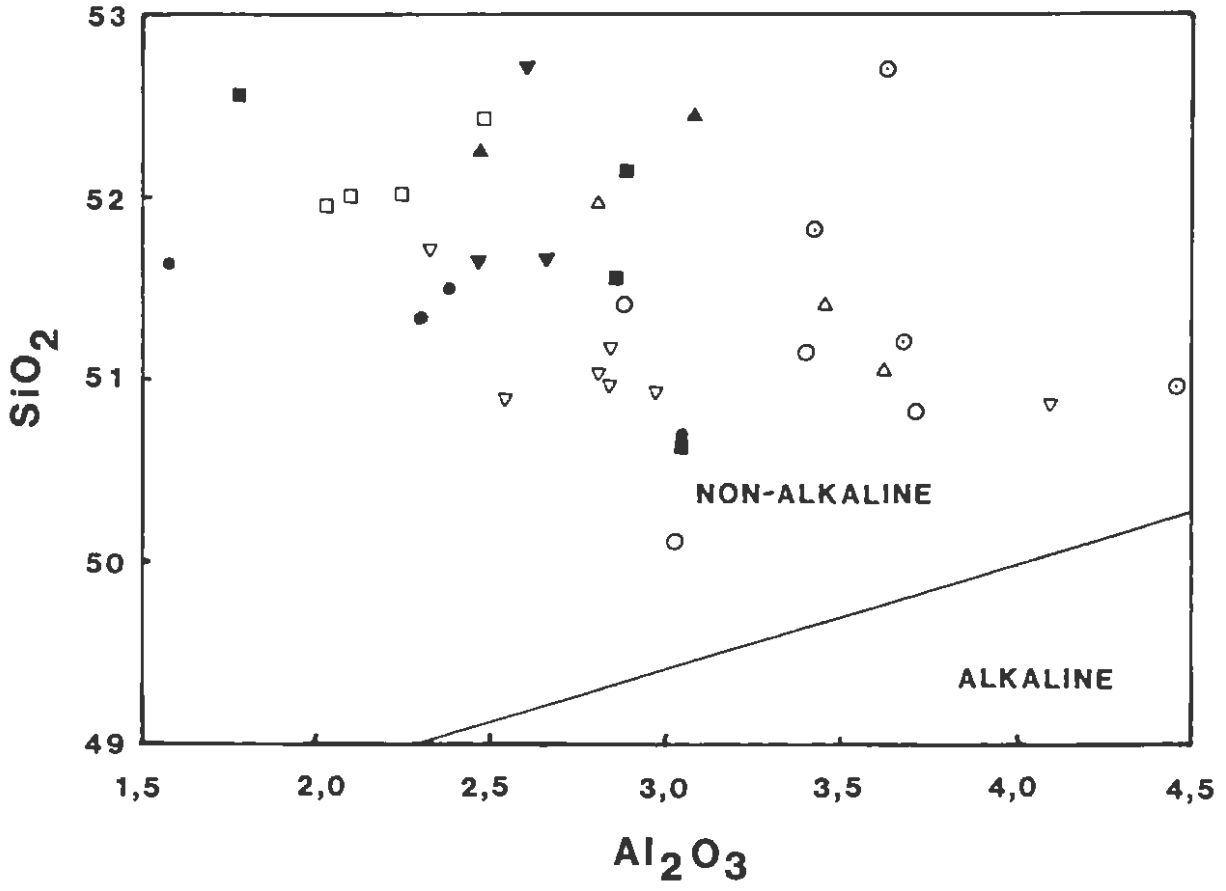

Figure 15 Plot discriminating between non-alkaline and alkaline magma types using SiO_2 and Al_2O_3 contents of pyroxenes (after Le Bas, 1962).

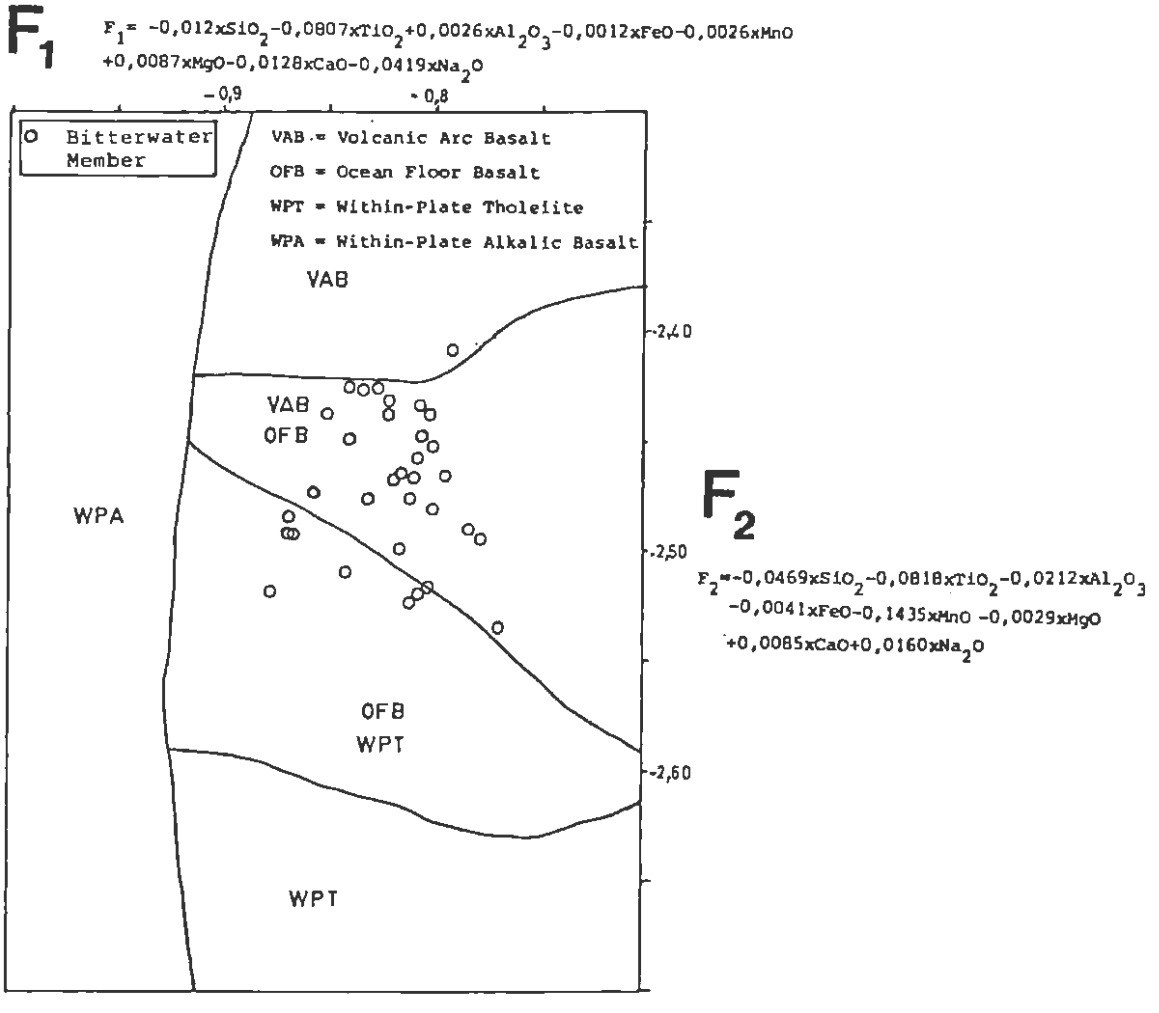

Figure 16 Plot of discriminant functions F_1 versus F_2 for the Bitterwater pyroxenes (after Nisbet and Pearce, 1977).

TABLE 3.1 PYROXENE ANALYSES BY MICROPROBE

Bitterwater Member

	IWJ140a	IWJ140b	IWJ140c	IWJ89a	IWJ89b	IWJ89c	IWJ89d	IWJ137a	IWJ137b	IWJ137c	IWJ139a	IWJ139b	IWJ139c	IWJ139d	IWJ72a	IWJ72b	IWJ72c	IWJ72d
SiO_2	51,40	51,05	51,96	50,95	51,20	51,81	52,70	51,63	51,65	52,72	52,01	52,00	51,95	52,43	52,13	51,54	52,56	50,62
TiO_2	0,74	0,70	0,71	0,60	0,62	0,63	0,51	0,82	0,63	0,65	0,56	0,45	0,47	0,59	0,51	0,64	0,49	0,54
Al_2O_3	3,46	3,62	2,81	4,46	3,68	3,43	3,63	2,47	2,67	2,61	2,25	2,10	2,03	2,49	2,89	2,86	1,78	3,05
FeO	7,35	7,46	9,91	6,84	6,60	7,38	7,38	9,82	7,91	8,16	7,23	6,62	6,88	7,88	7,31	7,31	7,61	6,46
MnO	0,20	0,21	0,28	0,20	0,20	0,20	0,20	0,28	0,25	0,25	0,18	0,17	0,18	0,23	0,21	0,21	0,22	0,20
MgO	15,42	15,67	16,67	15,29	15,85	15,91	16,43	15,10	15,53	16,03	15,24	15,82	15,81	15,92	16,70	16,14	16,62	16,81
CaO	20,77	20,21	17,45	20,45	21,10	20,84	20,15	19,28	20,53	19,87	21,08	21,25	20,76	20,77	18,83	19,57	19,08	18,97
Na_2O	0,28	0,36	0,23	0,40	0,31	0,30	0,52	0,27	0,23	0,21	0,96	0,25	0,21	0,28	0,32	0,29	0,24	1,09
Cr_2O_3	0,61	0,45	0,20	0,73	0,57	0,35	0,38	0,07	0,31	0,40	0,35	0,59	0,47	0,26	0,42	0,23	0,41	0,43
TOTAL	100,23	99,73	100,22	99,92	100,13	100,85	101,90	90,74	99,71	100,90	99,86	99,25	98,76	100,84	99,31	98,79	99,01	98,17
Recalculated as cations per 6 oxygens (Z = 2)																		
Si	1,898	1,893	1,919	1,881	1,888	1,899	1,905	1,927	1,920	1,930	1,930	1,934	1,941	1,924	1,928	1,922	1,954	1,900
Al	0,112	0,117	0,081	0,119	0,112	0,101	0,095	0,073	0,080	0,070	0,070	0,066	0,059	0,076	0,072	0,078	0,046	0,100
Ti	0,020	0,019	0,019	0,017	0,017	0,017	0,014	0,023	0,017	0,018	0,015	0,013	0,013	0,016	0,014	0,018	0,013	0,015
Al	0,038	0,041	0,041	0,075	0,048	0,047	0,050	0,036	0,037	0,043	0,028	0,026	0,030	0,032	0,054	0,048	0,032	0,035
Fe	0,227	0,231	0,306	0,211	0,203	0,226	0,223	0,307	0,246	0,250	0,224	0,206	0,215	0,242	0,226	0,228	0,237	0,203
Mn	0,006	0,006	0,009	0,006	0,006	0,006	0,006	0,009	0,008	0,008	0,006	0,005	0,005	0,007	0,006	0,006	0,007	0,006
Mg	0,848	0,866	0,918	0,841	0,871	0,870	0,887	0,839	0,860	0,875	0,843	0,876	0,879	0,872	0,919	0,895	0,918	0,938
Ca	0,821	0,803	0,690	0,809	0,834	0,818	0,780	0,771	0,818	0,779	0,839	0,847	0,831	0,816	0,746	0,782	0,760	0,763
Na	0,020	0,025	0,017	0,028	0,022	0,021	0,037	0,019	0,016	0,015	0,068	0,017	0,015	0,020	0,022	0,021	0,017	0,079
Cr	0,018	0,013	0,006	0,021	0,016	0,010	0,109	0,002	0,009	0,611	0,010	0,017	0,014	0,007	0,012	0,006	0,012	0,012
X + Y	2,008	2,015	2,006	2,008	2,017	2,016	2,017	2,006	2,009	1,998	2,034	2,008	2,002	2,012	1,999	2,004	1,996	2,049
At % Mg	44,72	45,57	47,94	45,21	45,64	45,44	46,93	43,79	44,70	45,97	44,24	45,43	45,64	45,17	48,61	46,98	47,95	49,26
Fe	11,97	12,17	15,99	11,33	10,65	11,81	11,81	15,99	12,78	13,12	11,76	10,67	11,17	12,52	11,94	11,96	12,35	10,65
Ca	43,31	42,26	36,06	43,45	43,71	42,75	41,26	40,22	42,51	40,90	44,00	43,90	43,19	43,30	39,45	41,06	39,70	40,09

TABLE 3.1 (continued)

	IWJ75a	IWJ75b	IWJ75c	IWJ75d	IWJ76a	IWJ76b	IWJ76c	IWJ76d	IWJ76e	IWJ76f	IWJ76g	IWJ77a	IWJ77b	IWJ77c	IWJ92a	IWJ92b	*17-1	x11-1
SiO_2	51,14	50,82	50,10	51,38	50,86	51,02	51,71	50,92	50,88	50,96	51,17	51,50	51,32	50,68	52,44	52,24	49,29	51,32
TiO_2	1,05	1,17	1,03	0,72	0,94	0,79	0,77	0,76	1,22	0,75	0,76	1,30	1,16	0,86	0,59	0,58	1,50	0,34
Al_2O_3	3,41	3,72	3,03	2,89	4,10	2,81	2,33	2,98	2,55	2,84	2,85	2,39	2,31	3,05	3,09	2,48	3,75	3,93
FeO	8,42	9,28	8,45	7,98	10,20	6,83	7,49	7,22	11,49	7,40	7,31	10,39	9,94	7,64	8,18	7,52	8,76	4,29
Fe_2O_3	0,00	0,00	0,00	0,00	0,00	0,00	0,00	0,00	0,00	0,00	0,00	0,00	0,00	0,00	0,00	0,00	2,16	1,87
MnO	0,17	0,27	0,21	0,24	0,25	0,22	0,19	0,20	0,31	0,19	0,19	0,28	0,28	0,21	0,24	0,18	0,24	0,11
MgO	14,93	14,12	14,87	15,35	13,89	15,31	15,36	15,40	14,75	15,80	15,93	14,70	14,67	15,63	16,16	16,31	13,21	17,97
CaO	21,06	20,28	20,65	20,10	18,74	22,30	22,10	21,68	18,75	21,32	21,49	20,44	20,77	21,75	19,37	20,24	20,62	19,19
Na_2O	0,42	0,54	0,39	0,14	1,53	0,25	0,15	0,26	0,33	0,31	0,21	0,30	0,31	0,28	0,48	0,17	0,30	0,14
Cr_2O_3	0,41	0,15	0,50	0,14	0,02	0,91	0,44	0,84	0,02	0,63	0,63	0,08	0,09	0,72	0,21	0,37	0,02	0,63
TOTAL	101,00	100,35	99,23	99,48	100,53	100,43	100,53	100,26	100,30	100,20	100,53	101,37	100,84	100,81	100,76	100,08	99,85	99,79
Recalculated as cations per 6 oxygens (Z = 2)																		
Si	1,885	1,889	1,884	1,914	1,891	1,888	1,911	1,888	1,903	1,889	1,890	1,904	1,906	1,873	1,921	1,926	1,854	1,876
Al	0,115	0,111	0,116	0,086	0,109	0,112	0,089	0,112	0,097	0,111	0,110	0,096	0,094	0,127	0,079	0,074	0,146	0,124
Ti	0,029	0,033	0,029	0,020	0,026	0,022	0,021	0,021	0,034	0,021	0,021	0,036	0,032	0,024	0,016	0,016	0,042	0,009
Al	0,033	0,052	0,018	0,040	0,070	0,011	0,013	0,018	0,015	0,013	0,013	0,008	0,007	0,006	0,054	0,034	0,020	0,046
Fe^{2+}	0,260	0,289	0,265	0,249	0,317	0.211	0,232	0,224	0,359	0,229	0,226	0,321	0,309	0,236	0,250	0,232	0,276	0,131
Fe^{3+}	0,000	0,000	0,000	0,000	0,000	0,000	0,000	0,000	0,000	0,000	0,000	0,000	0,000	0,000	0,000	0,000	0,061	0,051
Mn	0,005	0,008	0,006	0,007	0,008	0,007	0,006	0,060	0,010	0,006	0,006	0,008	0,008	0,006	0,007	0,006	0,008	0,003
Mg	0,821	0,782	0,833	0,852	0,770	0,845	0,847	0,851	0,823	0,873	0,877	0,811	0,813	0,862	0,883	0,896	0,740	0,979
Ca	0,832	0,808	0,832	0,802	0,747	0,884	0,875	0,861	0,752	0,847	0,850	0,810	0,827	0,861	0,760	0,800	0,831	0,752
Na	0,030	0,039	0,028	0,030	0,110	0,018	0,011	0,018	0,024	0,022	0,015	0,022	0,022	0,021	0,033	0,012	0,022	0,010
Cr	0,012	0,004	0,015	0,012	0,000	0,027	0,013	0,025	0,001	0,018	0,018	0,002	0,003	0,021	0,006	0,011	0,001	0,018
X + Y	2,021	2,014	2,027	2,011	2,048	2,024	2,016	2,023	2,018	2,029	2,026	2,018	2,021	2,036	2,010	2,005	2,00	1,999
At % Mg	42,93	41,65	43,14	44,77	41,98	43,54	43,35	43,97	42,54	44,79	44,92	41,78	41,73	43,98	46,63	46,49		
Fe	13,58	15,36	13,75	13,07	17,30	10,88	11,85	11,55	18,58	11,76	11,56	16,53	15,84	12,06	13,22	12,03		
Ca	43,49	42,99	43,11	42,16	40,72	45,58	44,79	44,48	38,88	43,45	43,52	41,69	42,43	43,96	40,14	41,48		

*17-1 Alkalic pyroxene (after Schweitzer et al., 1979)

x11-1 Tholeiitic pyroxene (after Schweitzer et al., 1979)

4.3 Feldspars

The general formula for the feldspar group minerals proposed by Frye (1981) is:

$$^{M}T_4O_8$$

where M represents large cations K^+, Na^+ and Ca^+ with trace amounts of Ba^{2+}, Sr^{2+}, Rb^+, Cs^+, Pb^{2+}, Fe^{2+}, Mg^{2+}, H_3O^+ and rare earth elements, while the T sites represent small cations Al^{3+} and Si^{4+} with trace amounts of Fe^{2+}, Fe^{3+}, P^{5+} and Ti^{4+} in tetrahedral coordination. Feldspars are framework silicates and can be divided into two solid solution series, the alkali feldspars where M represents Na^+ and/or K^+ and the plagioclase feldspars where M represents Na^+ and/or Ca^{2+}.

The feldspars in the lavas of the Dordabis Formation fall into three discrete groups, albite, oligoclase and labradorite, on the ternary diagram (Fig. 17). The feldspars from the Opdam Member (samples IWJ7 &

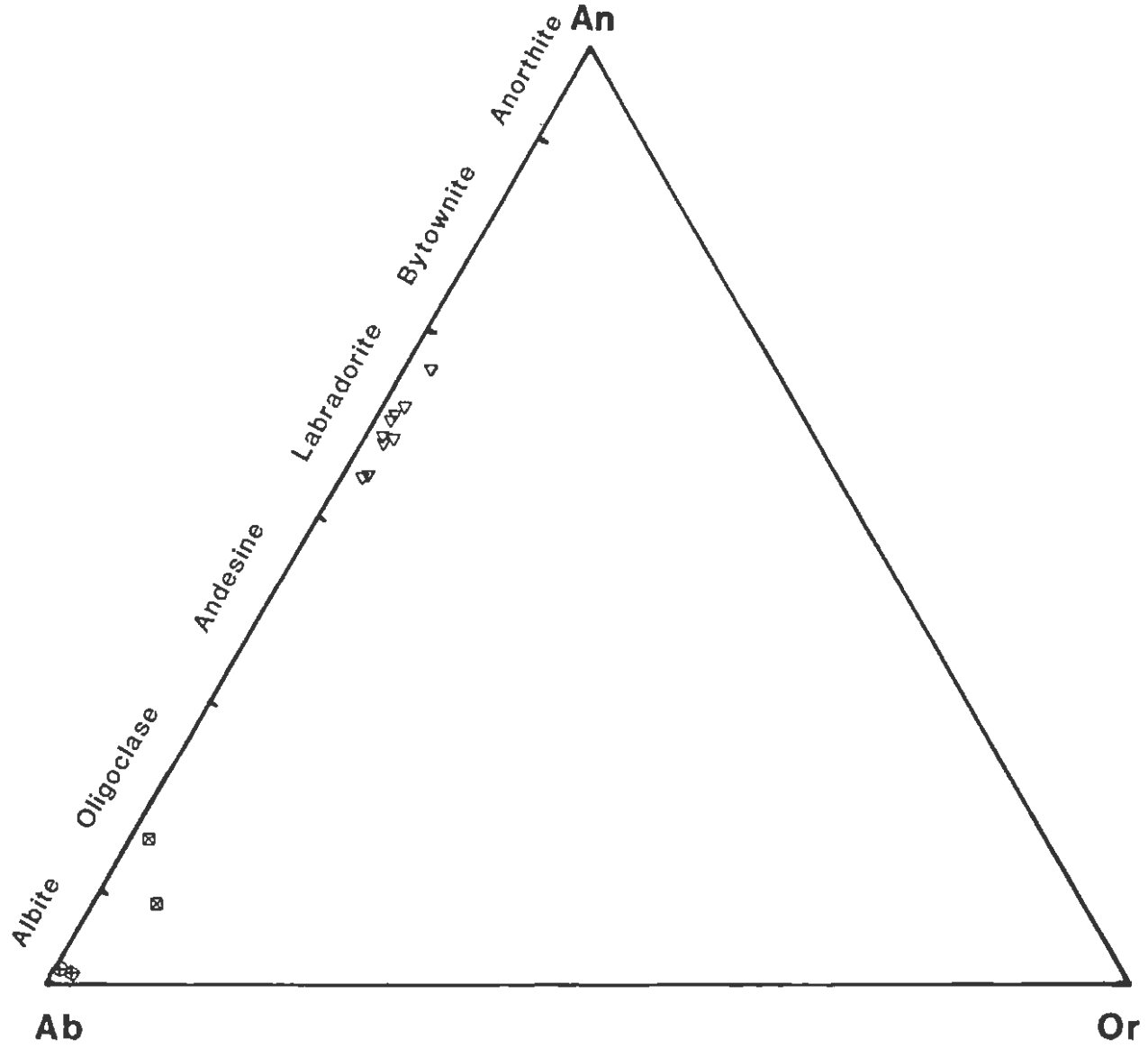

Figure 17 An-Ab-Or plots for Dordabis Formation feldspars.

IWJ156) are albitic in composition and exhibit a remarkably restricted chemical variation. These sodic plagioclases have an An content ranging from 0,0 to 1,7 and hence have uniformly low CaO and K_2O contents. The feldspars in the Opdam basalts have degraded to albite, calcite and clay minerals under greenschist facies metamorphic conditions.

In the less metamorphosed Bitterwater Member nearly all feldspars have altered to saussurite. Sample IWJ78 was collected from the large-feldspar blastoporphyritic lava on the farm Grasvlakte. The phenocrysts are highly altered to saussurite making microprobe analyses difficult. Analyses on small relict parts of the phenocrysts indicate that the feldspar was sodic oligoclase, although the presence of calcite, epidote and apatite in the altered phenocrysts indicate that the plagioclase may have originally had a higher anorthite content. The ophitic lava flow, represented by sample IWJ76, contains small relict labradorite laths which range in composition from An_{54} to An_{66} and which are regarded as primary.

TABLE 3.2 PLAGIOCLASE ANALYSES BY MICROPROBE

	Opdam Member (recrystallised plagioclase)					Bitterwater Member (Plagioclase chadacrysts in pyroxene oikocrysts)											Bitterwater Member (Large plagioclase phenocrysts)	
	IWJ156a	IWJ156b	IWJ156c	IWJ156d	IWJ156e	IWJ7a	IWJ7b	IWJ7c	IWJ76a	IWJ76b	IWJ76c	IWJ76d	IWJ76e	IWJ76f	IWJ76g	IWJ76h	IWJ76i	IWJ78a	IWJ78b
SiO_2	69,46	69,62	68,64	68,30	68,22	69,86	68,04	69,90	54,51	53,90	53,19	52,58	52,95	51,60	54,47	54,78	57,75	62,46	62,00
Al_2O_3	19,42	19,47	19,27	19,59	19,36	19,11	19,41	20,19	27,49	28,21	28,09	28,28	28,83	28,93	28,34	27,70	26,68	21,63	21,51
FeO	0,29	0,25	0,55	0,28	0,40	0,48	0,67	0,86	1,33	0,97	1,27	1,05	1,10	1,11	1,02	1,02	1,09	0,14	0,57
CaO	0,18	0,29	0,19	0,29	0,34	0,13	0,37	1,44	11,24	11,88	12,31	12,05	12,66	13,25	12,64	12,27	11,06	2,84	1,87
Na_2O	11,97	12,12	10,61	11,56	10,60	11,30	11,49	10,14	5,05	4,51	4,02	4,56	4,38	3,61	4,32	4,57	4,83	8,33	9,65
K_2O	0,08	0,11	0,11	0,00	0,07	0,04	0,09	0,16	0,34	0,39	0,36	0,36	0,30	0,27	0,32	0,40	0,48	0,26	1,03
TOTAL	101,39	101,86	99,37	100,02	98,99	100,91	100,06	102,68	99,96	99,86	99,24	98,88	100,22	98,77	101,10	100,74	101,89	95,66	96,63
Recalculated as cations per 8 oxygens																			
Si	2,998	2,994	3,011	2,986	3,004	3,021	2,982	2,985	2,479	2,452	2,440	2,423	2,410	2,384	2,450	2,473	2,561	2,863	2,842
Al	0,988	0,987	0,996	1,009	1,005	0,974	1,003	1,016	1,474	1,513	1,518	1,536	1,546	1,575	1,503	1,474	1,394	1,168	1,162
Fe	0,010	0,009	0,020	0,010	0,015	0,017	0,025	0,031	0,051	0,037	0,049	0,040	0,042	0,043	0,038	0,039	0,040	0,005	0,022
Ca	0,008	0,013	0,009	0,014	0,016	0,006	0,017	0,052	0,548	0,579	0,605	0,595	0,617	0,656	0,609	0,593	0,525	0,139	0,092
Na	1,002	1,011	0,902	0,980	0,905	0,947	0,976	0,839	0,445	0,398	0,357	0,407	0,386	0,323	0,377	0,400	0,415	0,074	0,858
K	0,004	0,006	0,006	0,000	0,004	0,002	0,005	0,009	0,020	0,023	0,021	0,021	0,017	0,016	0,018	0,023	0,027	0,015	0,060
SUM	5,011	5,020	4,945	4,999	4,948	4,967	5,008	4,932	5,016	5,002	4,990	5,023	5,018	4,998	4,996	5,002	4,963	4,931	5,036
Mol% An	0,82	1,30	0,97	1,37	1,73	0,63	1,74	0,00	54,08	57,93	61,51	58,13	60,45	65,91	60,66	58,38	54,29	15,58	9,10
Ab	98,75	98,11	98,36	98,63	97,84	99,14	97,75	98,97	43,97	39,80	36,35	39,81	37,85	32,49	37,52	39,35	42,90	82,72	84,94
Or	0,43	0,59	0,67	0,00	0,43	0,23	0,50	1,03	1,95	2,26	2,14	2,07	1,71	2,70	1,83	2,27	2,81	1,70	5,96

4.4 Epidotes

The general formula for epidote group minerals, after Deer et al. (1962) is:

$$X_2\ Y_3\ Z_3\ (O,OH,F)_3$$

in which X = Ca, Ce^{3+}, La^{3+}, Y^{3+}, Th, Fe^{2+}, Mn^{2+}, Mn^{3+}
Y = Al, Fe^{3+}, Mn^{3+}, Fe^{2+}, Mn^{2+}, Ti
Z = Si, Be

and the composition of the main members of the series is:

Zoisite Clinozoisite	$Ca_2\ Al.\ Al_2O.OH.Si_2O_7\ SiO_4$
Epidote	$Ca_2Fe^{3+}Al_2O_3.OH.Si_2O_7.SiO_4$
Piedmontite	$Ca_2(Mn^{3+}, Fe^{3+}, Al)_3\ O.OH.SiO_7.SiO_4$
Allanite	$(Ca, Ce, La, Y)_2\ (Mn^{2+}, Fe^{2+}, Fe^{3+}, Al)_3\ O.OH.Si_2O_7.SiO_4$

Epidote-clinozoisite series minerals occur in a wide variety of low to medium-grade metamorphosed rocks. Epidote is the most common mineral in this series because of its greater stability range, both towards high and low temperatures and because during metamorphism high oxygen fugacities often exist, favouring the development of iron-rich epidote (Liou, 1973). Liou (op. cit.) also found that epidotes become more aluminous with decreasing oxygen fugacity. If oxygen fugacities change with time an inverse relationship between iron and aluminium in epidote would be expected. Although only four of the points on Figure 18 suggest the presence of an inverse relationship between these elements, the author is confident that further analyses would substantiate this postulation.

Epidote, minor clinozoisite and zoisite occur in the metalavas, while piedmontite was recognised optically in the pink quartzites of the Dordabis Formation. The high magnesium content of the epidote in sample IWJ92 may be explained by the fact that it was sampled in a pyroxene-rich flow. Kerrick (1970) and Liou (1973) also recognised the strong influence that bulk rock composition has on epidote composition when they noted that epidotes in metabasic rocks have a higher Fe^{3+} content than epidotes in metasediments. Figure 19 illustrates how the iron content in the epidotes increases as the whole-rock iron content increases. To use the iron content of the epidotes in the Dordabis Formation to determine changes in metamorphic grade would be futile. The small changes in iron content that would occur within one metamorphic facies (greenschist)

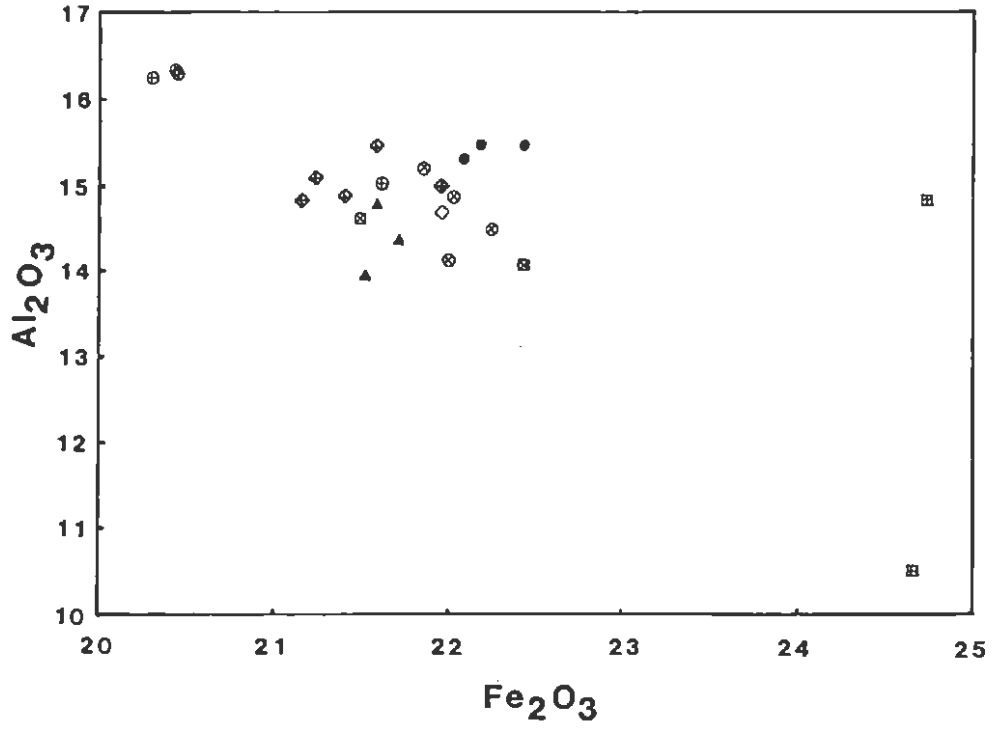

Figure 18 Fe_2O_3 versus Al_2O_3 variation diagram for epidotes from metalavas

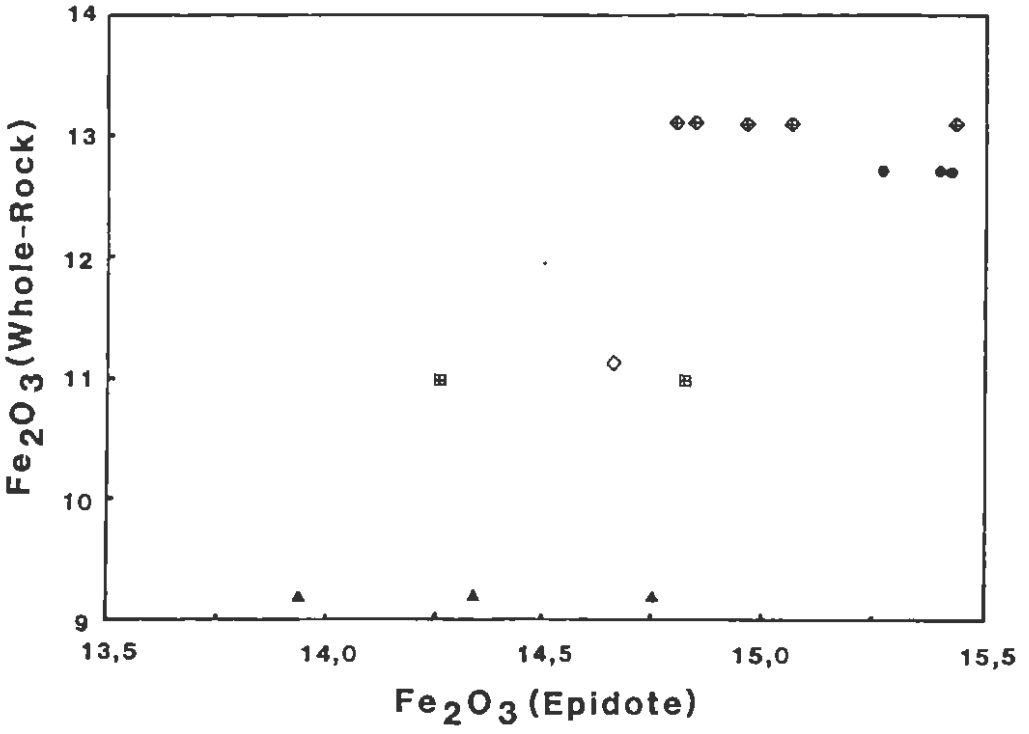

Figure 19 Plot of Fe_2O_3 (whole-rock) versus Fe_2O_3 (epidote) for the metalavas where Fe_2O_3 is total iron for both the whole-rock and the epidote analyses

would be minimal compared to the strong influences that bulk rock composition and oxygen fugacity have on epidote composition.

The number of ions was recalculated as cations per 25 oxygens, because the water content of epidote was not calculated. Average totals for oxygen-corrected microprobe analyses are about 98%. This indicates approximately 2% water content, which is in accordance with epidote analyses quoted by other authors (Deer et al., 1962 and Kerrick, 1970).

TABLE 3.3 EPIDOTE ANALYSES BY MICROPROBE

Opdam Member

	IWJ143a	IWJ143b	IWJ143c	IWJ156a	IWJ156b	IWJ156c	IWJ156d
SiO_2	37,77	37,87	37,90	37,39	37,03	37,50	36,54
Al_2O_3	21,71	21,97	24,66	20,46	20,32	21,63	20,45
Fe_2O_3	14,83	14,26	10,51	16,32	16,25	15,04	16,35
MnO	0,08	0,18	0,12	0,27	0,34	0,37	0,33
CaO	23,54	23,04	23,79	23,44	23,19	23,59	23,33
TOTAL	97,93	97,32	96,98	97,88	97,13	98,13	97,00
Recalculated as cations per 25 oxygens							
Si	6,054	6,086	6,040	6,039	6,029	6,013	5,968
Al	4,101	4,161	4,631	3,895	3,899	4,088	3,937
Fe	1,789	1,724	1,260	1,983	1,991	1,815	2,009
Mn	0,010	0,022	0,015	0,033	0,042	0,045	0,041
Ca	4,043	3,967	4,062	4,056	4,045	4,053	4,083
SUM	15,996	15,960	16,007	16,006	16,005	16,013	16,038

	IWJ7a	IWJ7b	IWJ7c	IWJ7d	IWJ7e
SiO_2	37,56	37,26	37,59	37,68	38,06
Al_2O_3	21,78	21,18	21,43	21,61	21,27
Fe_2O_3	14,97	14,81	14,85	15,44	15,07
MnO	0,35	0,32	0,21	0,34	0,30
CaO	23,50	23,22	23,42	23,69	23,12
TOTAL	98,16	96,79	97,50	97,18	97,82
Recalculated as cations per 25 oxygens					
Si	6,015	6,052	6,057	6,009	6,105
Al	4,111	4,054	4,070	4,062	4,021
Fe	1,804	1,810	1,800	1,853	1,819
Mn	0,043	0,040	0,025	0,041	0,037
Ca	4,032	4,041	4,043	4,048	3,974
SUM	16,005	15,996	15,995	16,013	15,956

Bitterwater Member

	IWJ117a	IWJ117b	IWJ117c	IWJ117d	IWJ86a	IWJ86b	IWJ77a
SiO_2	37,43	38,21	37,82	37,43	37,41	37,41	37,72
Al_2O_3	22,03	21,87	22,26	22,04	22,00	21,98	22,45
Fe_2O_3	14,16	15,23	14,48	14,86	14,68	14,68	15,43
MnO	0,16	0,20	0,20	0,23	0,20	0,28	0,29
CaO	24,16	23,71	23,72	23,95	23,58	23,52	23,38
TOTAL	97,94	99,22	98,48	98,51	97,87	97,87	99,27
Recalculated as cations per 25 oxygens							
Si	6,004	6,050	6,023	5,979	6,004	5,992	5,955
Al	4,165	4,081	4,178	4,149	4,161	4,149	4,177
Fe	1,709	1,814	1,735	1,786	1,773	1,769	1,833
Mn	0,020	0,024	0,024	0,028	0,024	0,034	0,035
Ca	4,152	4,022	4,047	4,099	4,055	4,036	3,955
SUM	16,049	15,991	16,008	16,041	16,017	15,979	15,955

	IWJ77b	IWJ77c	IWJ78a	IWJ78b	IWJ78c	IWJ92a	IWJ92b
SiO_2	38,14	37,54	37,60	38,63	37,33	37,78	37,53
Al_2O_3	22,21	22,10	21,60	21,54	21,73	22,44	21,50
Fe_2O_3	15,41	15,27	14,76	13,95	14,35	14,04	14,64
MnO	0,28	0,21	0,21	0,24	0,22	0,47	0,45
CaO	23,96	24,04	24,00	23,82	23,79	23,52	23,40
TOTAL	100,00	99,16	98,17	98,18	97,42	98,30	97,51
Recalculated as cations per 25 oxygens							
Si	6,000	5,963	6,026	6,156	6,020	6,021	6,047
Al	4,118	4,138	4,080	4,046	4,130	4,215	4,083
Fe	1,824	1,825	1,780	1,673	1,741	1,690	1,774
Mn	0,034	0,025	0,026	0,029	0,027	0,057	0,055
Ca	4,038	4,091	4,121	4,067	4,111	4,016	4,039
SUM	16,013	16,043	16,032	15,970	16,030	15,998	15,998

5. GEOCHEMISTRY OF THE LAVAS

5.1 Introduction

Whole-rock analyses for sixty three basic volcanic rocks from the Dordabis Formation are presented in Table 5 and Appendix 3. These include twenty samples from the Opdam Member and forty three samples from the Bitterwater Member which are represented on the diagrams by closed and open circles respectively. The analyses were performed using X-ray fluorescence spectrometry. Details of analytical techniques are given in Appendix 2 and sample locations are provided in Plans 1 and 2.

In geochemical studies of metamorphosed lavas it is essential to differentiate between the effects of alteration, as opposed to primary petrogenetic processes, on the compositional variation in a suite of lavas. The following chapter therefore deals in detail with chemical variation due to alteration.

5.2 Assessment of Alteration

5.2.1 General statement

Chemical alteration is regarded as any process that changes the original chemical composition of a rock. Metamorphism is usually considered to be isochemical, except with respect to volatile components such as H_2O and CO_2 (Winkler, 1979). However, element mobility is common in low grade metabasic rocks (Floyd, 1976; Coish, 1977; Beswick and Soucie, 1978). It is difficult to determine whether this alteration is due to metamorphism because the rocks have often also been sheared, metasomatised, weathered and have reacted with ground water.

Primary chemical variations are present in lavas due to magmatic differentiation, while secondary chemical variations due to alteration can be superimposed on primary variations. It is therefore essential to distinguish between alteration and differentiation trends by determining the mobility of the elements analysed. The Dordabis lavas have been sheared, folded, metamorphosed to greenschist facies, uplifted, and sub-aerially weathered. It is therefore possible that these metalavas have been chemically altered. This section evaluates the degree of

alteration with respect to volatile content, oxidation, and major and trace element concentrations.

5.2.2 Sample selection for analytical work

Samples of lava flows were selected for analysis on the basis of their appearance in handspecimen and after thin section examination. Metabasalts containing abundant veins or stringers of silica, chlorite and epidote were avoided. Alteration is not necessarily detectable in thin section or handspecimen and can result in significant chemical changes in the rock which need to be evaluated.

5.2.3 Volatile content

Volatile content was determined as loss on ignition (L.O.I.) by ashing the samples at 1000°C for about eight hours. Over 80% of the L.O.I. values range between 2% and 4%, although L.O.I. values up to 11,1% were recorded for some samples (see Fig. 20).

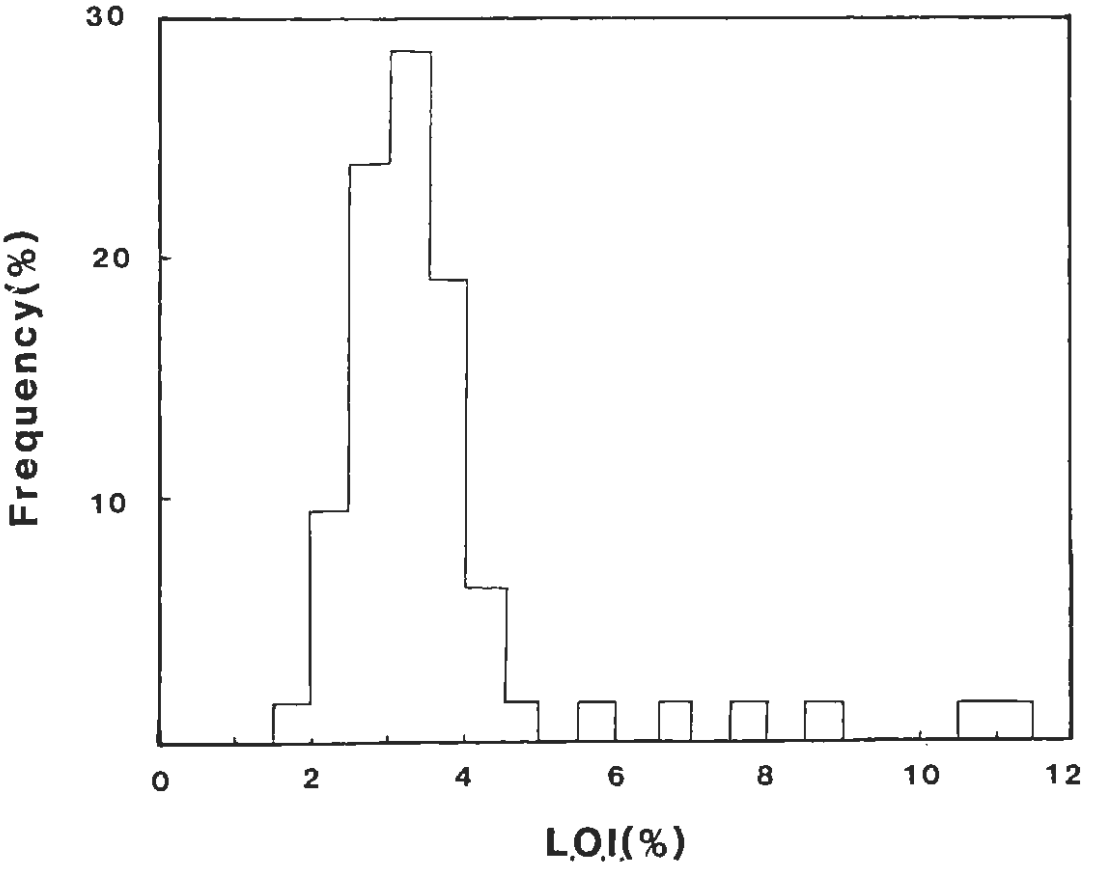

Figure 20 Frequency histogram illustrating the range in L.O.I. of the Dordabis Formation lavas

During the ashing of metabasalts the samples lose weight, by releasing volatiles (mainly H_2O^+ and minor CO_2), but gain weight by oxidation of FeO to Fe_2O_3. L.O.I. is therefore a net weight difference and is only a crude measure of the true volatile content. Although the L.O.I. of the Dordabis metalavas is higher than that of unaltered continental tholeiites, there is no way of knowing by how much the water content increased during alteration. During greenschist facies metamorphism the water content of basaltic lavas increases due to the the crystallisation of hydrous minerals, such as chlorite, which contains 12% water, and epidote which contains 2% water (Jolly, 1972). Miyashiro et al. (1969) showed that weathering also increases the water content of basalts. Unaltered continental tholeiites usually contain less than 1% volatiles, but as the Dordabis lavas have been metamorphosed to greenschist facies, it is understandable that samples have L.O.I. contents up to 11,1%.

There is some controversy as regards the use of water content of metalavas as a criterion for progressive alteration (discussed in 5.2.5). The Dordabis metalavas show no marked element variation with progressive hydration indicating that their volatile content is not directly related to any secondary chemical variation. Based on this uncertainty, geochemical analyses with higher volatile contents have not been rejected.

5.2.4 Bulk Fe_2O_3/FeO ratio

An estimate of the Fe_2O_3/FeO ratio is important, because it influences the C.I.P.W. norm. As the Fe_2O_3 content of a rock is tedious to measure using chemical techniques, and it is impossible to know how closely the measured Fe_2O_3/FeO in the rock reflects this ratio in the magma, various indirect methods of calculating Fe^{3+}/Fe^{2+} are discussed in this section. Irvine and Baragar (1971) have suggested that maximum $\%Fe_2O_3 = \%TiO_2 + 1,5$. Le Maitre (1976) suggests the use of a mean rather than a maximum oxidation value for volcanic rocks to be calculated by the formula:-

$$FeO/(FeO + Fe_2O_3) = 0,93 - 0,0042SiO_2 - 0,022(Na_2O + K_2O)$$

Le Maitre's (op. cit.) method used to calculate the ratio is rejected as Na_2O, K_2O and SiO_2 are thought to have been mobile in the Dordabis

metalavas (see section 5.2.5). Although TiO_2 is relatively immobile, Botha (1980) has shown that Irvine and Baragar's (op. cit.) maximum Fe_2O_3 value does not provide a close approximation of the primary Fe_2O_3 value in epidote/clinozoisite-rich and chlorite-rich zones in Witwatersrand triad metalavas. Since the Dordabis metalavas also contain epidote-rich and chlorite-rich zones this method of determining Fe_2O_3/FeO ratios has also been rejected. Ferric/ferrous ratios can be designated for various rock types. It is generally now accepted that the Fe_2O_3/FeO ratio in tholeiitic basaltic magmas lies in the range 0,1 to 0,2 (Brooks, 1976). The norms of the Dordabis metalavas were calculated using a value of 0,2 for this ratio.

5.2.5 Indexing the mobility of trace and major elements

It is essential to index the mobility of trace and major elements in the metalavas to determine whether geochemical trends are the result of primary or secondary chemical variation.

To illustrate the effect shearing has on the chemical composition of a rock, both highly sheared and unsheared parts of a single lava flow were sampled on the farm Grasvlakte. The sheared sample, IWJ68, is a lime-green mylonite and exhibits a crude foliation which anastomoses around scattered quartz porphyroblasts ranging in size from 1 to 3mm (Fig. 8L). The unsheared sample, IWJ69, is a fine-grained, blastophitic, dark purple-grey metabasalt.

Primary processes like within-flow differentiation usually result in limited variations in chemistry within a single lava flow. The larger differences in the chemical compositions of samples IWJ68 and IWJ69 are regarded as being the result of shearing.The most obvious difference (Appendix 3) is the apparent absolute loss of about 3,7% SiO_2 and the 5,8% gain in CaO in the mylonite. During shearing some SiO_2 is freed from the main mineral phases and leached away or recrystallised as quartz veins or as free quartz grains. Shearing has resulted in K_2O, Na_2O and Rb decreasing to close to zero while Sr and Cu have increased dramatically in the mylonite. TiO_2, P_2O_5, MnO, Ba, Y, Zr, Nb, Zn, Ni, Sc, La, Ce and Nd contents have not been significantly affected by the shearing. This example indicates that shearing can cause substantial mobility of SiO_2, K_2O, Na_2O, CaO, Rb, Sr and Cu.

Zirconium has been shown to be relatively immobile during shearing (see previous paragraph) and also during regional or ocean floor greenschist

facies metamorphism of basaltic rocks (Cann, 1970; Pearce and Cann, 1971; Floyd, 1976; Coish, 1977). It is however also very sensitive to igneous processes like fractional crystallisation or partial melting. Thus in a suite of differentiated metabasalts immobile elements exhibit rational variation trends, whereas mobile elements vary erratically when plotted against Zr (Wood et al., 1976 and Coish, 1977). Figures 30A to J and 31A to O show variations in major and trace element concentrations in relation to Zr contents for the Dordabis metalavas. SiO_2, K_2O, Na_2O, CaO, Rb, Sr, Cu, Ba, Co and Sc show no systematic variation trends, probably because they have been mobile. MgO, Al_2O_3, total iron, Zn and V have been mobile to a lesser extent and do not exhibit well-defined trends. In contrast TiO_2, P_2O_5, Y, Nb, Cr, Ni, La, Ce and Nd show well-defined variation trends and thus can be considered as immobile. Pearce and Norry (1979) have explained the stability of Ti, Zr, Nb and Y in terms of their high field strength (charge/radius ratio). Coish (1977) also found that TiO_2, P_2O_5, Y, Cr, Zr and Ni remain stable during metamorphism. Floyd (1976) has compared the composition of similar but progressively more altered (spilitised) greenstones. In order to estimate the effect of secondary chemical variation he plotted various elements against H_2O^+, the latter being regarded as an index of alteration. Floyd (op. cit.) found that although variable, CaO, Sr, K, Rb and Ba show a general decrease, while Na_2O shows a wide scatter and a small increase in basaltic rocks with progressive hydration. His study also illustrated that Co, Cr, Ni, Li, Cu, Rb and Zn show no marked variation with progressive hydration. The Dordabis metalavas show no significant element variation when plotted against L.O.I, although Na_2O and SiO_2 exhibit an ill-defined negative correlation with L.O.I. (Figs. 21A & B).

Beswick and Soucie (1978) used a graphical procedure whereby chemical data for a suite of metavolcanic rocks may be tested to detect and correct for metasomatic modifications of individual sample compositions. The assumptions initially made are that Al_2O_3 remains immobile during alteration, and that the altered rocks initially had compositions which would conform with well-defined trends shown to be present in relatively unaltered post-Mesozoic suites. Their method involved plotting the analytical data in terms of oxide molecular proportion ratios in the form log X/Z versus log Y/Z, where X, Y and Z are molecular proportions. On such a plot 'X' metasomatism will cause an original composition to be displaced parallel to the log X/Z axis, 'Y' metasomatism will cause displacement parallel to the log Y/Z axes and 'Z' metasomatism will displace the original composition along a 45° positively sloping line. A

unique solution for a suite of metamorphosed lavas can only be obtained by using a set of such diagrams. K_2O is used as the ratioing oxide Z, because it largely remains in the liquid phase during early and middle stages of fractionation, prior to the crystallisation of alkali feldspar.

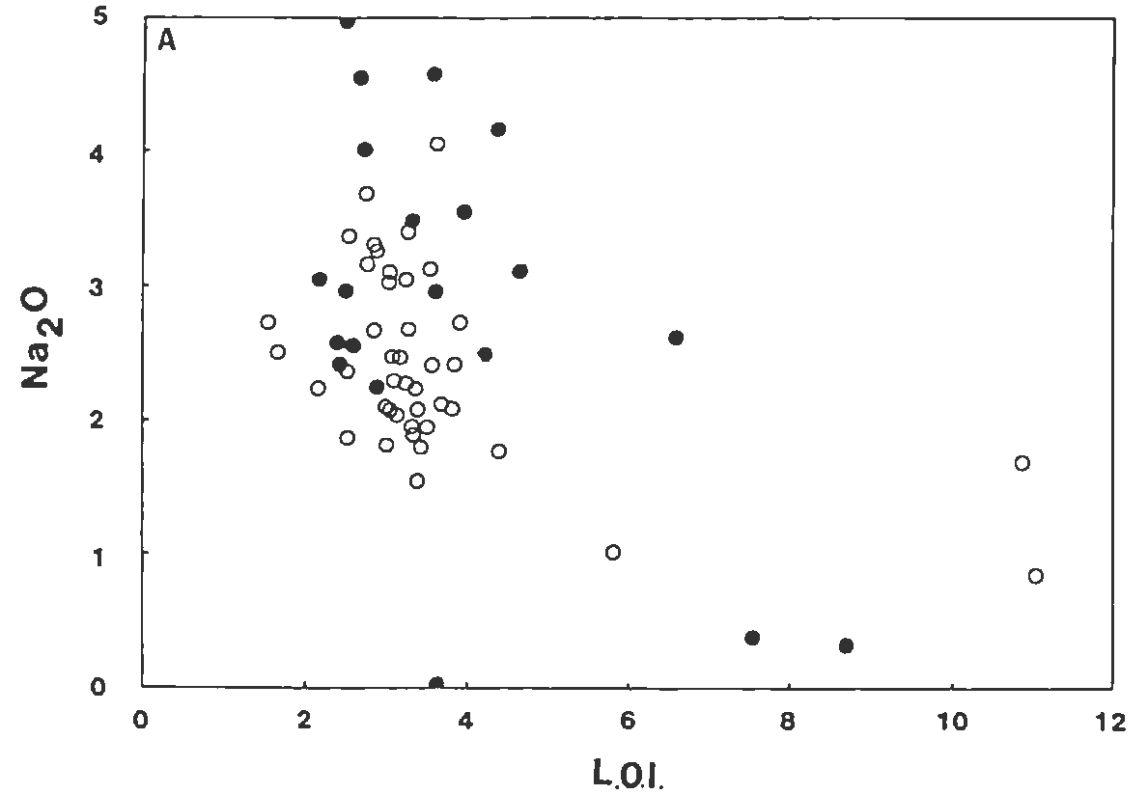

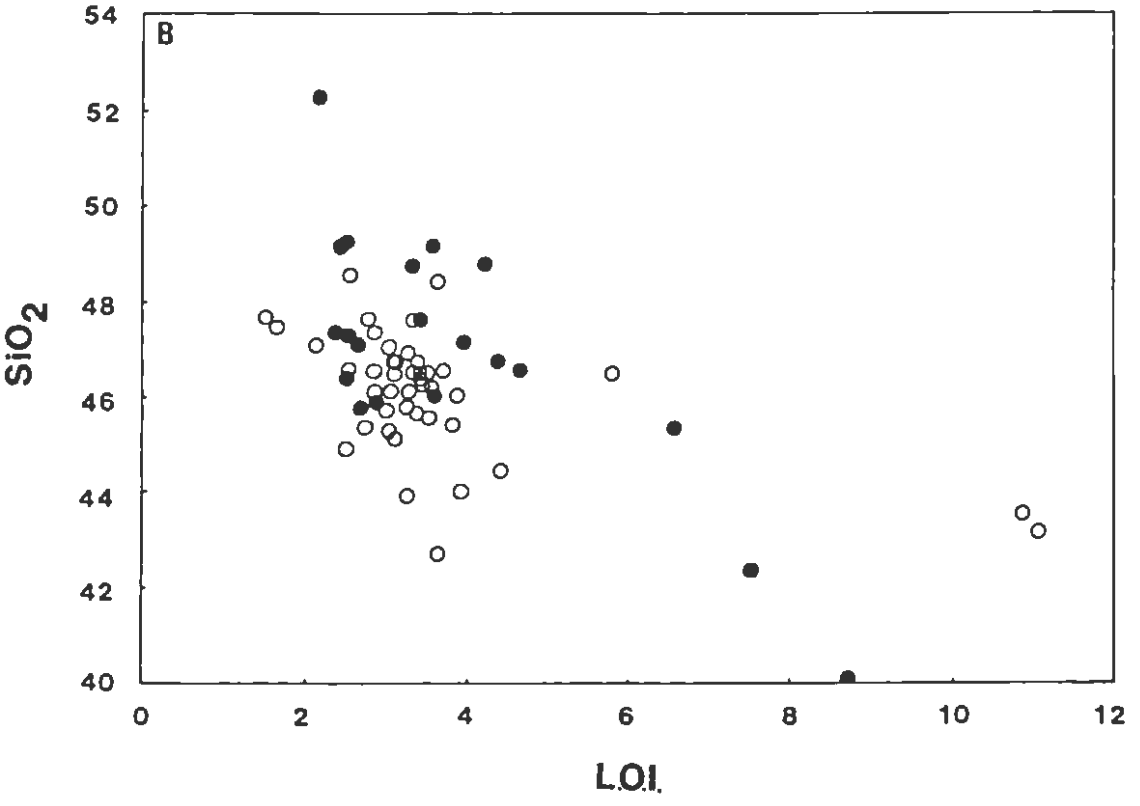

Figure 21A Plot of Na_2O versus L.O.I. for the Dordabis lavas
B Plot of SiO_2 versus L.O.I. for the Dordabis lavas (● Opdam basalts, ○ Bitterwater basalts).

In applying this method to the Dordabis lavas it must be realised that the Zr versus Al_2O_3 plot (Fig. 30C) indicates that Al_2O_3 may be slightly mobile. If this is the case an initial assumption is not met. It must also be recognised that the lavas used by Beswick and Soucie (op. cit.) were oceanic basalts and hence differ compositionally from the Dordabis suite which are shown to be continental tholeiites (see section 5.3). This method has therefore been used qualitatively to demonstrate chemical alteration. The preceding discussion has shown that SiO_2 is much more mobile than Al_2O_3 in the Dordabis metalavas. Figures 22A and B illustrate that the Dordabis metalavas are SiO_2 and CaO-deficient and perhaps slightly enriched in Al_2O_3. This results in the average Dordabis metalava plotting along the unaltered post-Mesozoic trend on the log CaO/K_2O versus log SiO_2/K_2O graph (Fig. 22C). Low ratios in Figure 22C and in Figure 22D plot off the post-Mesozoic trend on a line with a 45° slope, indicating possible mobility of K_2O. The Dordabis metalavas plot close to the post-Mesozoic trend on the log SiO_2/K_2O and log CaO/K_2O versus log Fm/K_2O (Figures 22D & E), indicating possible Fm (sum of the molecular proportions of total FeO, MgO and MnO) depletion if the metalavas are depleted in SiO_2 and CaO.

Figure 22(A to E) Plot of the logarithms of the major oxide molecular proportion ratios (after Beswick and Soucie, 1978).

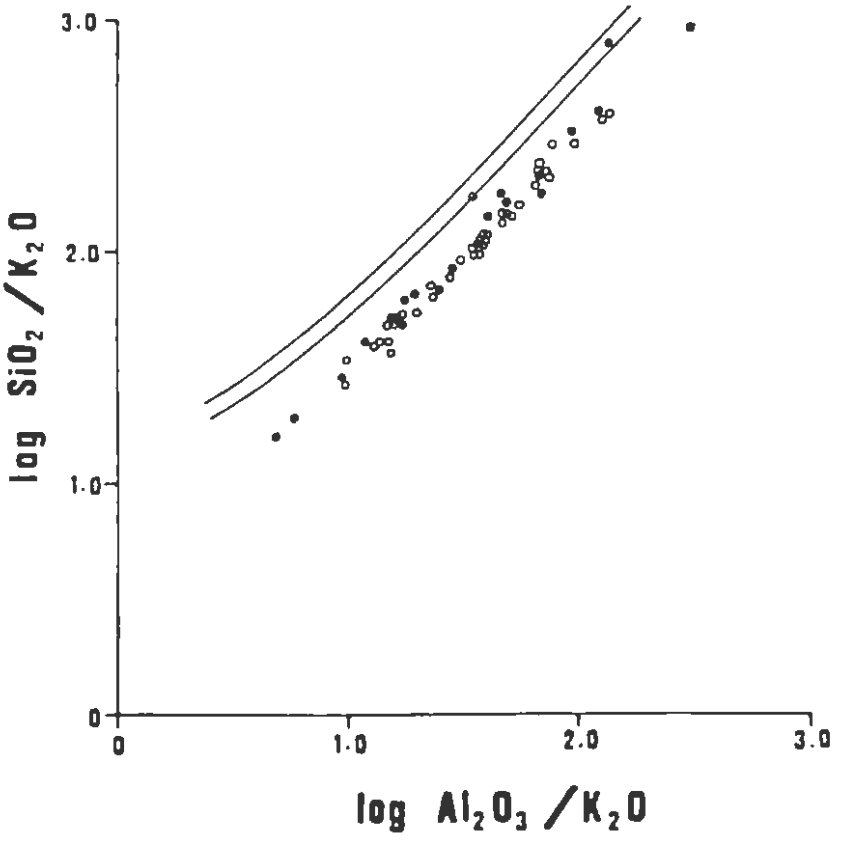

Figure 22A

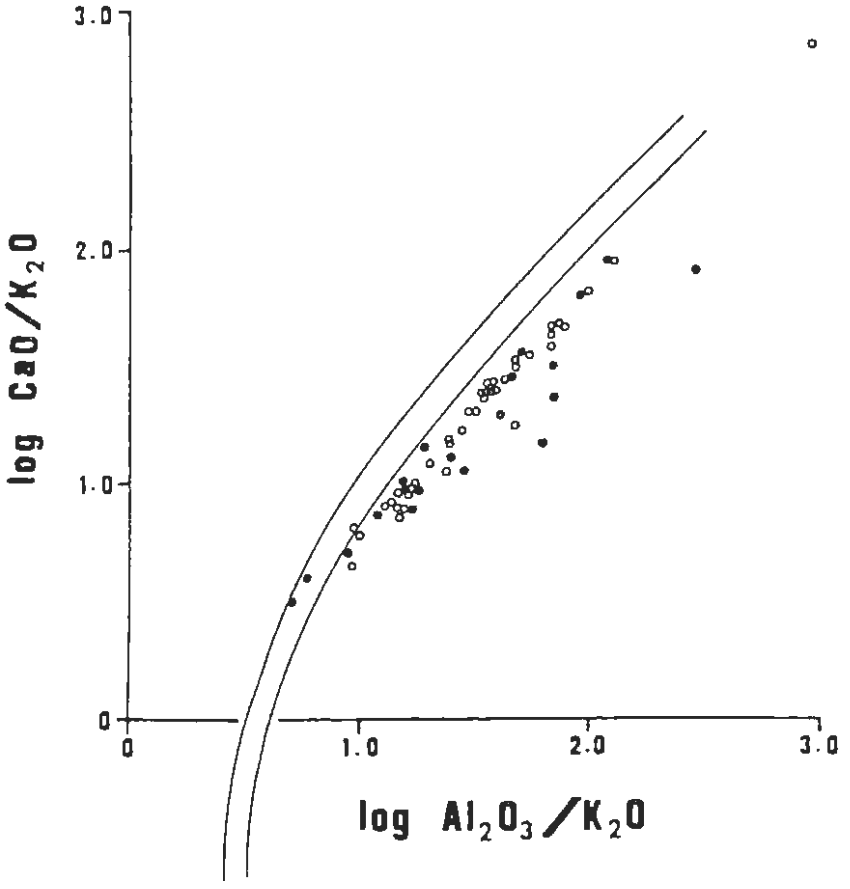

Figure 22B

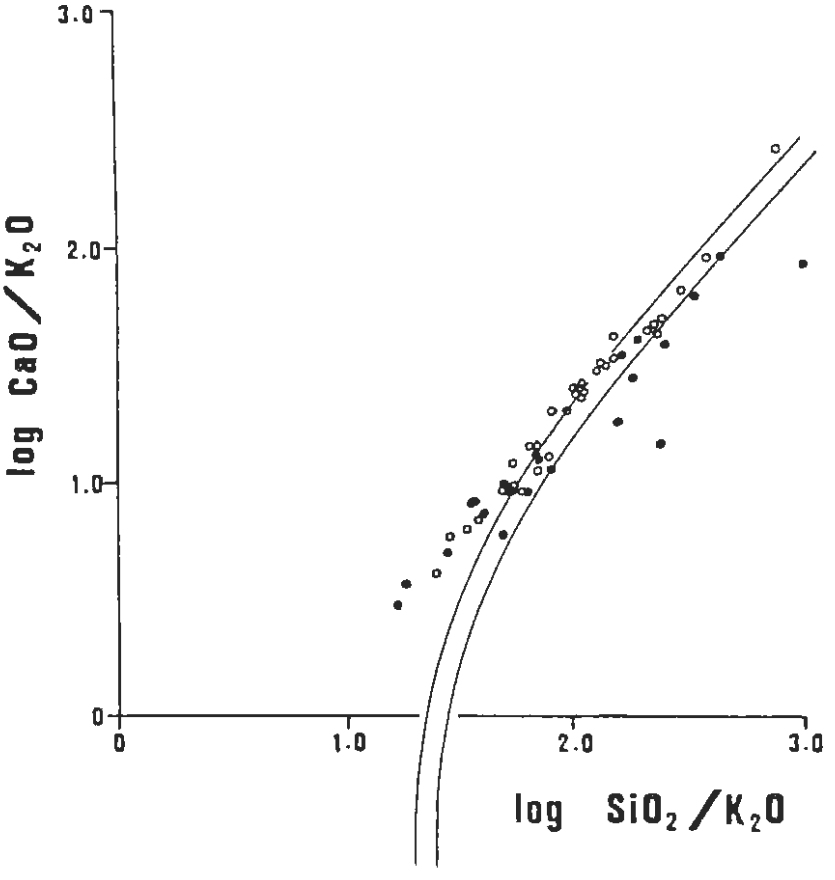

Figure 22C

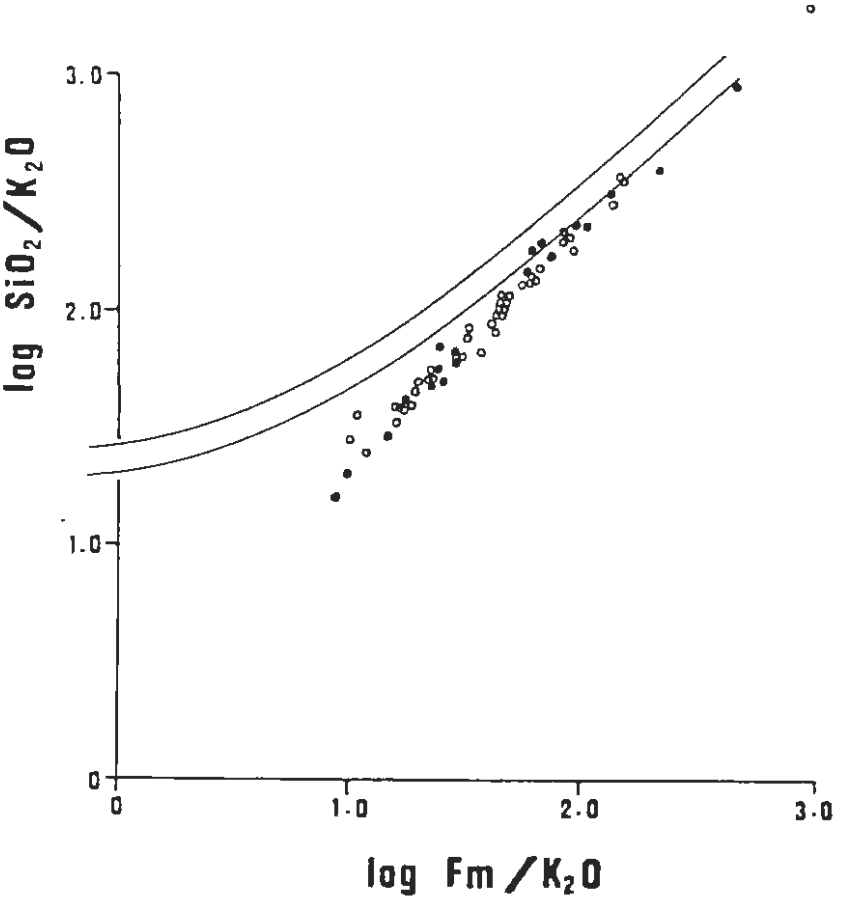

Figure 22D

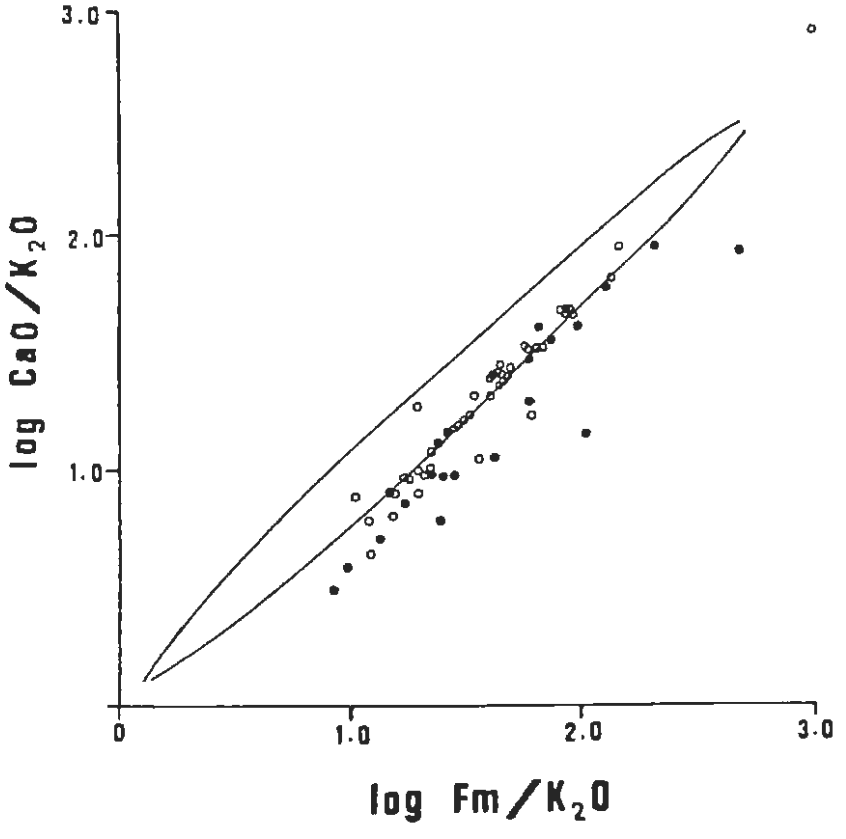

Figure 22E

Having used a number of approaches to discuss element mobility in the Dordabis Formation metavolcanics, it is now possible to construct a table classifying various elements in terms of their relative mobilities during greenschist facies metamorphism (Table 4).

TABLE 4 Index of element mobility in the Dordabis Formation metavolcanics

Mobile elements		Partially mobile elements		Immobile elements	
Na_2O	Ba	SiO_2	Zn	TiO_2	Nb
K_2O	Rb	Al_2O_3	Cu	P_2O_5	Y
CaO	Sr	Fe_2O_3	Ni		Zr
	Co	MnO	Cr		La
	Sc	MgO	V		Ce
					Nd

Alteration during greenschist facies metamorphism, shearing and sub-aerial weathering does not seem to result in uniform enrichments or depletions in any elements, (especially trace elements) but rather tends to produce non-proportional variation in the concentrations of mobile elements. Silica may be an exception to this rule. Beswick and Soucie's (1978) graphical procedure indicates that the Dordabis lavas are generally depleted in SiO_2, which is possible considering the sheared nature of many of the metalavas, especially in the Opdam Member.

TABLE 5 MAJOR AND TRACE ELEMENT ANALYSES NORMALISED TO 100% FREE OF VOLATILES

Opdam Member

	IWJ143	IWJ145	IWJ146	IWJ147	IWJ148	IWJ149	IWJ150	IWJ151	IWJ152	IWJ153	IWJ2	IWJ3	IWJ4	IWJ5
SiO_2	54,32	48,42	47,78	50,30	46,22	44,37	49,26	47,44	49,12	48,72	49,77	47,81	48,13	49,36
TiO_2	0,89	1,94	4,40	1,55	4,13	4,16	2,03	2,53	2,20	2,25	1,69	2,07	2,42	2,91
Al_2O_3	14,22	14,49	13,13	14,52	14,08	14,29	14,05	14,82	14,45	14,41	14,68	15,08	15,35	15,52
Fe_2O_3	10,99	13,79	18,11	12,88	18,07	19,07	15,60	17,19	15,20	15,84	11,75	15,02	15,69	14,98
MnO	0,18	0,20	0,20	0,20	0,27	0,24	0,20	0,24	0,19	0,20	0,16	0,21	0,17	0,23
MgO	7,08	7,54	5,41	6,96	4,99	5,50	6,97	5,74	5,96	5,08	7,75	6,48	6,60	8,43
CaO	8,80	10,61	10,28	9,74	8,92	18,62	7,60	8,50	18,73	9,43	10,87	8,37	5,78	4,50
Na_2O	3,15	2,60	0,00	3,58	0,41	0,35	3,29	2,31	2,66	2,81	2,42	3,05	4,63	3,70
K_2O	0,30	0,29	0,11	0,15	2,42	2,87	0,80	0,93	1,22	0,95	0,77	1,67	0,94	0,05
P_2O_5	0,07	0,12	0,57	0,13	0,49	0,52	0,20	0,30	0,28	0,32	0,12	0,24	0,29	0,30
TOTAL	100,00	100,00	100,00	100,00	100,00	100,00	100,00	100,00	100,00	100,00	100,00	100,00	100,00	100,00
Ba	0	105	52	42	532	555	130	363	440	347	200	396	267	41
Rb	5,8	12,6	6,1	2,5	78,7	86,4	29,7	31,4	35,0	35,2	30,2	56,7	30,6	1,6
Sr	133	188	188	172	101	130	182	290	268	269	175	275	239	106
Y	18,8	28,4	67,9	29,8	67,8	67,6	31,8	48,6	41,5	40,9	24,3	36,1	38,9	46,1
Zr	52	82	359	95	328	325	122	212	183	183	81	155	174	209
Nb	2,1*	4,1	31,0	6,2	26,2	25,5	7,4	13,5	14,5	14,0	7,1	9,3	13,3	15,7
Zn	99	133	179	123	192	207	154	189	153	139	110	131	139	228
Cu	177	102	414	142	371	453	160	160	121	173	92	73	126	187
Ni	101	108	135	111	157	166	154	151	159	156	141	179	187	137
Co	54	68	64	55	66	72	70	74	67	61	58	68	70	78
Cr	139	59	105	164	127	99	186	96	114	144	311	177	137	128
V	221	312	351	291	390	422	345	329	279	276	278	289	300	408
Sc	37	46	36	45	45	45	51	40	36	36	41	37	36	47
La	1*	8*	26	2*	26	24	5*	18	18	14	7*	13	14	8*
Ce	21	28	102	35	132	99	28	78	67	67	23	65	29	38
Nd	12	23	71	22	79	75	25	46	44	43	19	39	-	32

* Concentrations below determination limits

TABLE 5 (continued)

	Opdam Member						Bitterwater Member							
	IWJ6	IWJ7	IWJ8	IWJ9	IWJ10	IWJ11	IWJ12	IWJ13	IWJ14	IWJ15	IWJ16	IWJ17	IWJ19	IWJ20
SiO_2	49,38	49,15	51,82	51,29	51,37	47,62	47,11	48,06	47,98	46,85	48,36	49,28	48,60	47,92
TiO_2	1,93	1,95	2,19	2,71	1,73	1,55	1,15	1,18	1,21	0,70	1,11	1,22	1,12	1,40
Al_2O_3	17,23	17,72	14,22	13,84	14,89	16,02	15,46	17,34	16,64	16,78	17,40	16,51	16,89	16,28
Fe_2O_3	12,75	13,12	14,46	16,70	12,89	16,92	16,71	11,21	12,10	10,72	11,14	11,15	11,30	11,03
MnO	0,17	0,19	0,20	0,18	0,18	0,16	0,16	0,18	0,18	0,16	0,17	0,14	0,14	0,15
MgO	4,05	3,74	5,29	6,38	7,58	6,45	7,30	8,02	7,63	11,54	7,88	7,45	8,34	9,05
CaO	9,15	10,55	6,42	3,22	8,39	6,37	7,54	10,17	11,21	11,06	11,48	11,78	11,12	10,67
Na_2O	4,40	3,05	4,82	5,17	2,61	4,18	3,81	3,11	2,50	1,87	2,15	1,94	2,19	2,71
K_2O	0,70	0,25	0,34	0,22	0,21	0,56	0,66	0,62	0,43	0,24	0,23	0,42	0,22	0,71
P_2O_5	0,25	0,28	0,25	0,29	0,15	0,18	0,10	0,12	0,12	0,07	0,10	0,10	0,09	0,09
TOTAL	100,00	100,00	100,00	100,00	100,00	100,00	100,00	100,00	100,00	100,00	100,00	100,00	100,00	100,00
Ba	214	92	147	103	70	208	218	171	187	124	63	155	77	146
Rb	21,8	7,9	11,9	6,5	4,6	19,7	23,4	15,4	9,9	5,7	5,6	9,9	6,6	22,3
Sr	228	447	164	88	225	184	336	262	227	223	196	209	197	219
Y	32,8	34,1	47,5	43,8	23,2	31,3	22,9	20,6	21,9	13,7	18,6	18,6	19,9	20,4
Zr	143	146	183	195	86	106	64	67	69	35	56	53	63	60
Nb	10,6	11,4	12,7	15,7	6,3	8,3	2,1*	2.1*	3,1	2.1*	3,1	4,1	4,2	3,1
Zn	135	117	150	177	117	144	104	108	107	90	91	90	91	92
Cu	70	413	533	149	389	73	173	41	101	22	106	81	49	45
Ni	104	86	107	138	174	137	177	167	204	387	182	180	234	218
Co	55	47	56	69	60	62	55	58	65	72	57	54	63	57
Cr	58	52	87	116	225	211	425	309	306	440	379	374	372	327
V	238	237	376	346	219	299	280	237	268	172	225	227	224	217
Sc	28	25	52	49	29	38	41	36	38	29	34	35	32	32
La	9	14	14	14	1*	32	1*	3*	4*	3*	6*	3*	1*	3*
Ce	53	63	51	73	18	18	23	28	26	15	11*	20	22	20
Nd	33	35	37	44	16	22	17	21	20	13	17	11	14	10

* Concentrations below determination limits

TABLE 5 (continued)

Bitterwater Member

	IWJ21	IWJ49	IWJ50	IWJ51	IWJ52	IWJ53	IWJ54	IWJ56	IWJ57	IWJ58	IWJ59	IWJ60	IWJ61	IWJ62
SiO_2	48,04	50,87	48,04	49,40	45,57	47,46	46,92	46,50	48,76	48,71	48,30	47,99	47,91	47,89
TiO_2	1,09	1,31	1,16	1,47	1,23	1,28	1,19	1,19	1,15	1,04	1,11	1,14	1,33	1,30
Al_2O_3	16,97	16,03	17,04	15,69	16,91	16,79	17,26	17,92	17,46	17,07	16,92	16,87	16,42	16,82
Fe_2O_3	11,24	11,63	11,55	12,46	11,39	11,48	11,29	12,00	10,95	10,58	11,56	11,19	11,60	11,67
MnO	0,14	0,18	0,15	0,20	0,17	0,16	0,17	0,16	0,16	0,15	0,15	0,16	0,16	0,19
MgO	8,62	8,85	8,31	7,36	8,53	6,83	8,69	9,32	7,25	7,86	8,16	8,69	8,92	8,02
CaO	9,80	6,40	10,82	9,09	12,47	11,86	11,80	8,07	9,55	10,42	9,29	10,32	9,35	9,99
Na_2O	2,29	4,26	2,51	3,26	3,14	3,48	2,13	2,87	3,38	2,76	3,37	2,50	3,20	2,76
K_2O	1,70	0,35	0,30	0,91	0,48	0,57	0,46	1,86	1,22	1,29	1,02	1,04	0,97	1,23
P_2O_5	0,11	0,13	0,12	0,16	0,10	0,09	0,09	0,11	0,12	0,10	0,12	0,11	0,15	0,13
TOTAL	100,00	100,00	100,00	100,00	100,00	100,00	100,00	100,00	100,00	100,00	100,00	100,00	100,00	100,00
Ba	281	122	86	243	106	195	107	204	144	373	145	129	186	196
Rb	53,9	11,2	6,8	26,6	14,1	14,4	12,3	58,2	37,5	27,6	29,1	29,9	28,5	38,7
Sr	210	225	259	263	378	253	216	175	286	185	224	191	189	209
Y	20,7	24,2	20,9	24,9	20,8	19,6	18,7	21,2	19,6	18,4	18,7	17,5	23,9	21,8
Zr	64	76	64	90	57	57	60	68	59	52	57	57	81	69
Nb	3,1	4,2	2.1*	2,1*	4,2	2,1*	2,1*	2,1*	3,1	2,0*	2,1*	4,1	4,2	5,2
Zn	91	118	109	107	103	90	104	116	93	92	90	86	104	107
Cu	45	40	29	45	26	79	34	24	39	26	25	28	26	28
Ni	234	154	183	147	228	178	177	246	140	184	236	233	220	172
Co	60	63	60	60	66	58	60	69	54	59	61	61	65	62
Cr	273	354	340	283	404	371	371	374	326	390	407	352	324	296
V	243	260	240	299	259	244	248	255	250	231	242	224	264	266
Sc	36	41	38	43	42	38	39	36	37	36	36	35	36	43
La	2*	5*	8*	0*	0*	-	7*	4*	5*	2*	2*	1*	4*	1*
Ce	34	21	13	29	5*	-	12*	14	-	17	17	21	29	19
Nd	18	18	15	24	35	-	14	15	23	12	13	11	22	18

* Concentrations below determination limits

TABLE 5 (continued)

Bitterwater Member

	IWJ64	IWJ89	IWJ88	IWJ87	IWJ86	IWJ85	IWJ84	IWJ83	IWJ82	IWJ79	IWJ68	IWJ69	IWJ70	IWJ71
SiO_2	49,99	47,15	49,17	47,37	47,59	47,19	49,40	48,91	48,90	48,18	44,40	47,88	48,38	47,18
TiO_2	1,21	1,20	1,06	1,15	1,10	1,21	1,19	1,17	1,17	1,11	1,13	1,15	1,09	1,11
Al_2O_3	15,13	17,11	16,47	17,29	17,49	17,50	17,35	17,17	17,78	17,07	17,28	16,57	16,71	17,25
Fe_2O_3	11,02	11,66	11,07	11,65	11,08	11,26	11,09	11,03	11,79	10,84	12,31	11,35	11,22	11,53
MnO	0,17	0,15	0,13	0,16	0,16	0,15	0,14	0,14	0,13	0,16	0,17	0,16	0,16	0,15
MgO	8,32	8,89	8,60	8,72	8,50	8,74	7,53	7,44	9,27	8,17	7,47	9,16	8,65	8,44
CaO	10,49	11,10	11,15	11,61	10,77	11,12	12,02	12,00	8,67	11,43	17,07	10,99	11,25	11,73
Na_2O	3,44	2,14	1,89	1,59	2,34	1,99	1,05	1,88	0,94	2,53	0,03	2,10	1,99	2,15
K_2O	0,22	0,47	0,34	0,33	0,88	0,73	0,13	0,13	1,22	0,41	0,02	0,52	0,44	0,35
P_2O_5	0,11	0,12	0,12	0,13	0,11	0,11	0,12	0,11	0,11	0,11	0,12	0,12	0,11	0,12
TOTAL	100,00	100,00	100,00	100,00	100,00	100,00	100,00	100,00	100,00	100,00	100,00	100,00	100,00	100,00
Ba	62	139	106	95	271	182	18	77	205	144	138	143	96	97
Rb	4,9	9,2	7,1	7,5	21,4	17,5	2,1	5,6	40,3	10,0	2,1	13,7	8,5	9,7
Sr	329	200	185	199	175	189	217	216	56	175	591	229	179	211
Y	20,6	19,6	18,1	20,8	17,7	20,7	19,1	22,5	17,0	18,6	23,9	19,6	18,7	20,8
Zr	53	61	58	62	56	57	59	68	62	55	62	61	56	66
Nb	2,1*	2,1*	3,2	4,2	3,1	2,1*	4,3	4,5	2,3*	2,1*	2,1*	4,1	2,1*	5,2
Zn	104	95	91	99	92	99	95	83	102	95	100	96	99	96
Cu	29	59	34	112	30	30	53	25	253	34	926	47	51	30
Ni	164	243	231	243	200	192	164	184	163	168	337	345	228	232
Co	56	62	60	64	59	61	59	56	54	56	56	64	62	64
Cr	387	340	324	342	357	396	407	346	374	310	359	302	314	327
V	216	241	231	238	240	244	249	249	272	236	276	220	230	248
Sc	41	35	36	35	37	38	34	42	44	36	38	32	34	37
La	3*	3*	1*	5*	1*	1*	0*	4*	4*	2*	2*	3*	0*	6*
Ce	20	19	18	16	14	15	34	18	13	21	22	23	17	21
Nd	14	17	14	10	12	13	28	14	14	18	21	20	13	19

* Concentrations below determination limits

TABLE 5 (continued)

Bitterwater Member

	IWJ72	IWJ73	IWJ74	IWJ75	IWJ76	IWJ77	IWJ78
SiO_2	48,55	48,04	48,39	47,75	46,27	46,84	48,44
TiO_2	1,06	2,90	2,53	1,61	1,42	1,51	1,22
Al_2O_3	16,66	13,77	14,46	16,41	16,40	15,96	21,04
Fe_2O_3	10,97	16,12	16,08	12,08	12,28	12,71	9,19
MnO	0,15	0,22	0,19	0,17	0,17	0,18	0,13
MgO	8,61	5,82	5,48	8,04	8,54	18,93	4,85
CaO	11,60	9,15	9,04	10,88	12,42	11,19	10,36
Na_2O	1,86	2,27	2,54	2,41	1,91	2,36	3,25
K_2O	0,43	1,46	1,01	0,46	0,45	0,16	1,37
P_2O_5	0,11	0,24	0,30	0,19	0,15	0,16	0,16
TOTAL	100,00	100,00	100,00	100,00	100,00	100,00	100,00
Ba	107	398	298	133	199	67	352
Rb	11,2	40,9	30,6	10,4	13,1	3,4	38,2
Sr	193	158	208	209	195	167	354
Y	18,6	50,1	48,0	27,7	23,7	26,0	21,9
Zr	60	213	198	103	82	96	86
Nb	2,1*	17,4	13,3	7,2	5,2	5,2	6,3
Zn	96	162	151	113	103	114	91
Cu	37	95	204	106	127	73	47
Ni	279	130	143	233	249	238	109
Co	61	60	49	62	62	69	46
Cr	320	150	107	304	304	415	153
V	227	373	297	213	221	264	184
Sc	35	43	39	33	32	35	25
La	3*	21	18	10	-	10	*3
Ce	22	90	80	42	22	27	11
Nd	19	54	49	32	19	-	11

* Concentrations below determination limits

5.3 Classification

In this chapter an attempt is made to classify the Dordabis Formation lavas on the basis of chemical composition, as metamorphic recrystallisation has precluded any petrographic classification. During this century numerous chemical classifications of volcanic rocks using major elements, normative mineralogy, trace elements and cation contents have been proposed by various authors including Irvine and Baragar (1971), Winchester and Floyd (1977) and Jensen (1976).

The elaborate major element and normative mineralogy classification scheme of Irvine and Baragar (1971) involves the use of numerous diagrams to classify volcanic rocks. Irvine and Baragar (op. cit.) distinguish between alkaline and subalkaline volcanics by plotting alkalies against silica. Although widely scattered, most of the Dordabis lavas plot in the subalkaline field (Fig. 23A). Further classification by the plotting of normative plagioclase against Al_2O_3 content (Fig. 23B) shows that although most of the Dordabis lavas plot in the tholeiitic field, a

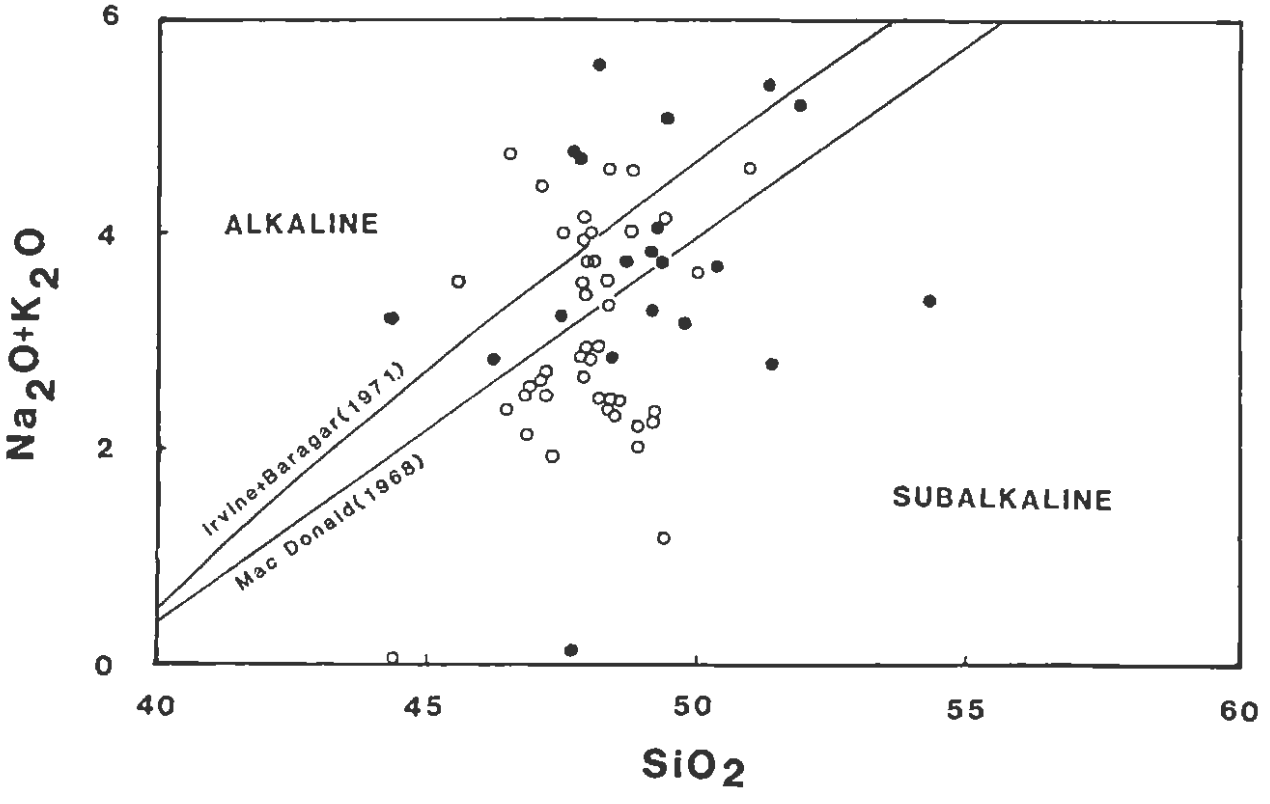

Figure 23A Alkalies versus silica diagram with dividing lines proposed by Irvine and Baragar (1971) and Mac Donald (1968). (Plots in weight percent)

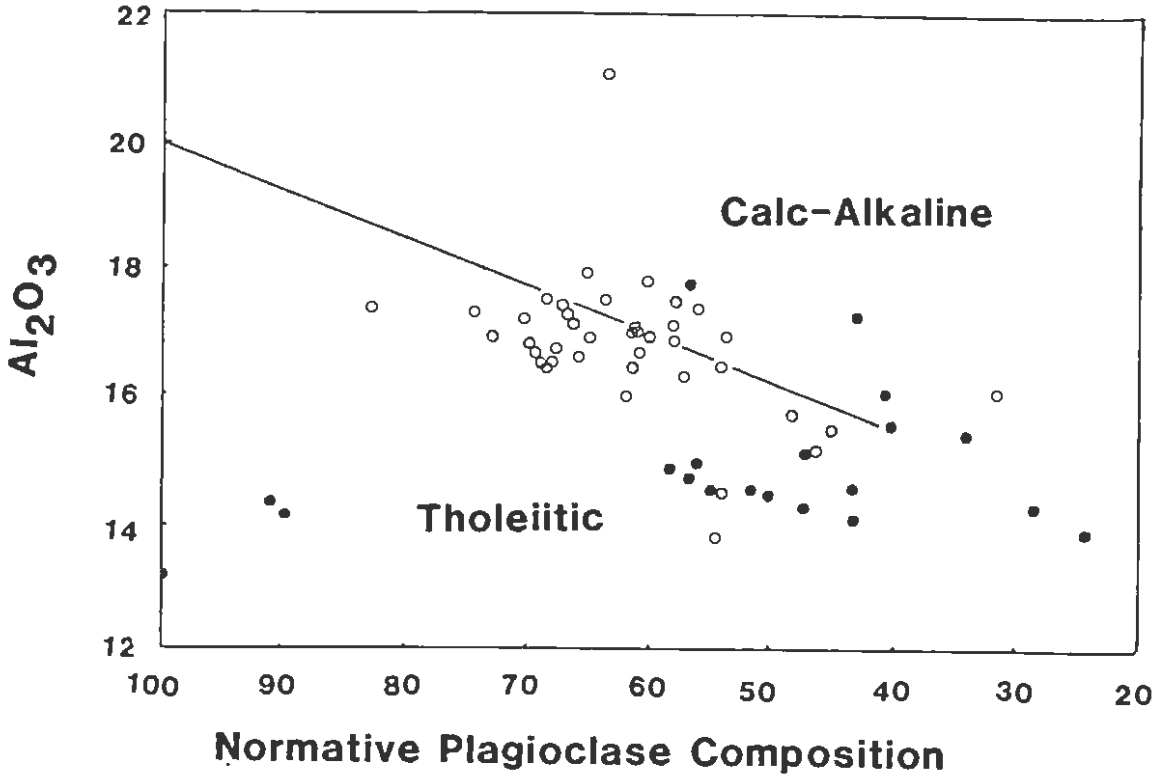

Figure 23B Al_2O_3 versus normative plagioclase composition plot for the Dordabis metalavas (after Irvine and Baragar, 1971).

number also plot in the calc-alkaline field. The extreme mobility of the alkalies and to a lesser extent CaO and SiO_2 mobility during alteration, result in the Dordabis metalavas being only partially successfully classified according to the Irvine and Baragar scheme. An AFM plot of the Dordabis lavas (Fig. 24) shows a distinct iron enrichment trend, which is characteristic of tholeiites.

A logical alternative classification would be to use immobile trace elements with fractionation tendencies that parallel those of the alkalies, MgO, FeO and CaO and display characteristic patterns for different volcanics.

Floyd and Winchester (1975) used plots of Nb/Y versus Zr/P_2O_5 (Fig. 25) to distinguish between oceanic tholeiites, continental tholeiities and alkali basalts. Although there is good separation between the alkali basaltic and tholeiitic fields, there is overlap between the oceanic and continental tholeiitic fields resulting in no meaningful separation between these two groups. The Dordabis lavas plot in the area of overlap between continental and oceanic tholeiitic basalts on Figure 25 and along the boundary between andesite/basalt field and sub-alkaline basalt field

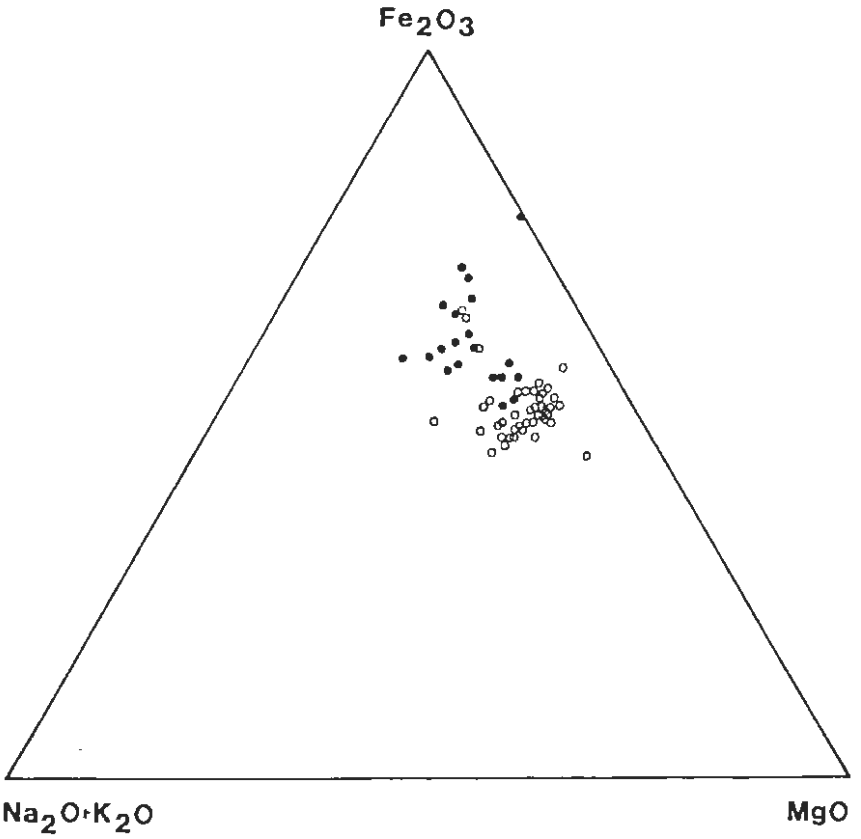

Figure 24 AFM diagram illustrating an iron enrichment trend in the Dordabis metabasalts

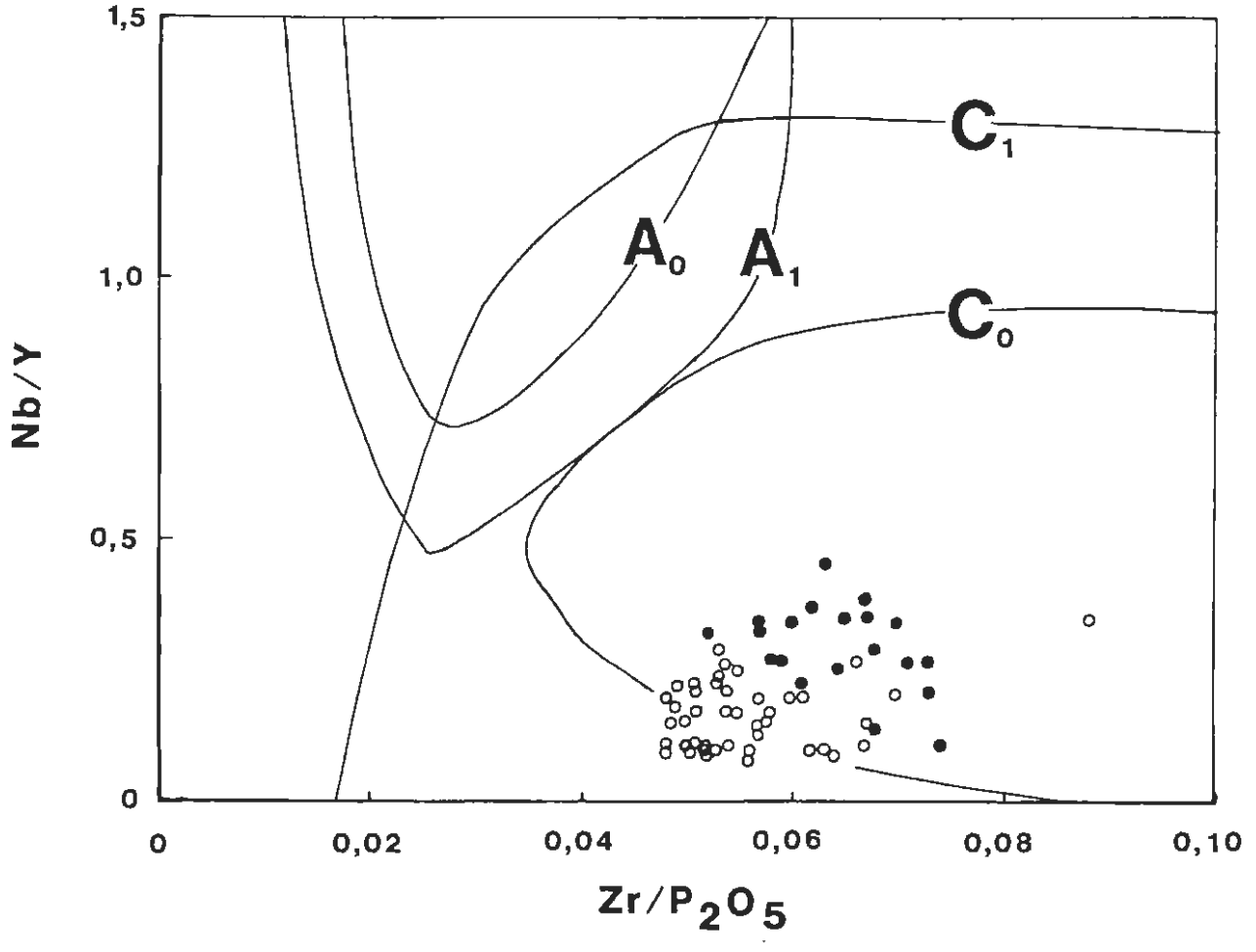

Figure 25 Nb/Y versus Zr/P_2O_5 discrimination diagram where oceanic alkali basalts are represented by fields enclosed by line A_0, continental alkali basalts by A_1, oceanic tholeiitic basalts by C_0 and continental tholeiitic basalts by C_1 (after Floyd and Winchester, 1975)

on the Winchester and Floyd's (1977) diagram (Fig. 26A). Winchester and Floyd's (op. cit.) Zr/TiO_2 versus Ce diagram (Fig. 26B) indicates that the Dordabis lavas are basalts rather than andesites. The classification scheme of Davies et al. (1979) provides a clear distinction between Archaean magnesian, tholeiitic and calc-alkaline suites. This classification scheme uses immobile trace-elements and although it is designed for altered Archaean volcanic rocks, it also provides a good separation between Proterozoic mafic volcanic magma types. The Opdam lavas all plot in the tholeiitic field, while most of the Bitterwater lavas plot in the transitional area between the tholeiitic and magnesian fields (Fig. 27).

Jensen (1976) proposed a cation plot as an alternative method for classifying subalkaline volcanic rocks, using the less mobile major elements Al_2O_3, $FeO+Fe_2O_3+TiO_2$ and MgO. On the Jensen cation plot (Fig. 28) arrows indicate komatiitic, tholeiitic and calc-alkalic trends and lines separate rock types. Figure 28 shows the strong iron enrichment trend exhibited by the Dordabis lavas, especially the Opdam member whose $FeO + Fe_2O_3 + TiO_2$ cation content increases from 23,3 to 36,7%. The Opdam Member lavas are mostly high-iron tholeiitic basalts, although a few samples plot in the high-magnesium tholeiitic and basalt fields. The Bitterwater Member lavas usually plot in the high-magnesium tholeiitic area, although a few more differentiated samples plot in the high-iron tholeiitic area.

Chemical classification schemes like that of Irvine and Baragar (1971) using mobile oxides such as Na_2O, K_2O, SiO_2 and CaO, and normative mineralogy are only partially successful in classifying the altered Dordabis metalavas. Alternative schemes using immobile trace elements suggest that the Dordabis lavas are tholeiitic basalts, probably of a continental affinity. A problem with these plots is that most of them use incompatible element ratios that tend to reflect the ratios in the mantle sources, which are known to be heterogeneous. Morrison (1978) has therefore suggested that trace element diagrams should only be used to identify magma types and their evolutionary trends, but not their palaeotectonic environments.

Jensen's cation plot unsuccessfully distinguishes between high-iron tholeiitic basalts, high-magnesium tholeiitic basalts and basalts, because they all have similar MgO contents (see Fig. 28). Generally classification schemes require basalts to have more than 8 to 10% MgO to

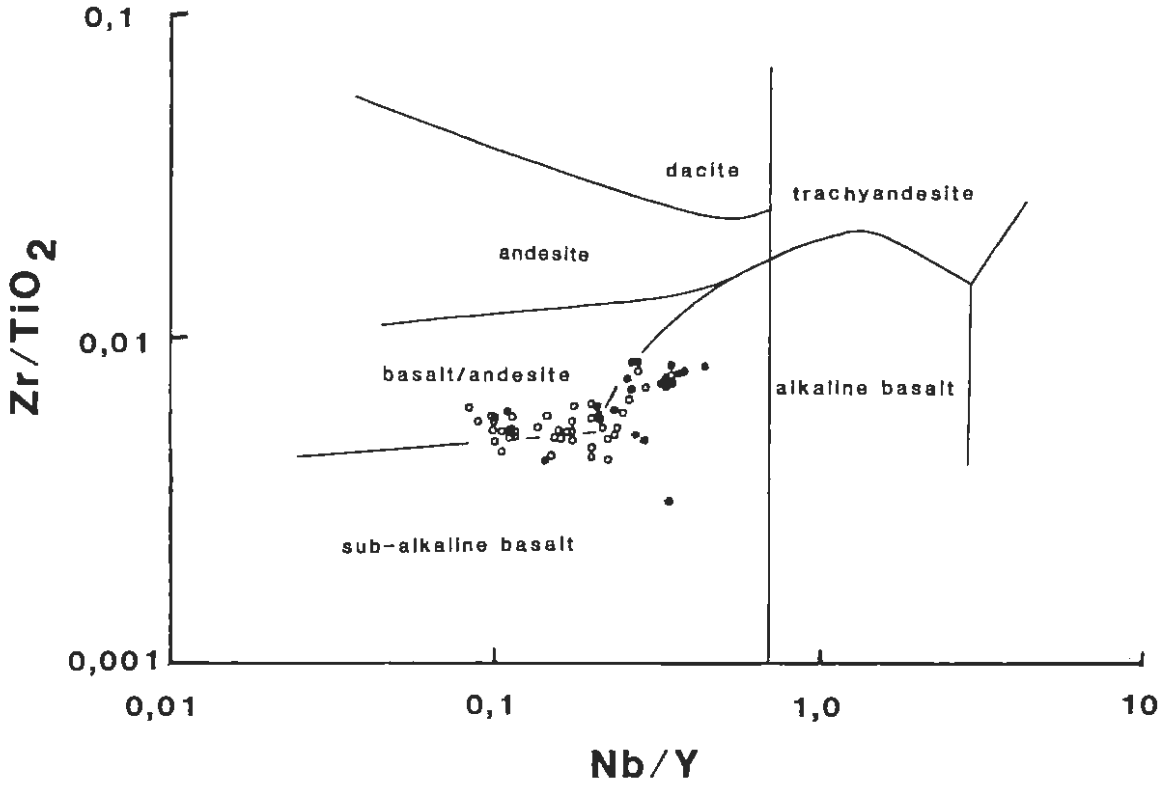

Figure 26A Zr/TiO_2 versus Nb/Y volcanic rock discrimination digram (after Winchester and Floyd, 1977)

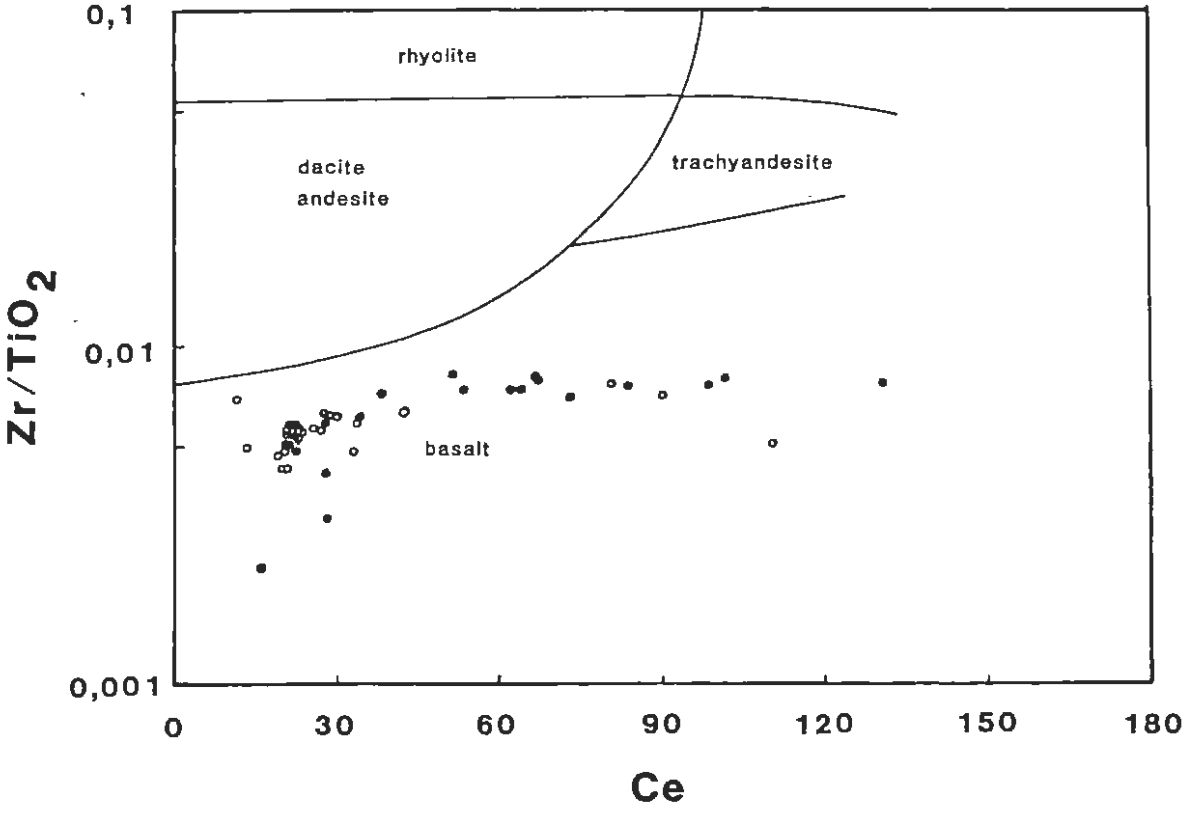

Figure 26B Zr/TiO_2 versus Ce volcanic rock discrimination diagram (after Winchester and Floyd, 1977)

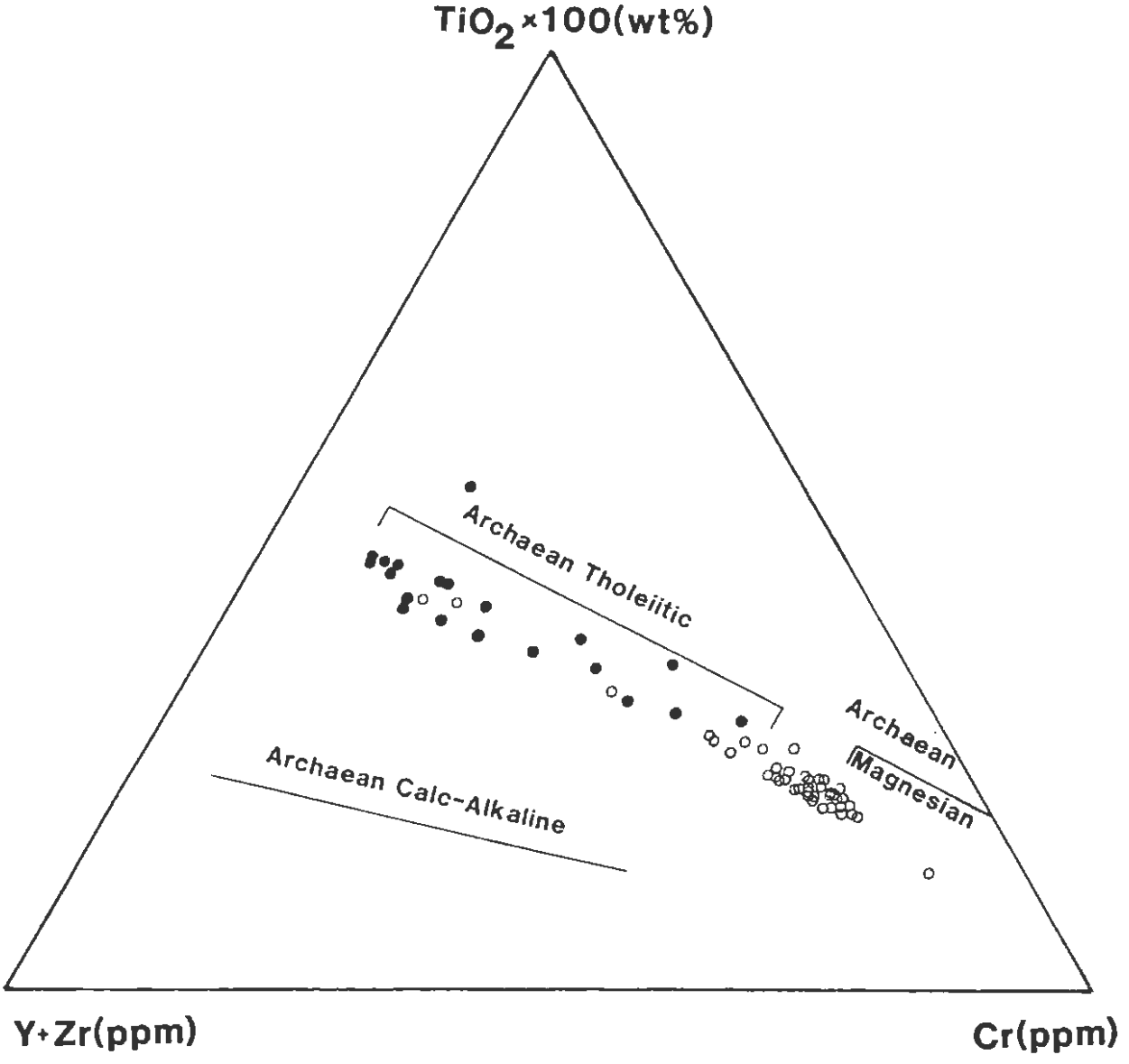

Figure 27 TiO_2 x 100 versus Y + Zr versus Cr discrimination plot based on various Archaean suites from Australia (after Davies et al., 1979)

be called high-magnesium basalts, which is not always the case in the Jensen plot. However a number of the Bitterwater lavas do fall in the magnesian field on the Davies et al. plot (Fig. 27). The AFM diagram (Fig. 24) illustrates the strong iron enrichment trend in the Dordabis lavas, with the Opdam basalts generally having higher iron and lower magnesium contents than the Bitterwater basalts.

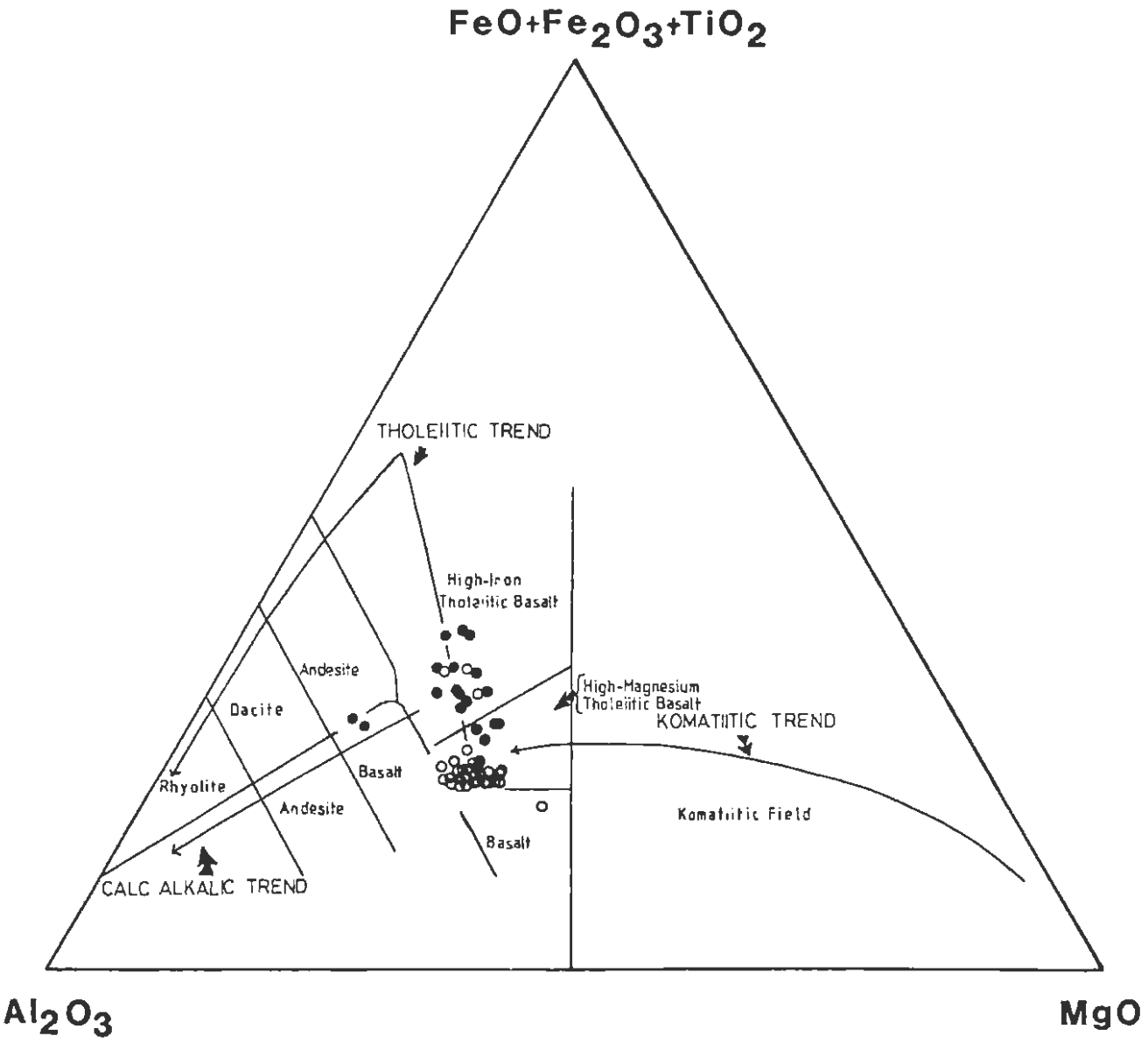

Figure 28 Jensen Cation Plot illustrating the tholeiitic trend in the Dordabis metabasalts (after Jensen, 1976)

5.4 Major Element Geochemistry

5.4.1 Introduction

Major element concentrations were determined in duplicate using X-ray fluorescence spectrometry according to the techniques described in Appendix 2. All iron is determined as Fe_2O_3 and major element data is given in this section in the form of anhydrous values normalised to 100 percent. Original analyses including L.O.I. and norms are given in Appendix 2.

5.4.2 Major element variations

The general major element compositional character of the Dordabis volcanic suite is illustrated by the diopside-olivine-hypersthene-quartz-nepheline normative diagram (Fig. 29). All tholeiites by definition must contain normative hypersthene (Yoder and Tilley, 1962). The nepheline normative Dordabis metabasalts have probably been depleted in SiO_2 or enriched in alkalies during alteration.

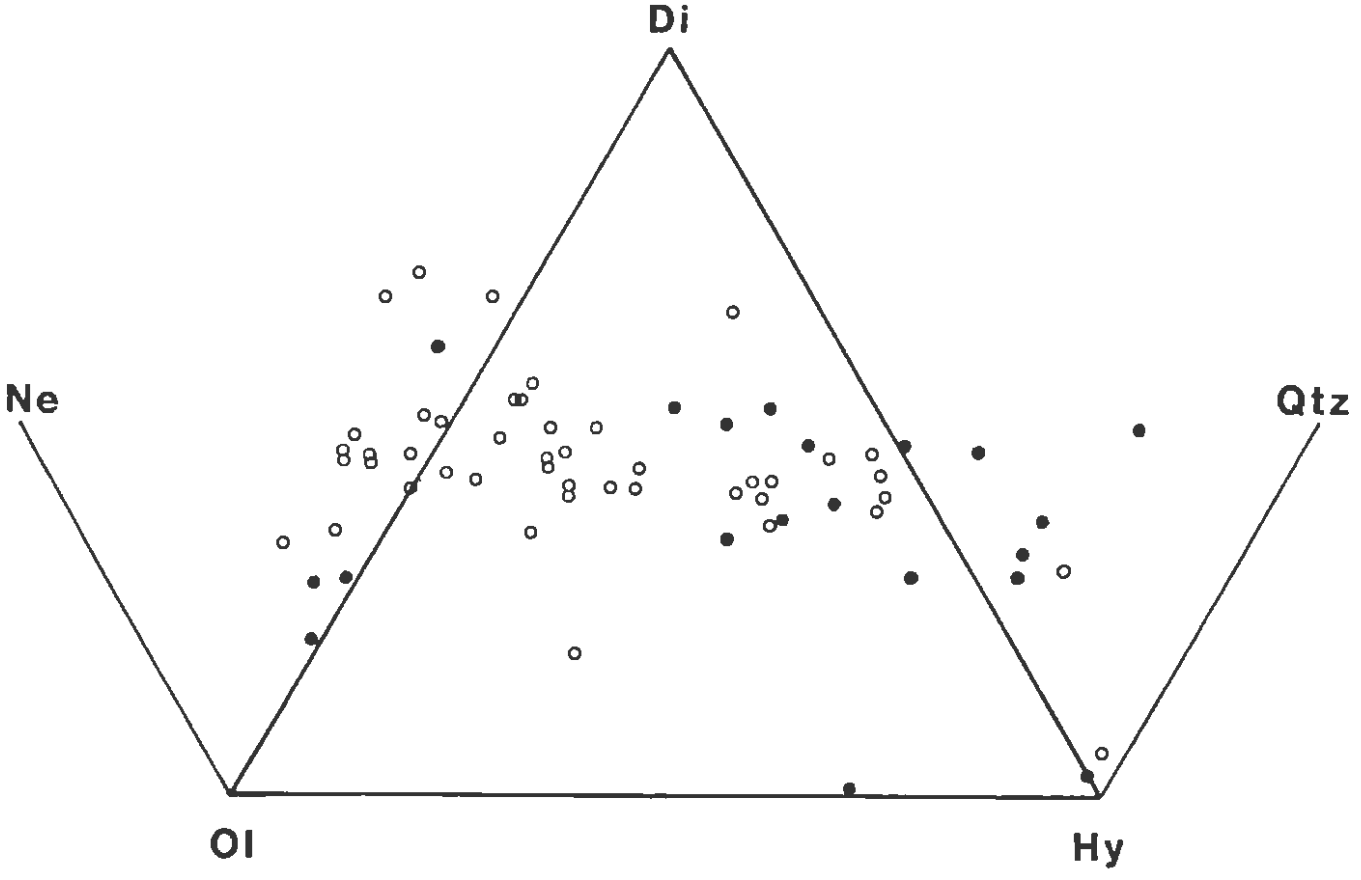

Figure 29 Normative diopside-olivine-hypersthene-quartz-nepheline diagram illustrating the composition of the Dordabis lavas

Major element chemical variation is quantitatively discussed with the aid of Zr variation diagrams (Figs. 30A to J). Zr is chosen as the abscissa in the variation diagrams (Figs. 30 and 31) because it is immobile and incompatible and it can be precisely determined by X-ray fluorescence spectrometry. Zr concentration increases with differentiation in basaltic systems. Major oxide variations with differentiation can therefore readily be identified on Figures 30A to J.

Major oxides exhibiting coherent variation trends with Zr are the immobile oxides TiO_2 and P_2O_5 (Figs. 30 B and J). Both oxides are enriched during differentiation, with TiO_2 varying from 0,9 to 4,2% in the Opdam lavas and from about 0,7 to 2,9% in the Bitterwater lavas. P_2O_5 concentrations vary in a similar manner from 0,07 to 0,57% in the Opdam lavas and from 0,07 to 0,30% in the Bitterwater lavas.

Al_2O_3, MgO and CaO contents generally decrease (Figs. 30C, F and G), while MgO and Fe_2O_3 contents usually increase (Figs. 30F and D) with differentiation. Al_2O_3, MgO and CaO concentrations vary from about 18%, 13% and 4% in the more primitive lavas to about 13%, 3% and 12% respectively in the more evolved lavas. Fe_2O_3 concentrations plot in a well-defined trend on Figure 30D, with concentrations ranging from 10 to 19%. MnO contents are low and vary from 0,13% in the more primitive basalts to 0,27% in the more differentiated samples. Because SiO_2 and the alkalies (Na_2O and K_2O) were mobile (see section 5.2.5), no systematic variation trends are evident in Figures 30A, H and I.

The Bitterwater basalts generally have higher Al_2O_3, MgO and CaO contents, and lower TiO_2, Fe_2O_3 and P_2O_5 contents than the Opdam basalts. IWJ78, the large-feldspar phyric lava, plots off the variation trend on most major element diagrams. This sample has higher Al_2O_3 and lower Fe_2O_3 and MgO concentrations than the other metalavas and is therefore less basic in composition than the average Dordabis Formation lavas. Its compositional characteristics can be accounted for by the presence of large quantitites of plagioclase phenocrysts.

The Dordabis metalavas are basaltic in composition and it would therefore be expected that plagioclase, pyroxene and olivine were probably fractionating phases. These phases contain virtually no Zr and their bulk compositions would therefore plot along the ordinate on the major element diagrams (Figs. 30A to J).

Variation diagrams of major elements showing reasonable coherence illustrate the chemical evolution of the liquids that crystallised as the Dordabis basalts. However, alteration and the presence of porphyritic lavas has introduced scatter in some of these variation trends, making quantitative modelling of differentiation trends impractical. Dashed lines on Figures 30A to J represent envelopes enclosing possible liquid lines of descent for the Dordabis metabasalts.

The Al_2O_3 variation diagram (Fig. 3DC) indicates that an extract containing 16 to 19% Al_2O_3 is required to produce the observed trend of decreasing Al_2O_3 with Zr. Relict feldspar phenocrysts analysed from the Bitterwater basalts contain about 28% Al_2O_3 (see section 4.3). This suggests that the fractionating assemblage contained less than 70% plagioclase, and probably included mafic phases, as is indicated by the positive correlation of Fe_2O_3 and negative correlation of MgO with progressive differentiation (Figs. 30D and F). Less than 70% plagioclase in the fractionating assemblage cannot alone account for the 9 to 14% CaO required to generate the CaO trend observed in Figure 30G. Another phase with more than 9 to 14% CaO must therefore also have been fractionating.

This phase is probably clinopyroxene, which, in the Bitterwater Member, contains 17 to 22% CaO (see section 4.2). These relict clinopyroxenes also contain approximately 50 to 53% SiO_2. The relict plagioclase phenocrysts analysed contain 53 to 58% SiO_2 (see section 4.3). The SiO_2 variation diagram (Fig. 30A) indicates the extract contained between 46% and 50% SiO_2. Although alteration has probably caused SiO_2 depletion (see section 5.2.5), this variation trend indicates that olivine was possibly also an important fractionating phase. Fractional crystallisation is discussed in more depth with the aid of trace element data in section 5.5.

The Opdam metabasalts generally have higher concentrations of TiO_2, Fe_2O_3 and P_2O_5, and lower concentrations of Al_2O_3 and CaO compared to the Bitterwater metabasalts. This suggests that the Opdam metalavas are generally more differentiated and hence compositionally more evolved than the Bitterwater metalavas. Compositional overlap, especially shown by strongly differentiated elements (e.g. P_2O_5 and TiO_2), is indicative of a co-genetic relationship between the two members. This is further assessed with the aid of trace element data in section 5.5.

Figure 30(A-J) Major element variation diagrams (weight % oxides) using Zr as the abscissa (● Opdam basalts, ○ Bitterwater basalts). Dashed lines enclose liquid lines of decent and solid lines enclose modelled element behaviour during fractional crystallisation.

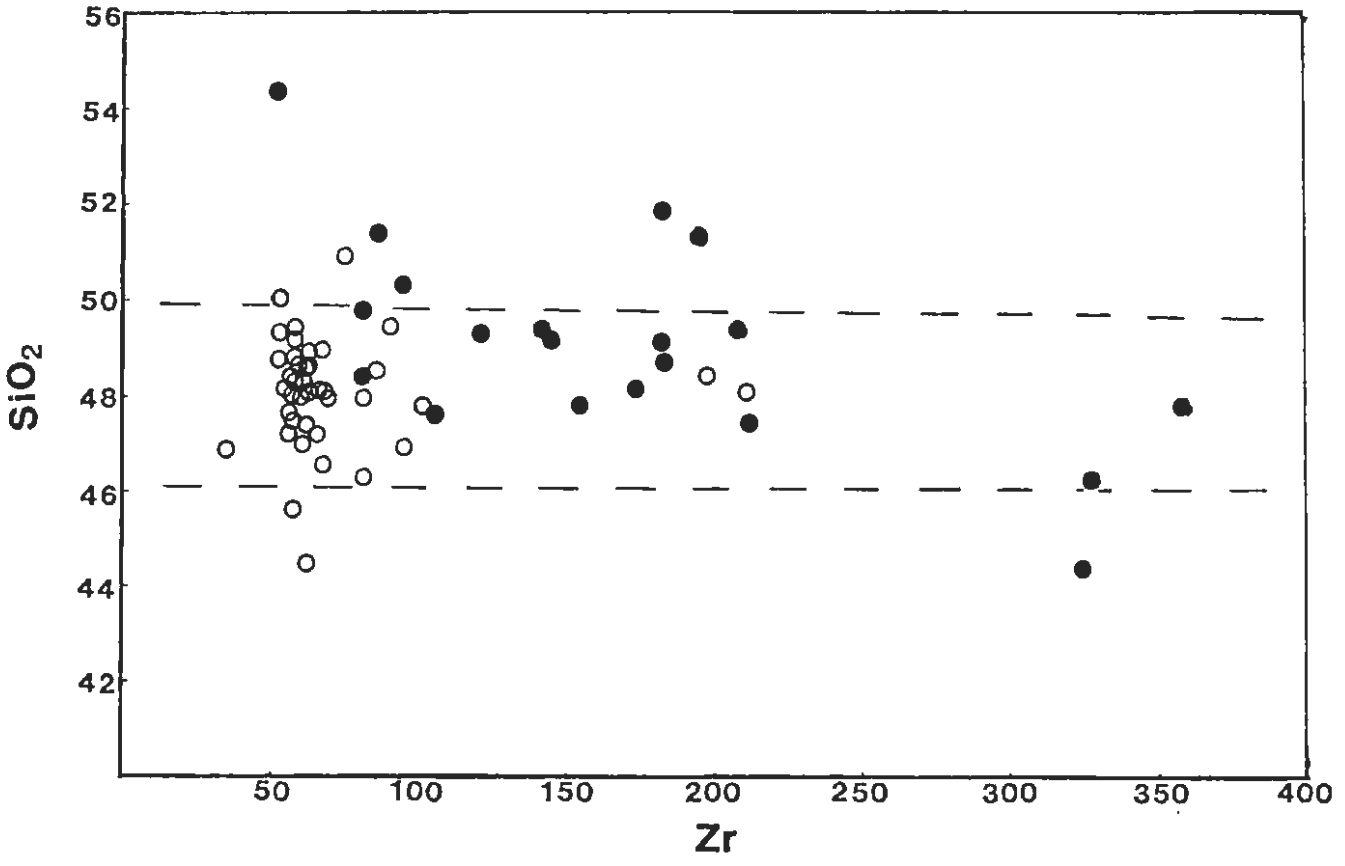

Figure 30A

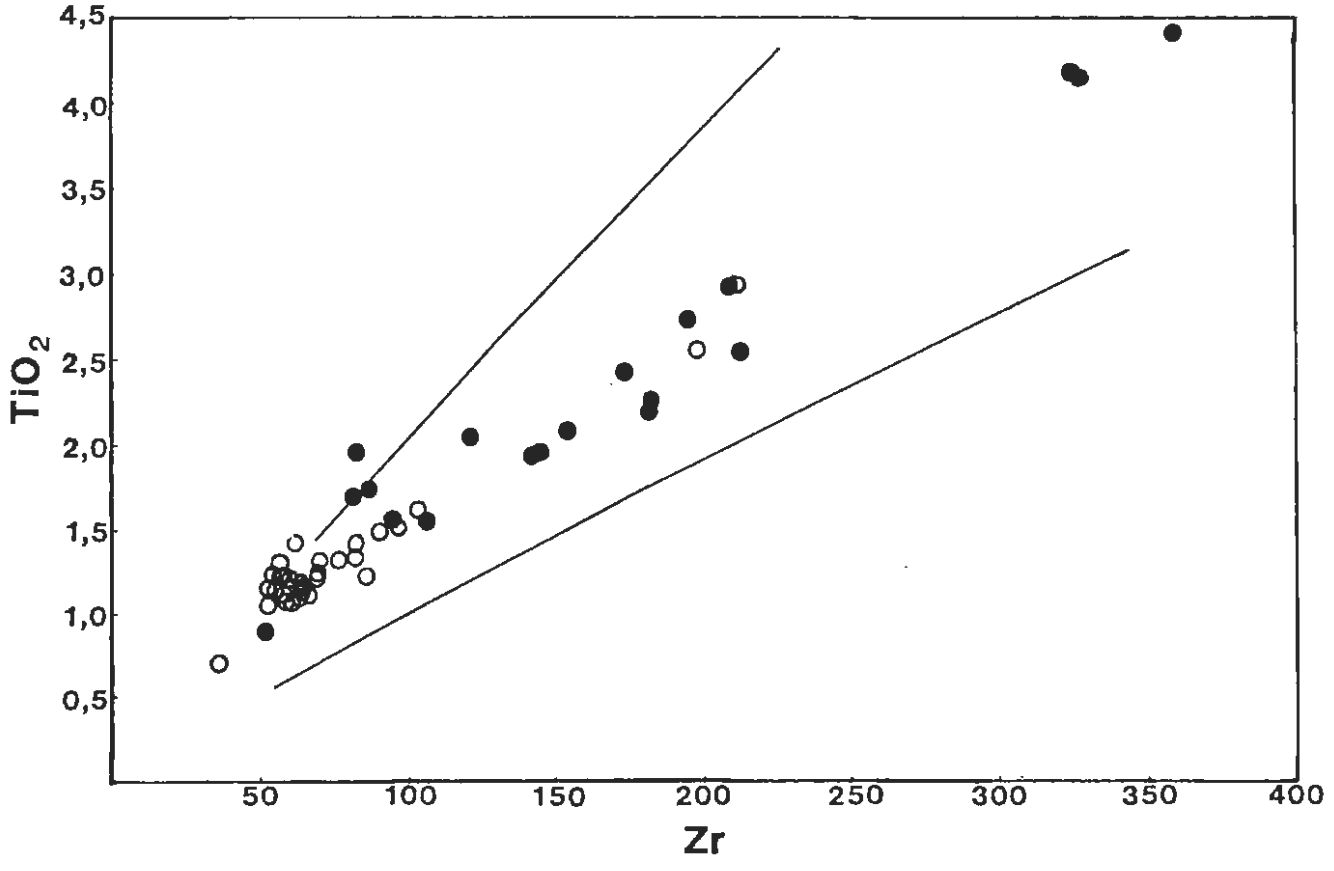

Figure 30B

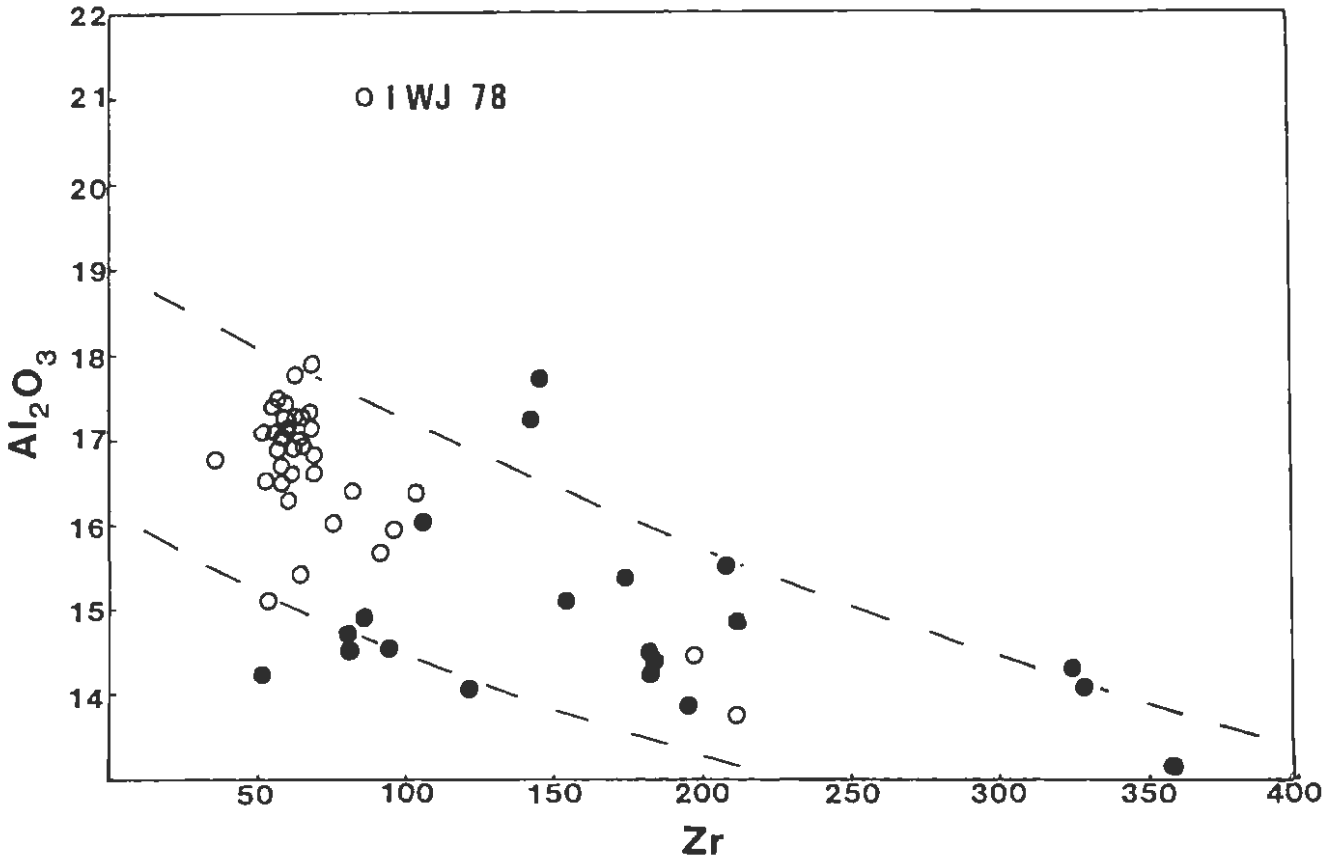

Figure 30C

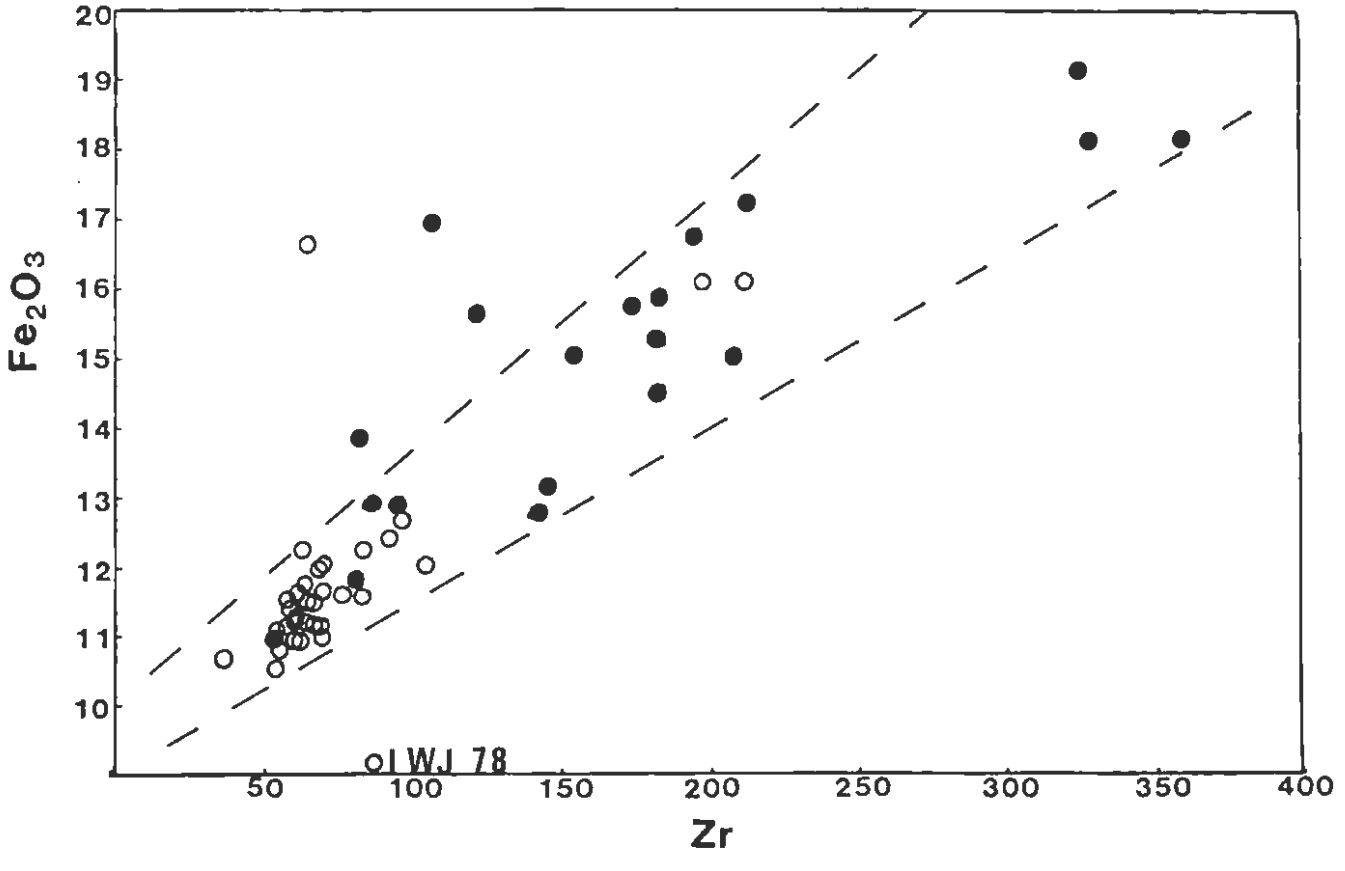

Figure 30D

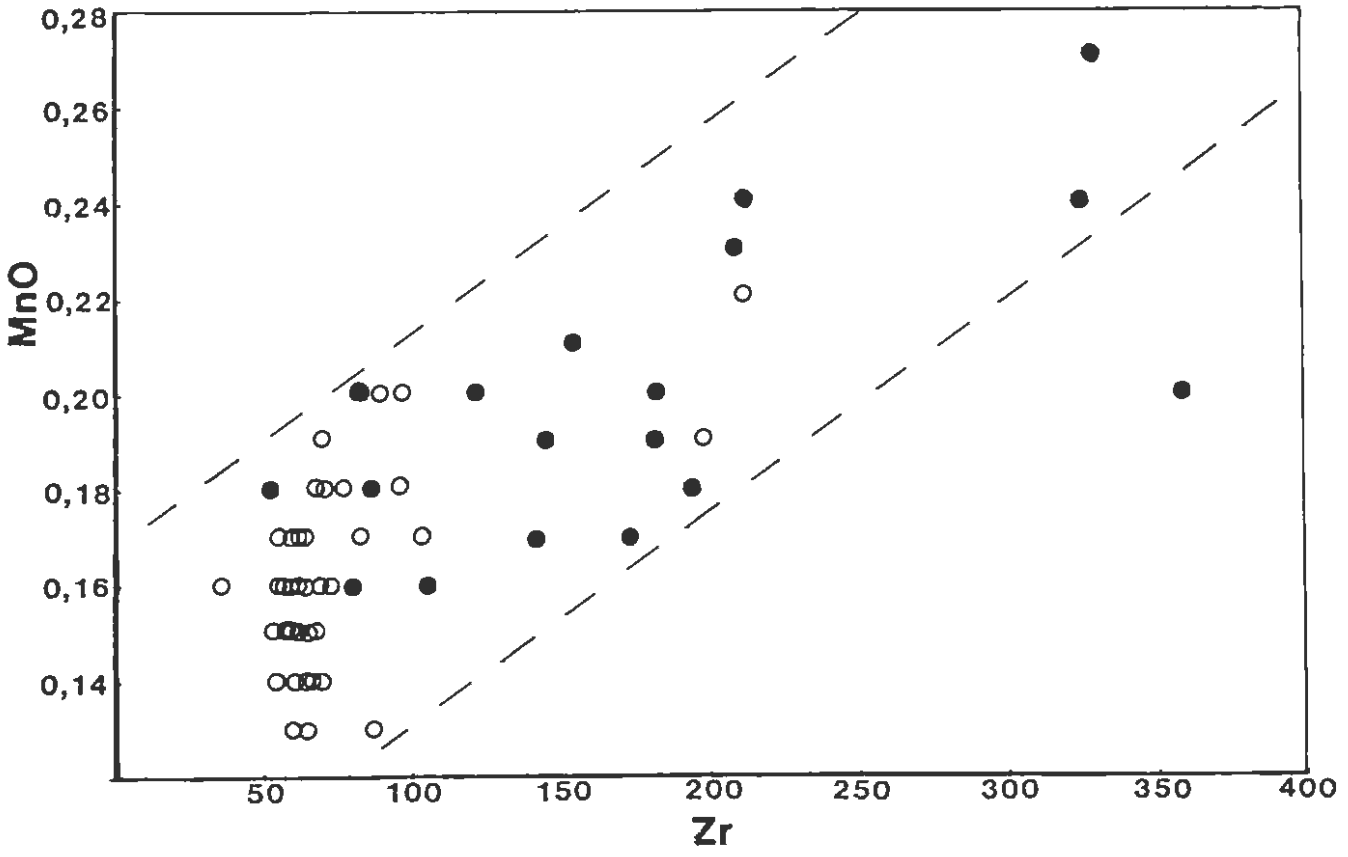

Figure 30E

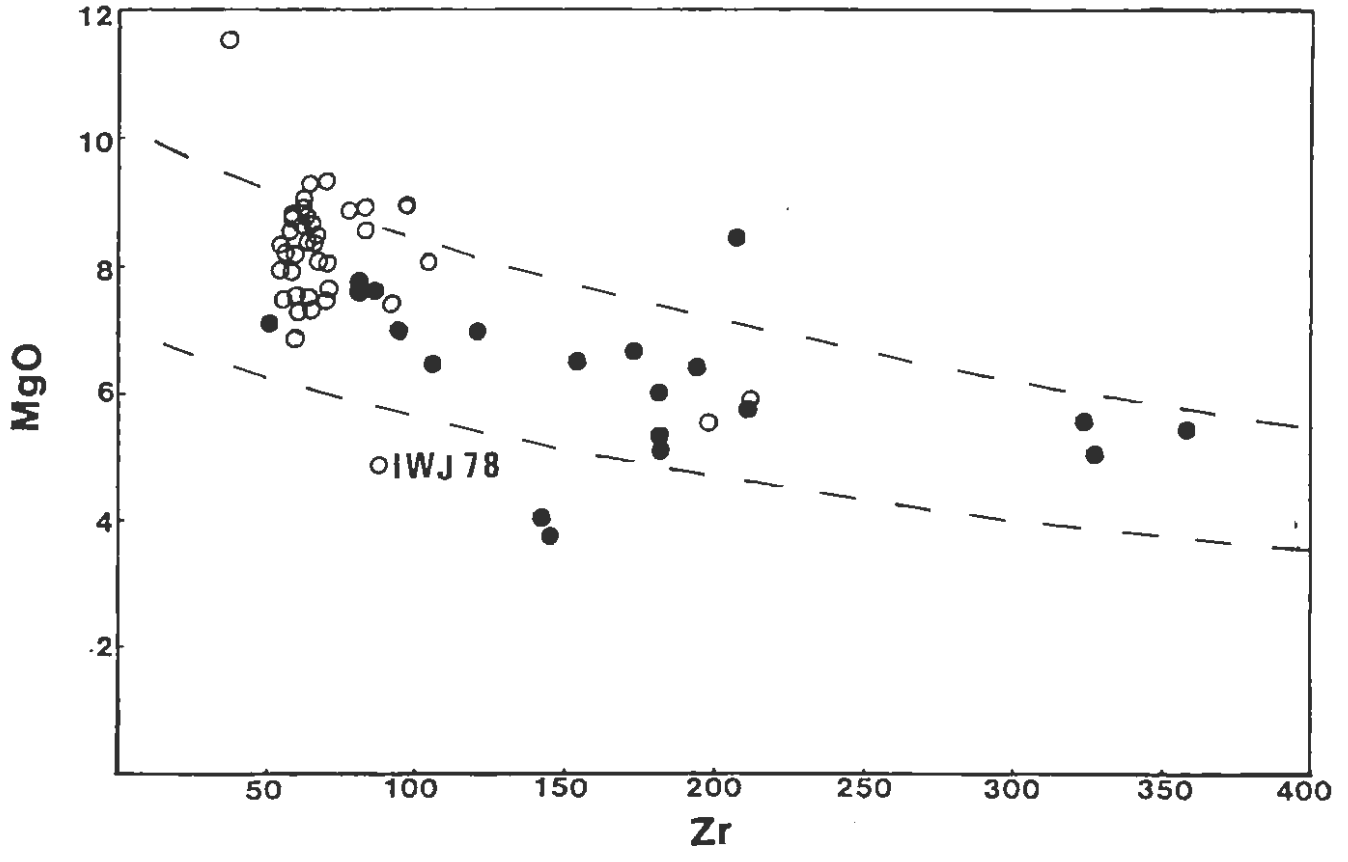

Figure 30F

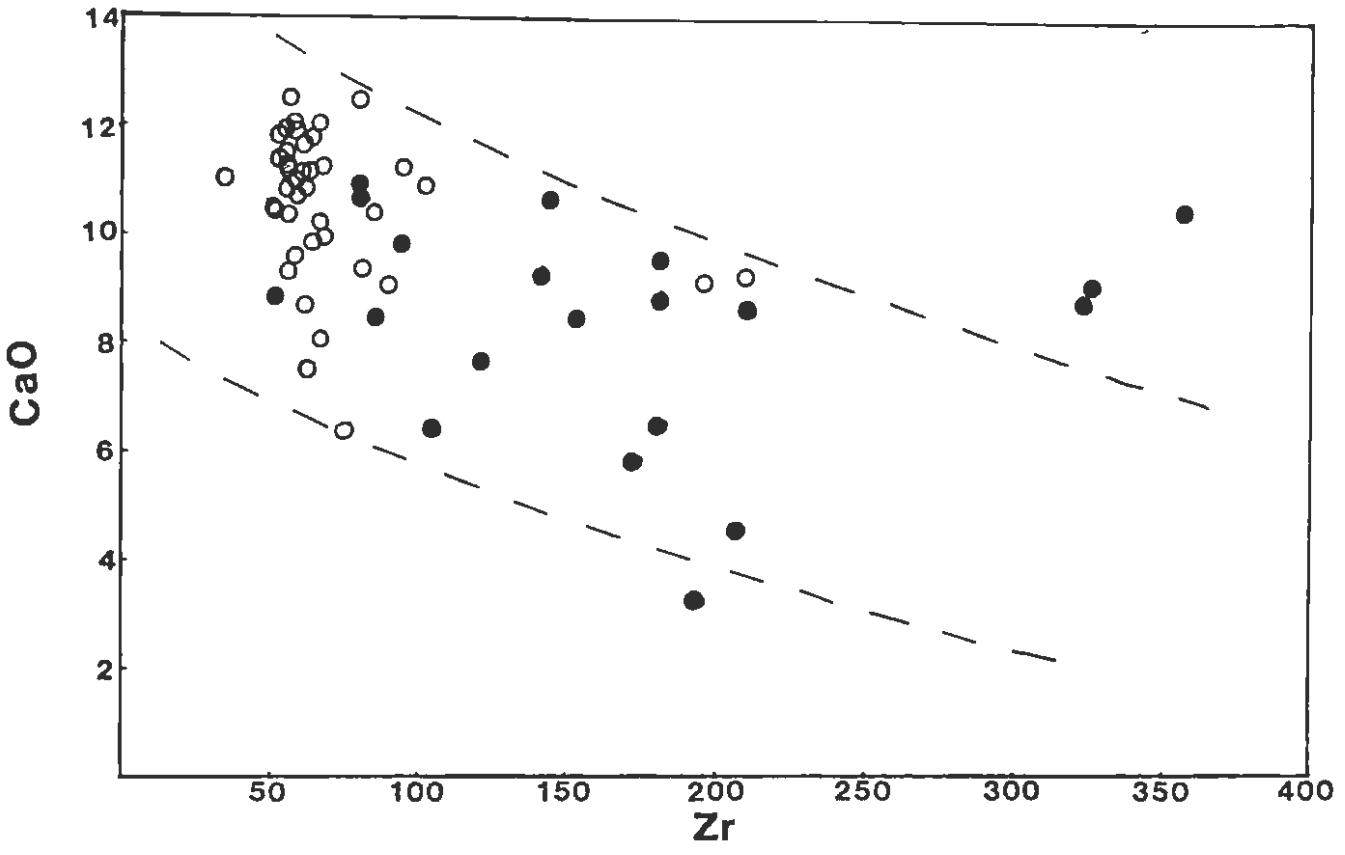

Figure 30G

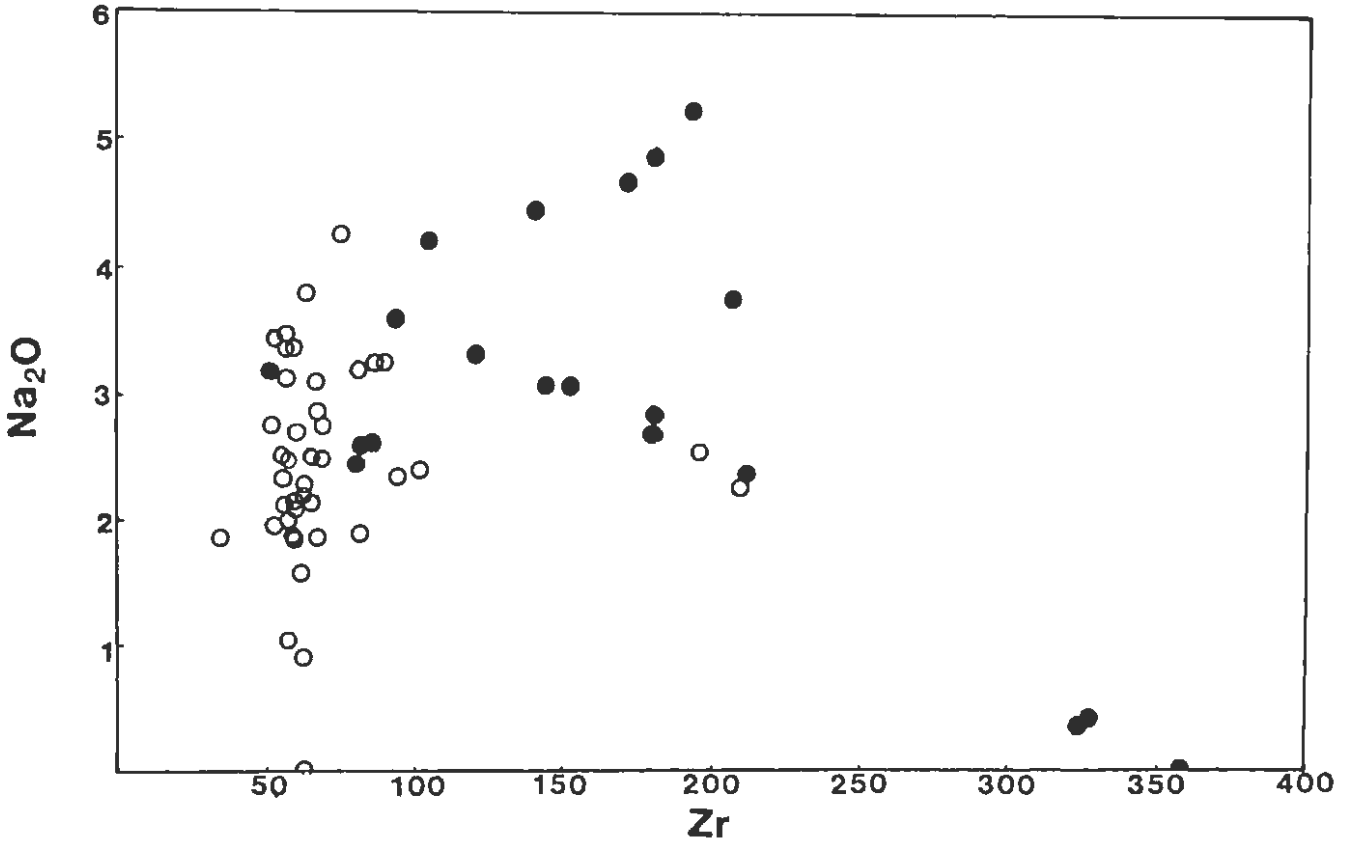

Figure 30H

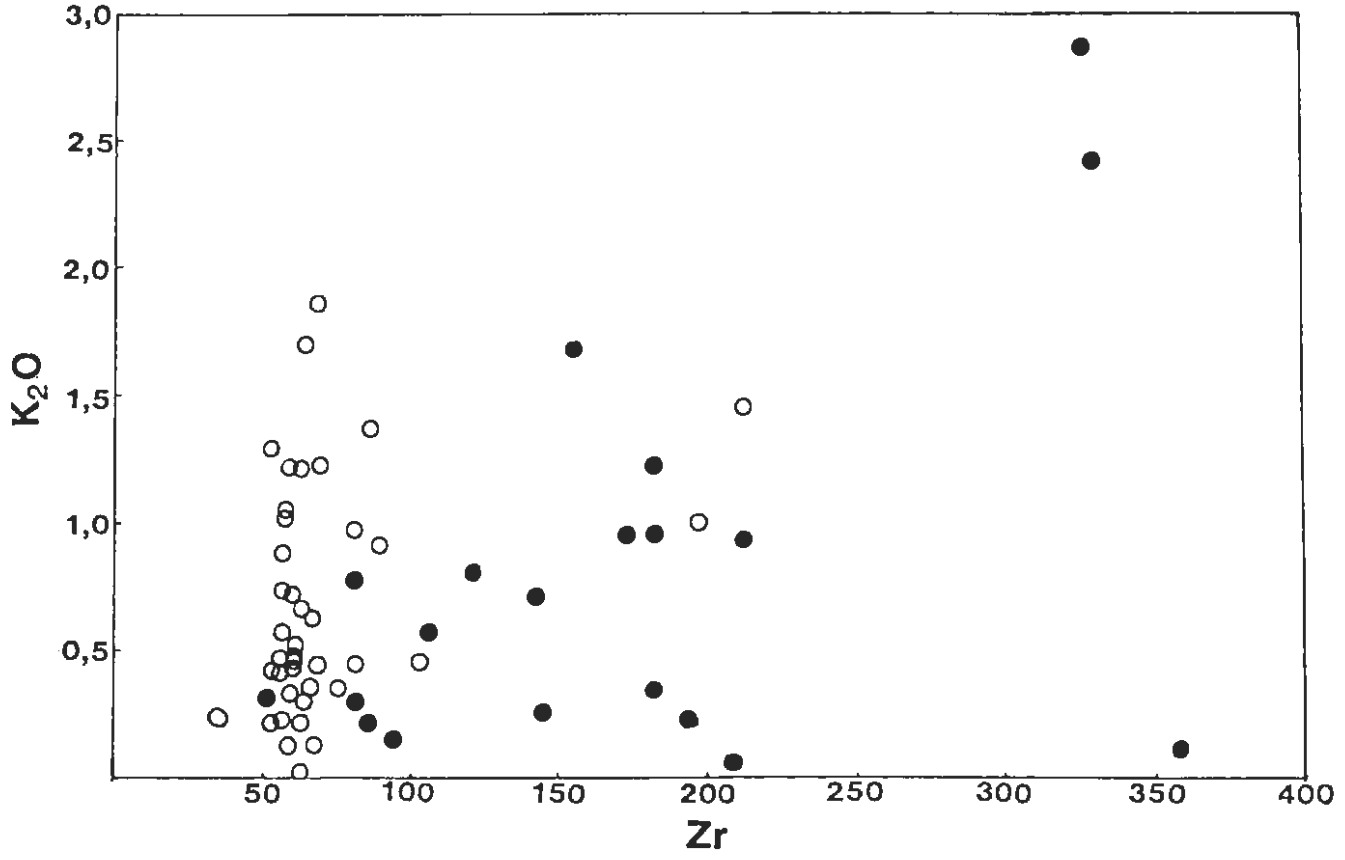

Figure 30I

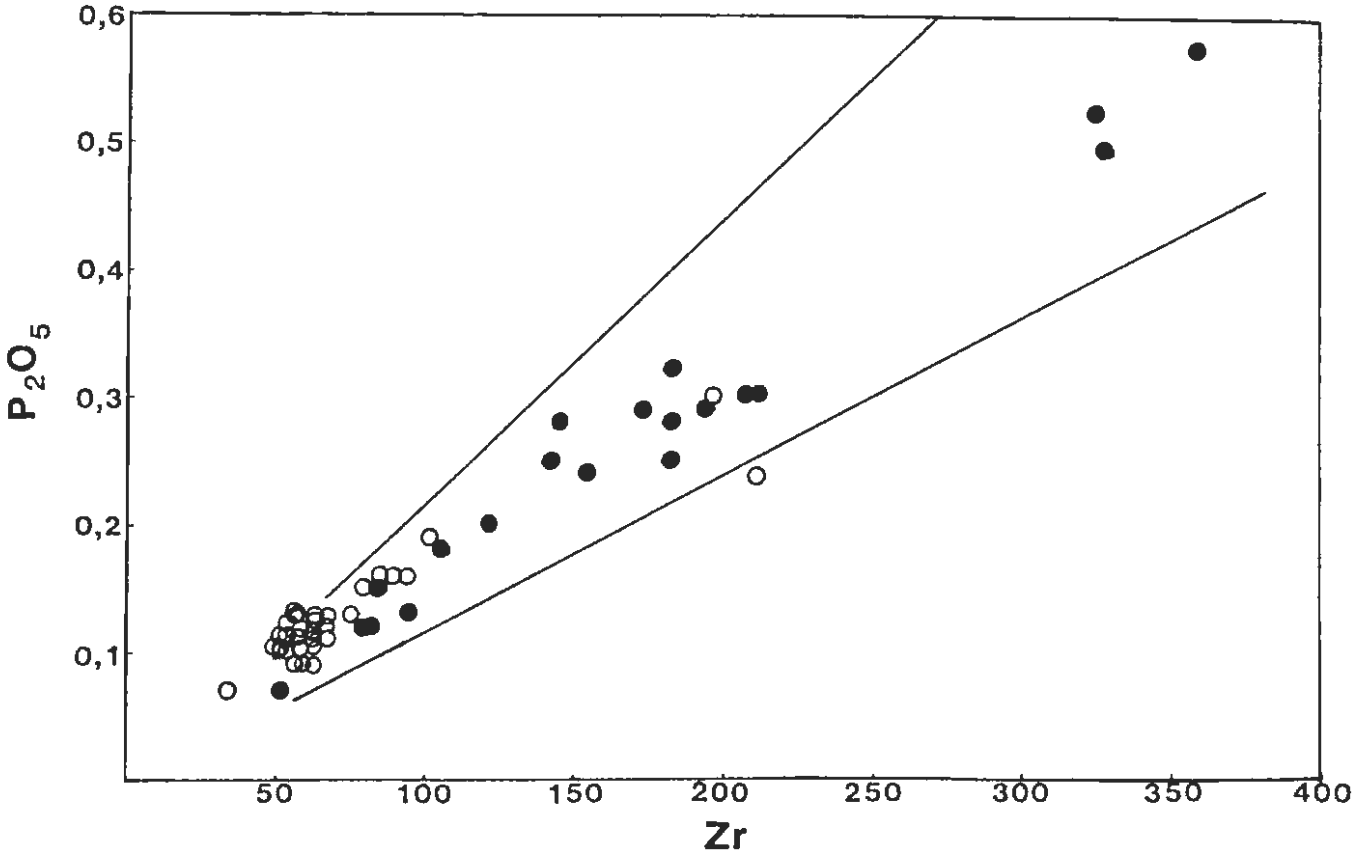

Figure 30J

Figure 31(A-O) Trace element variation diagrams (in parts per million) using Zr as the abscissa (● Opdam basalts, ○ Bitterwater basalts) where L.L.D. represents the lower limits of determination. Solid lines enclose modelled trace element behaviour during fractional crystallisation.

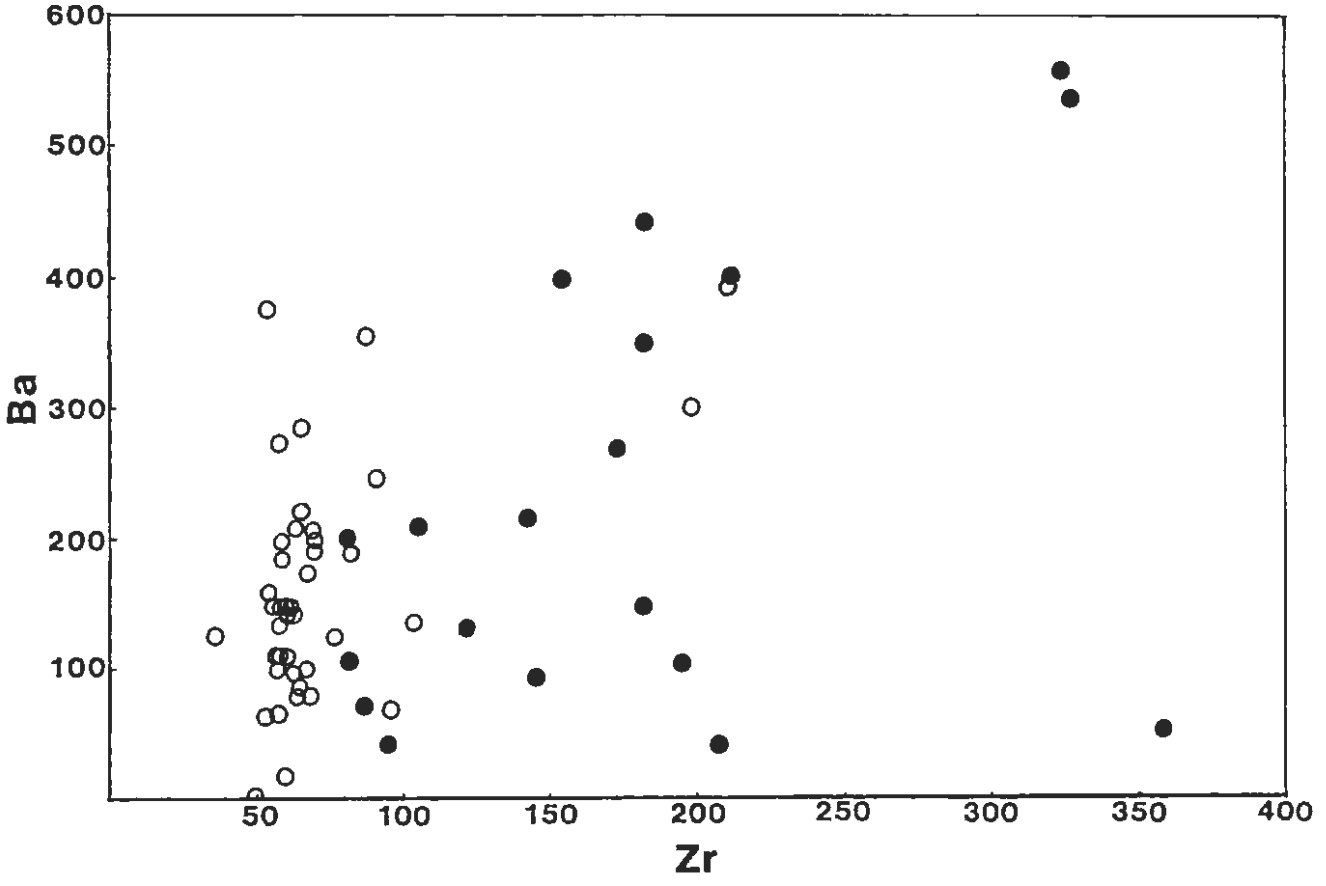

Figure 31A

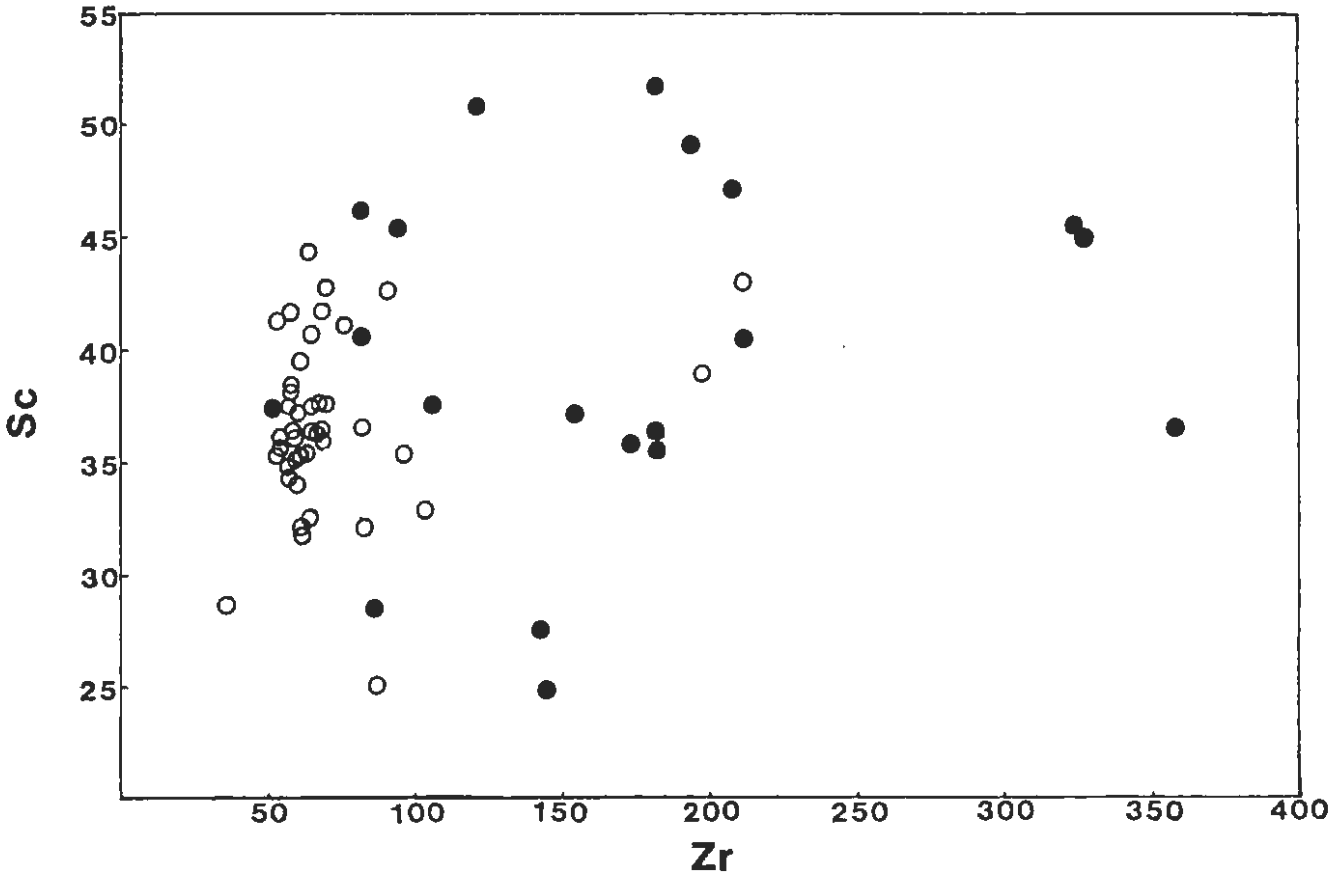

Figure 31B

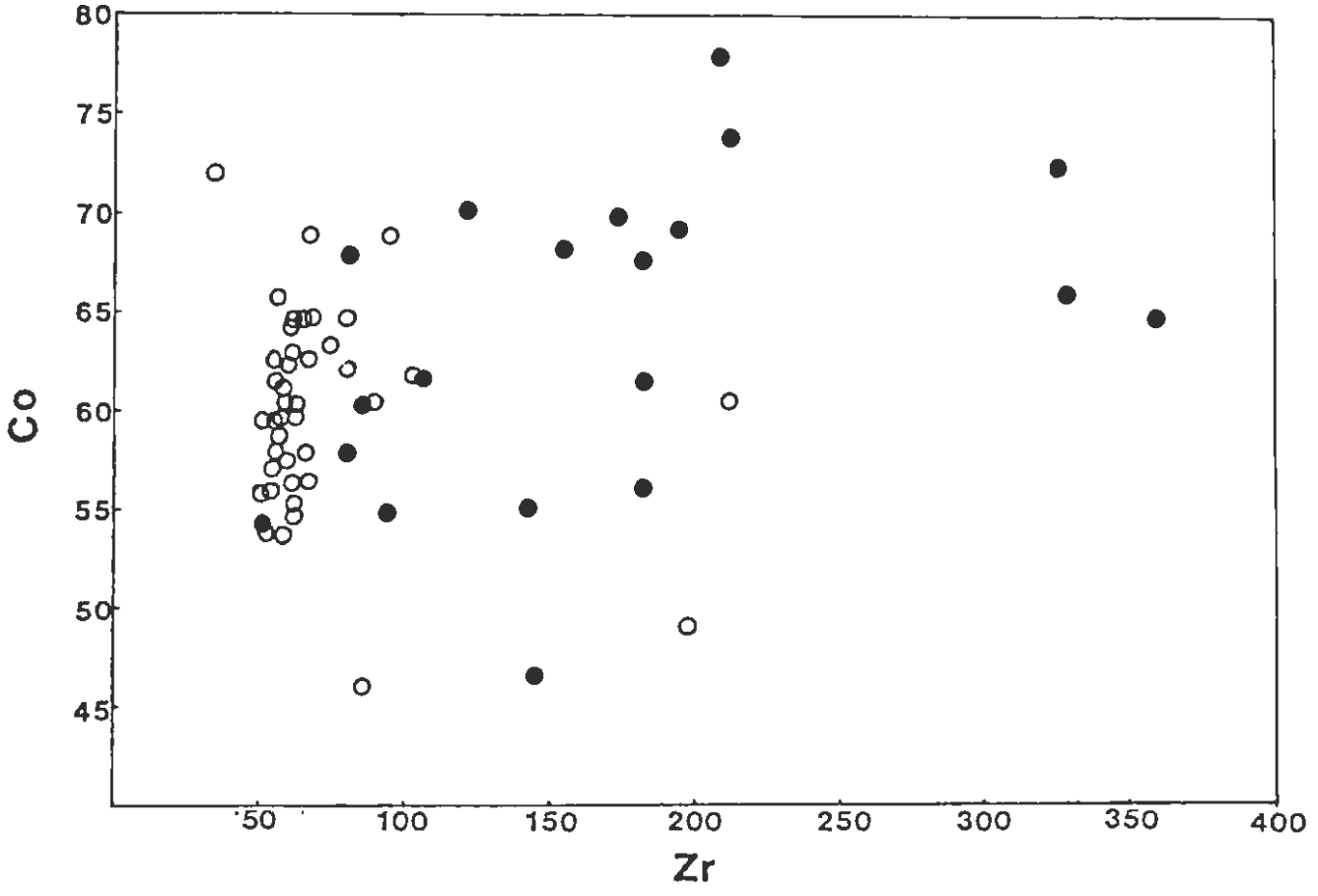

Figure 31C

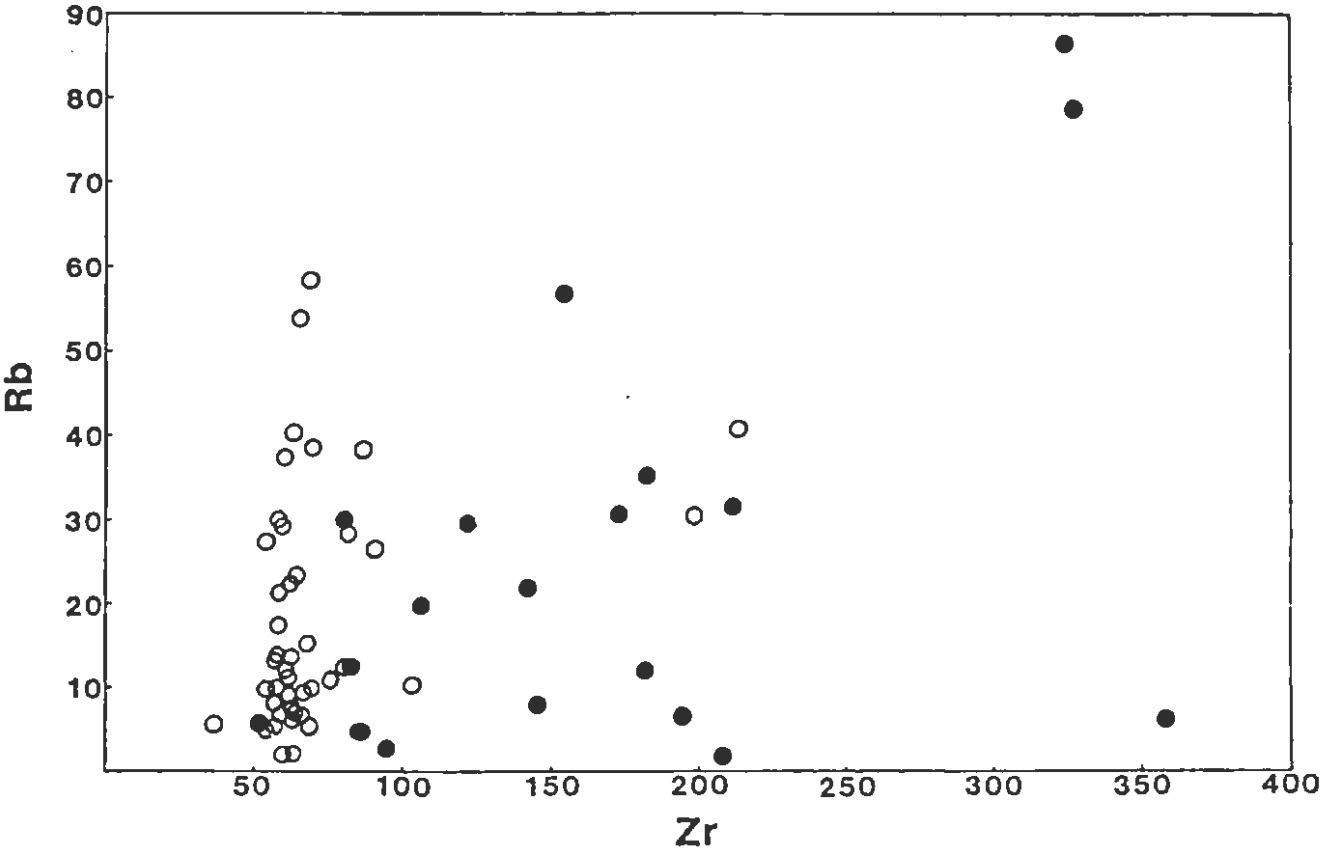

Figure 31D

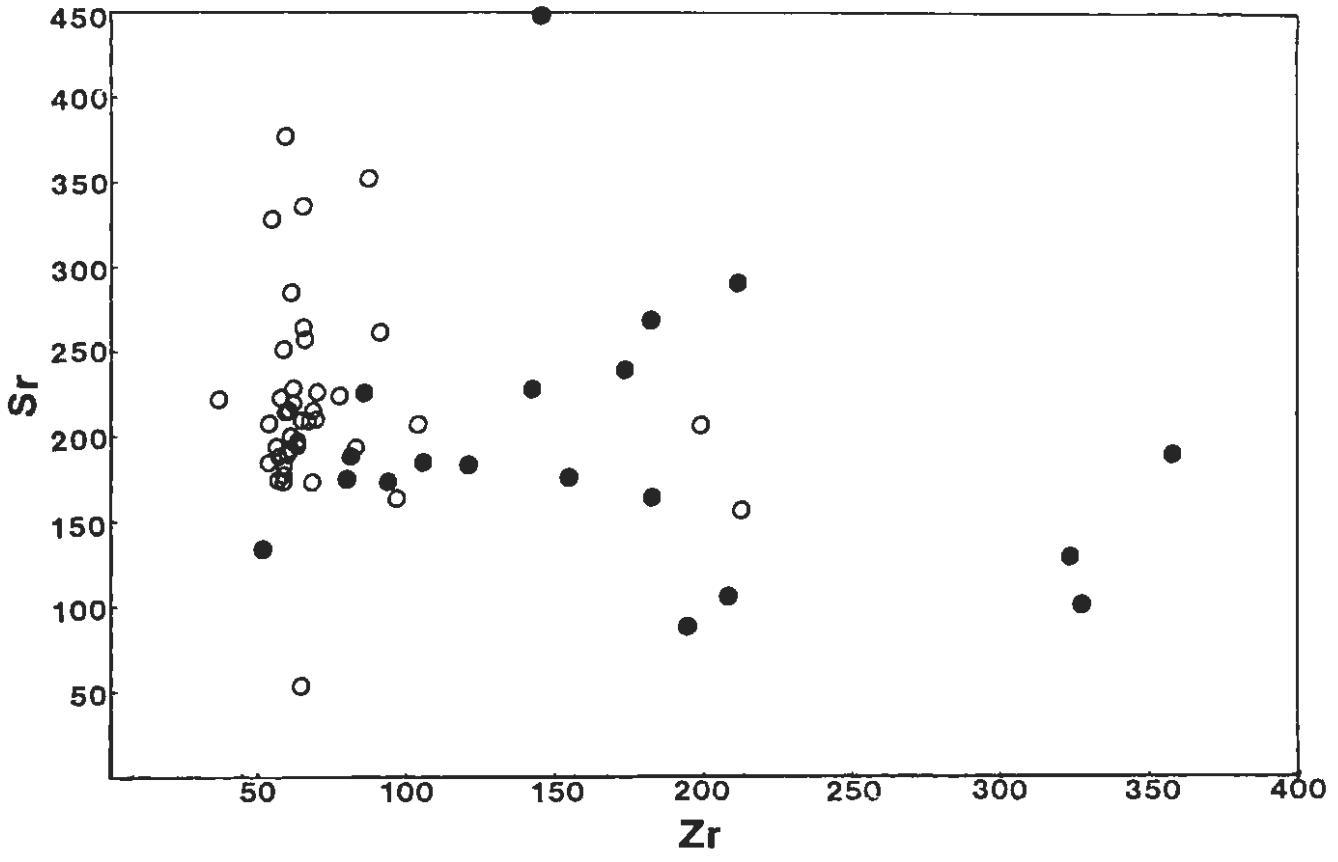

Figure 31E

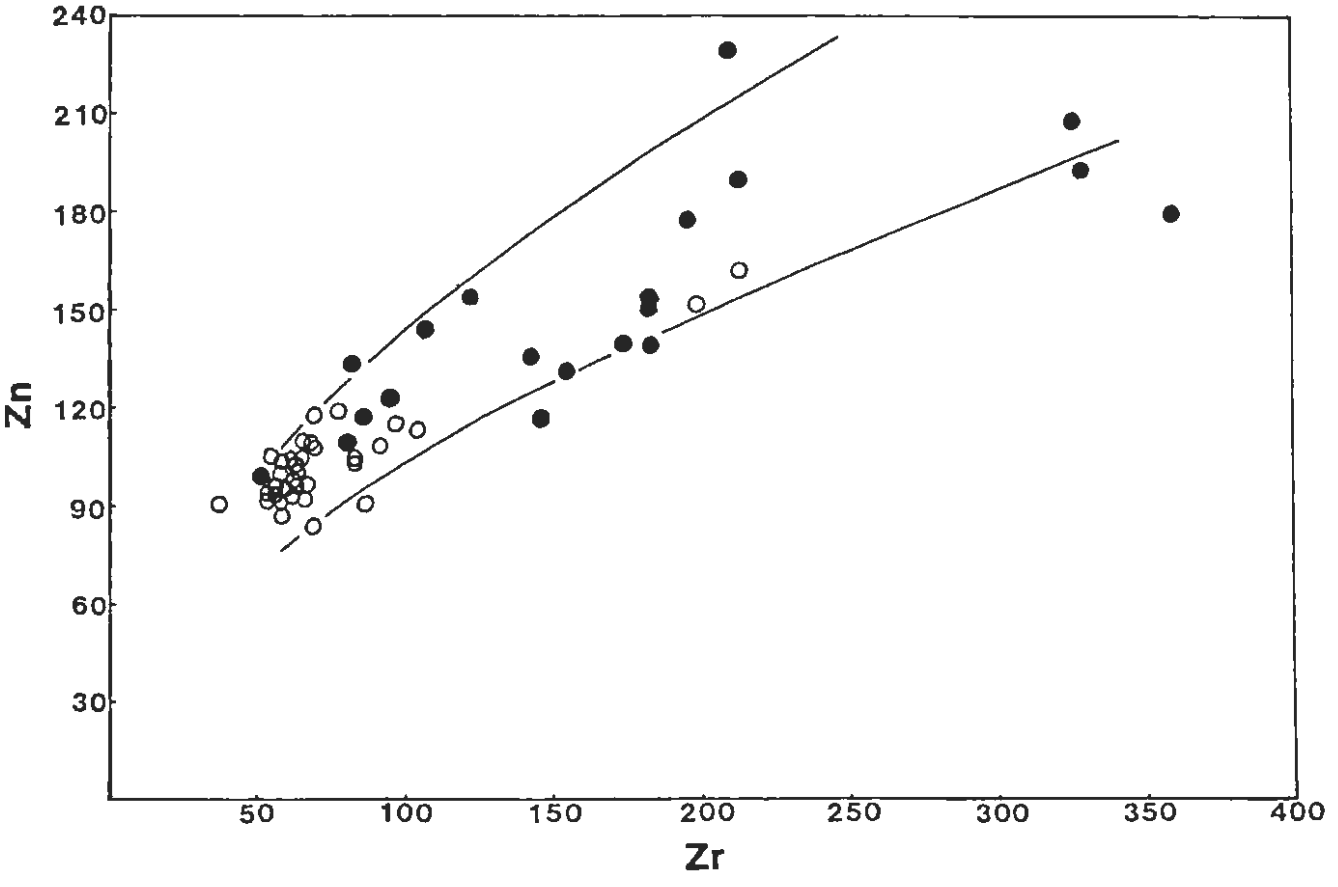

Figure 31F

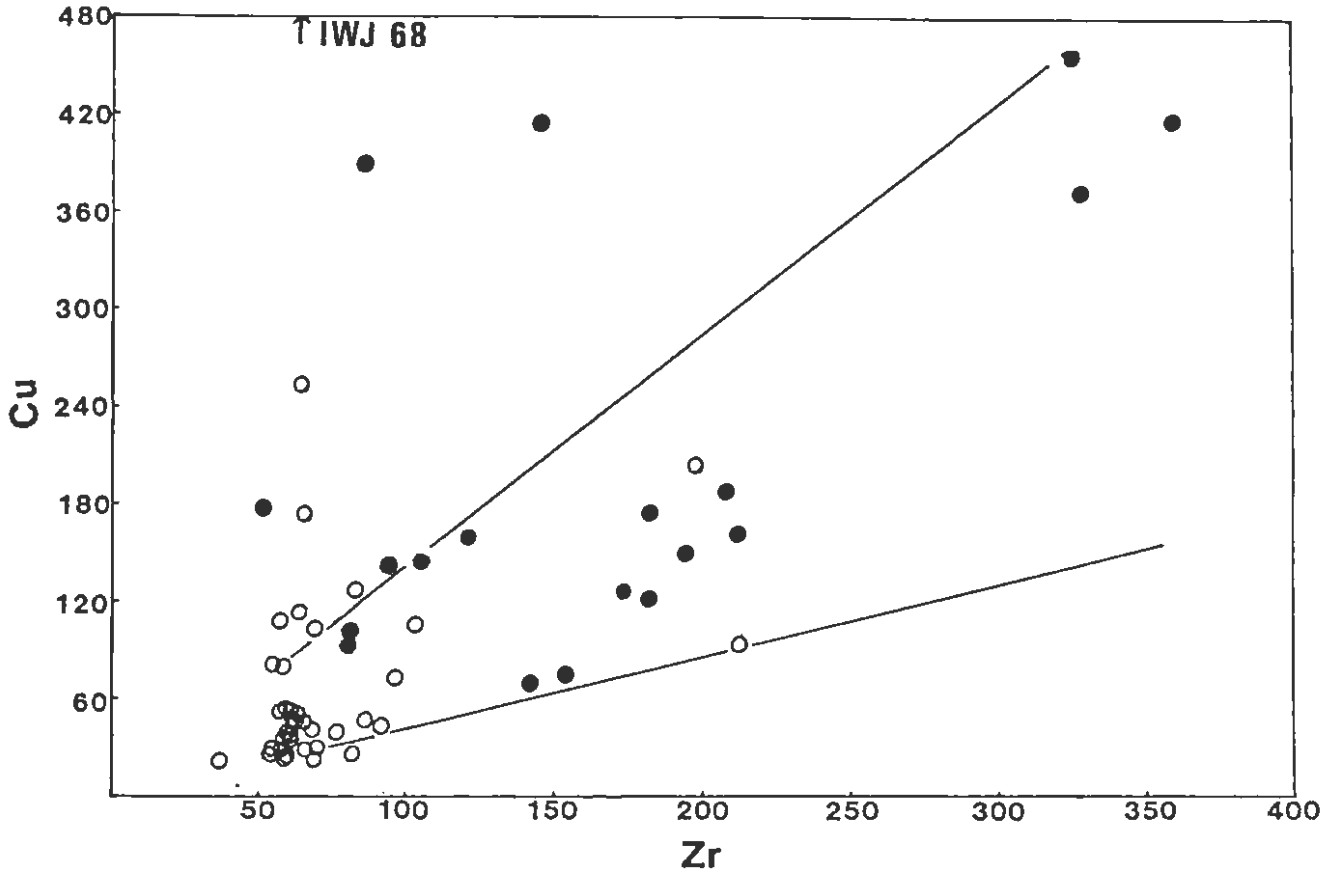

Figure 31G

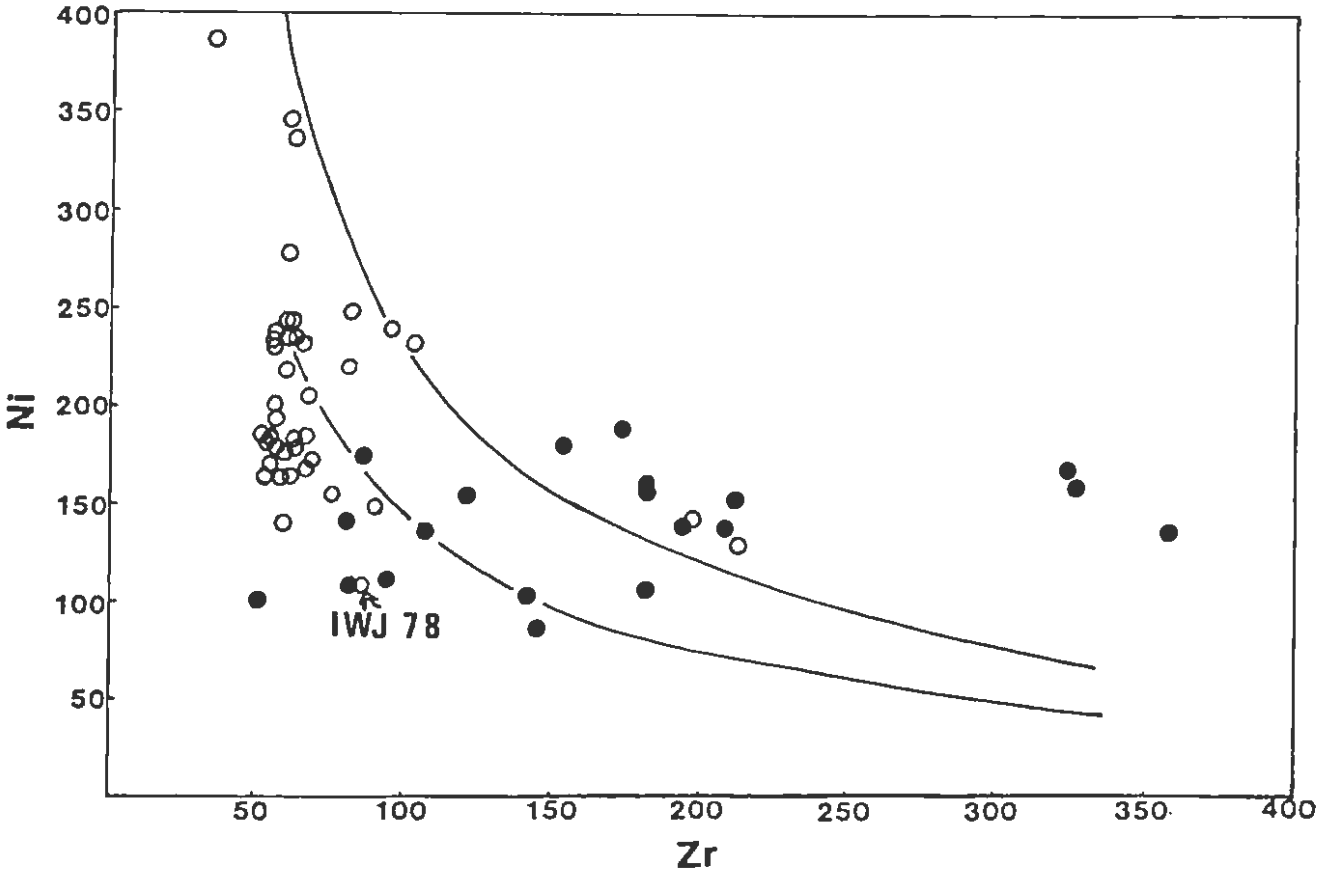

Figure 31H

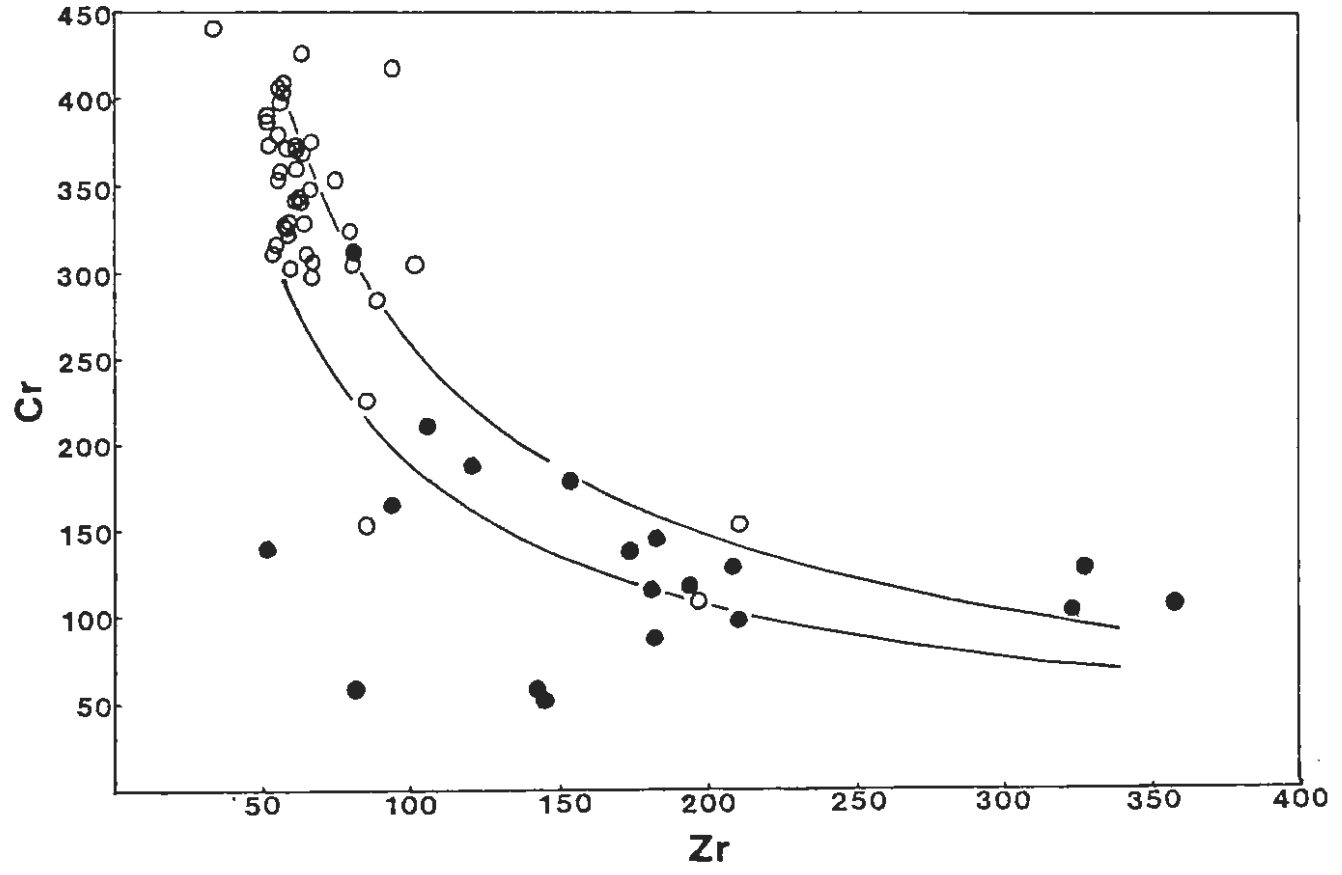

Figure 31I

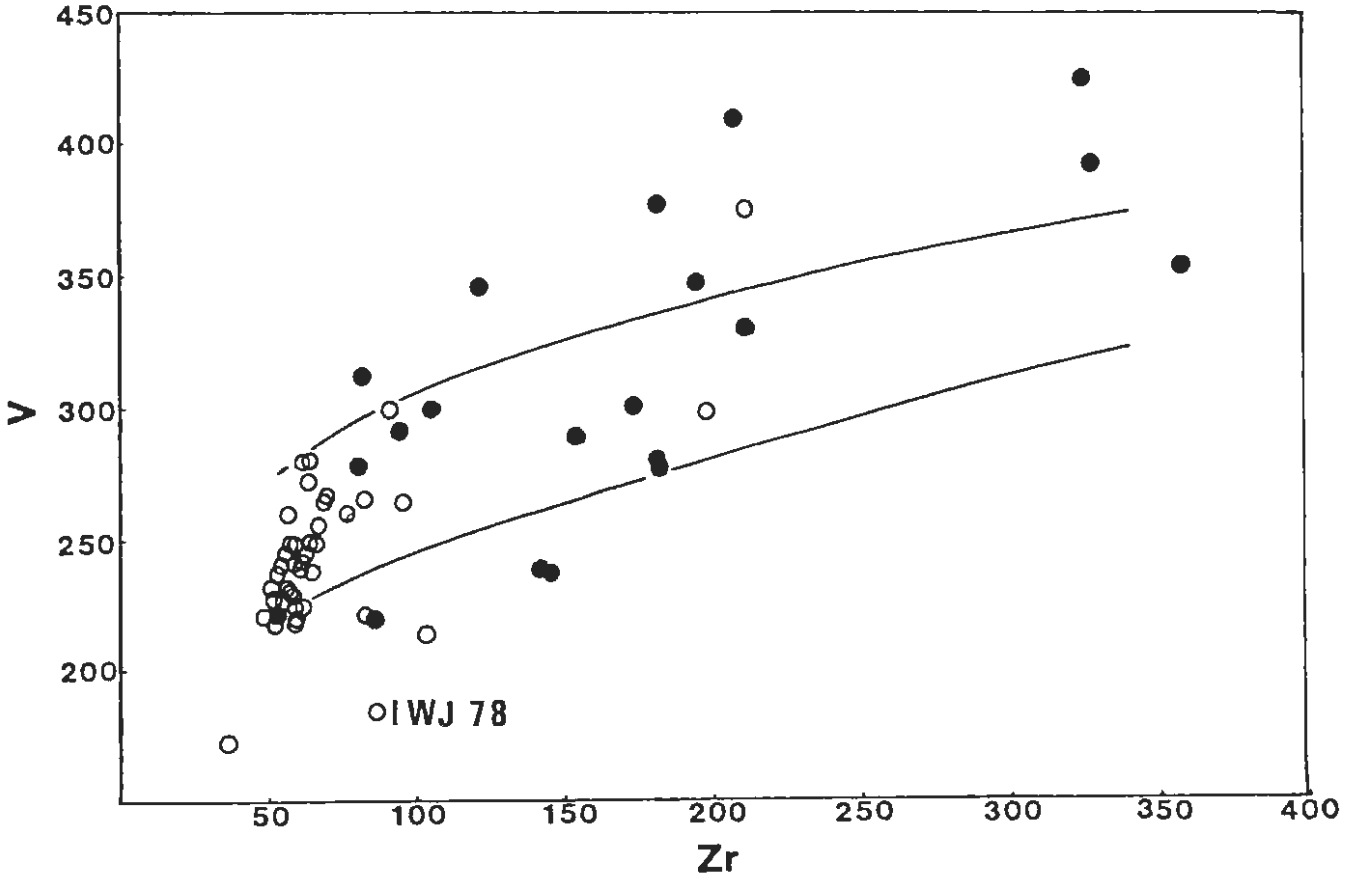

Figure 31J

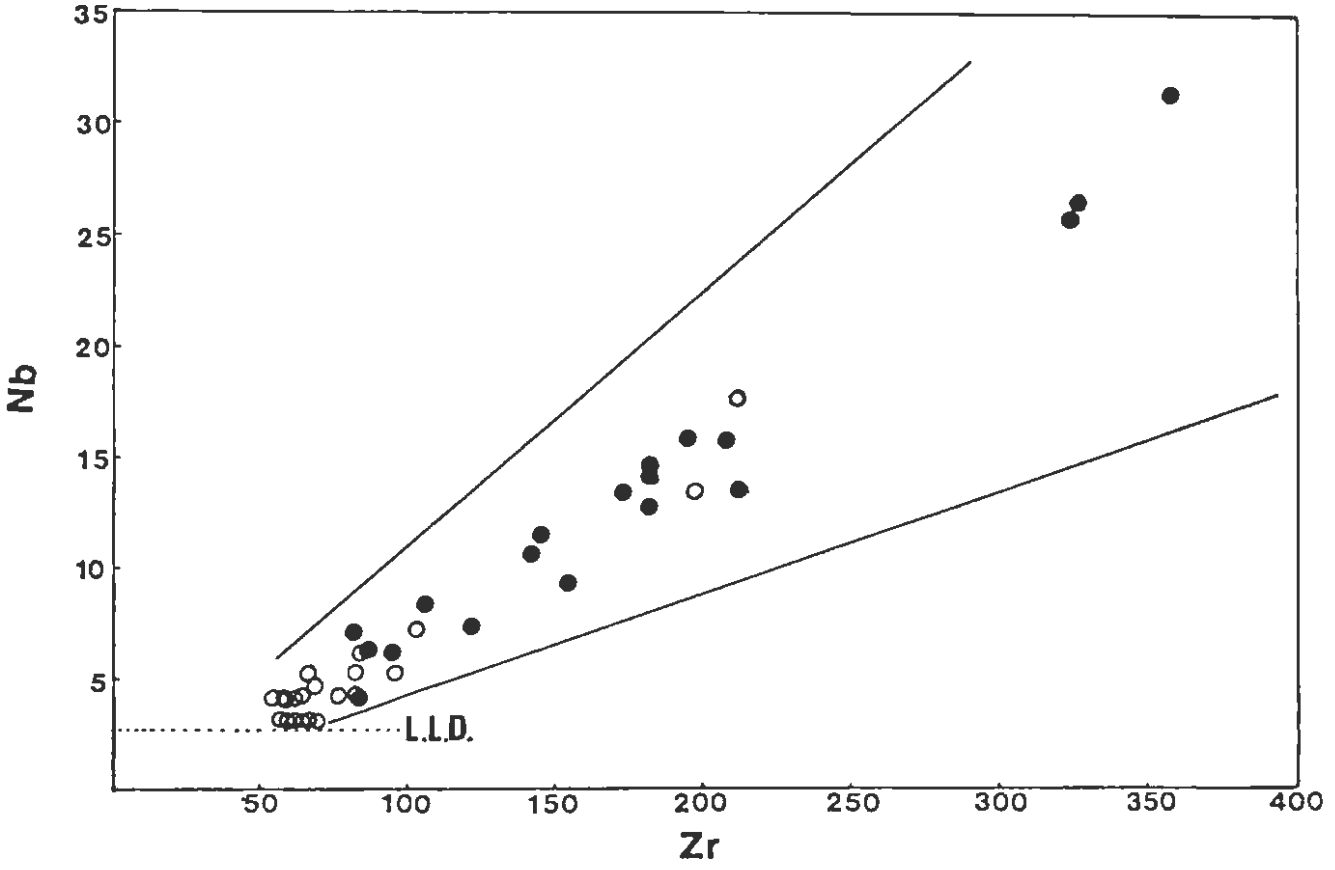

Figure 31K

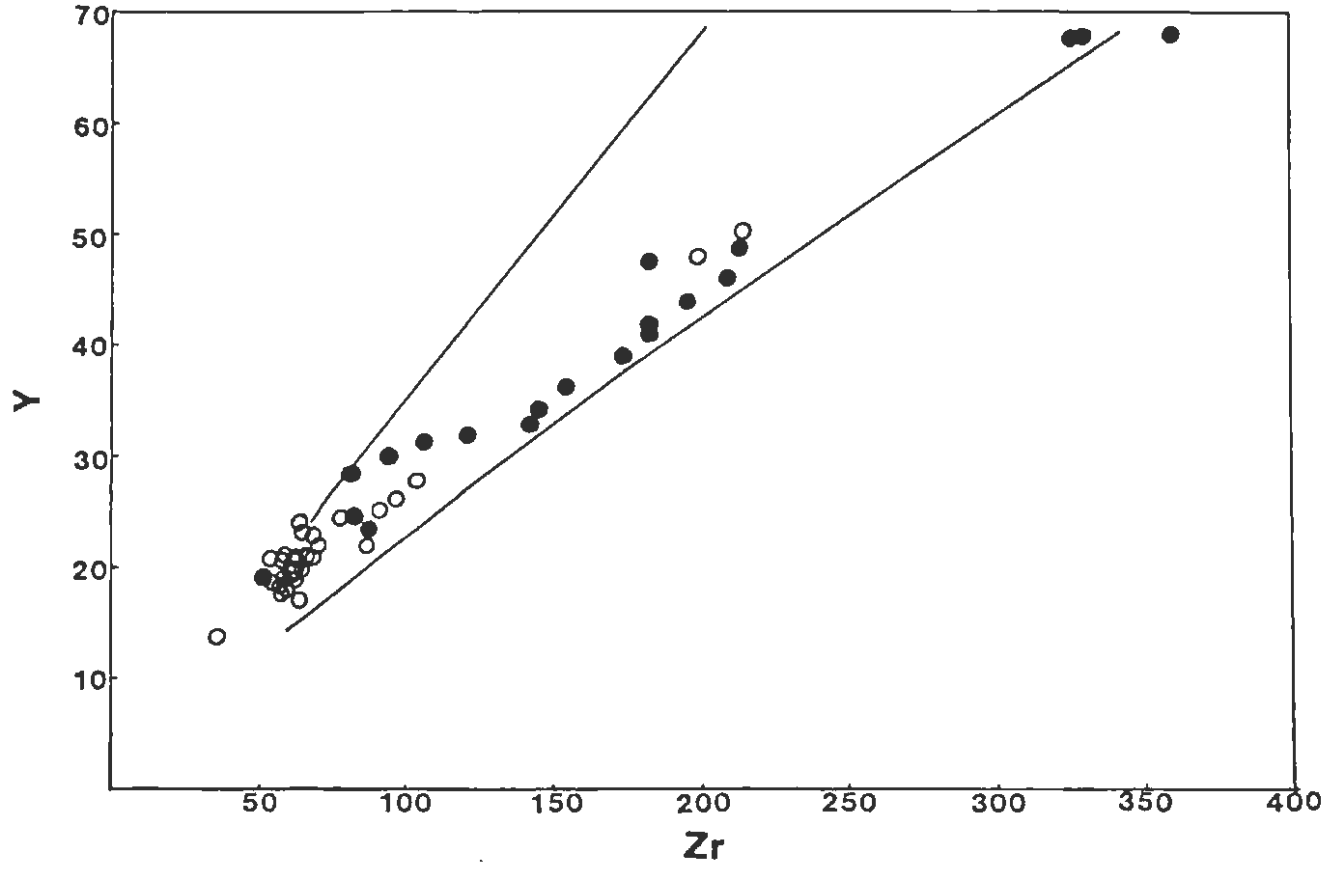

Figure 31L

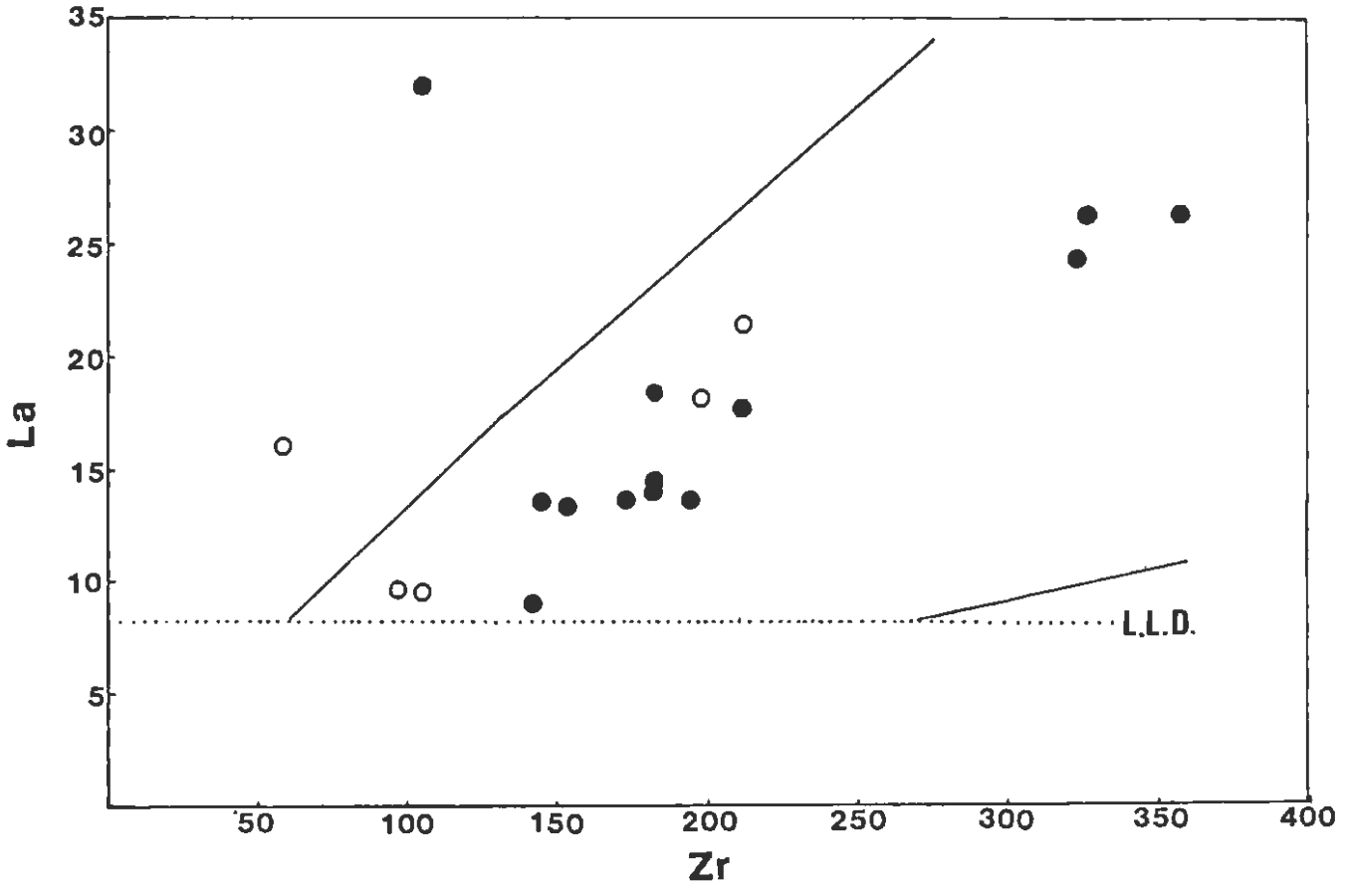

Figure 31M

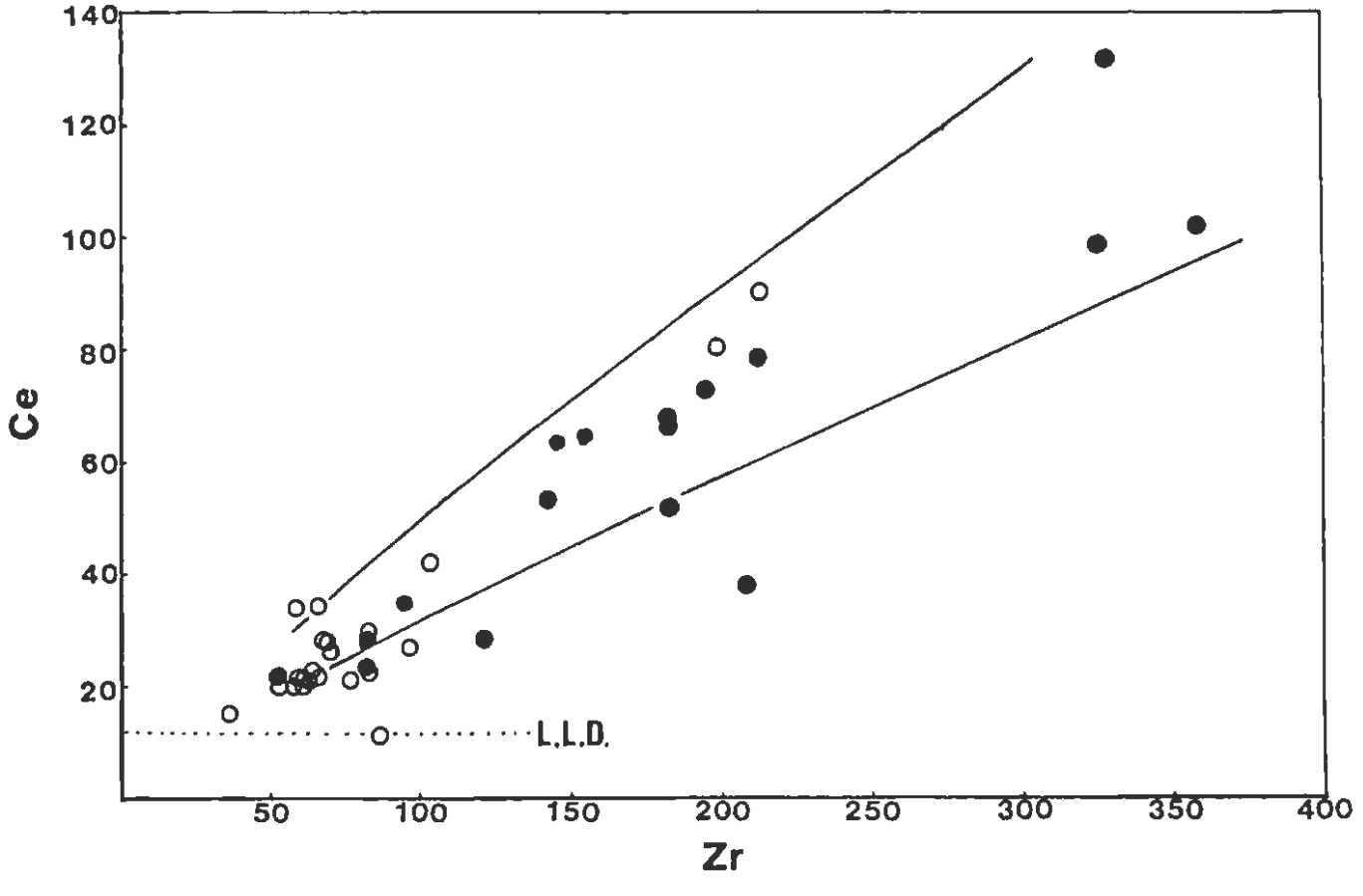

Figure 31N

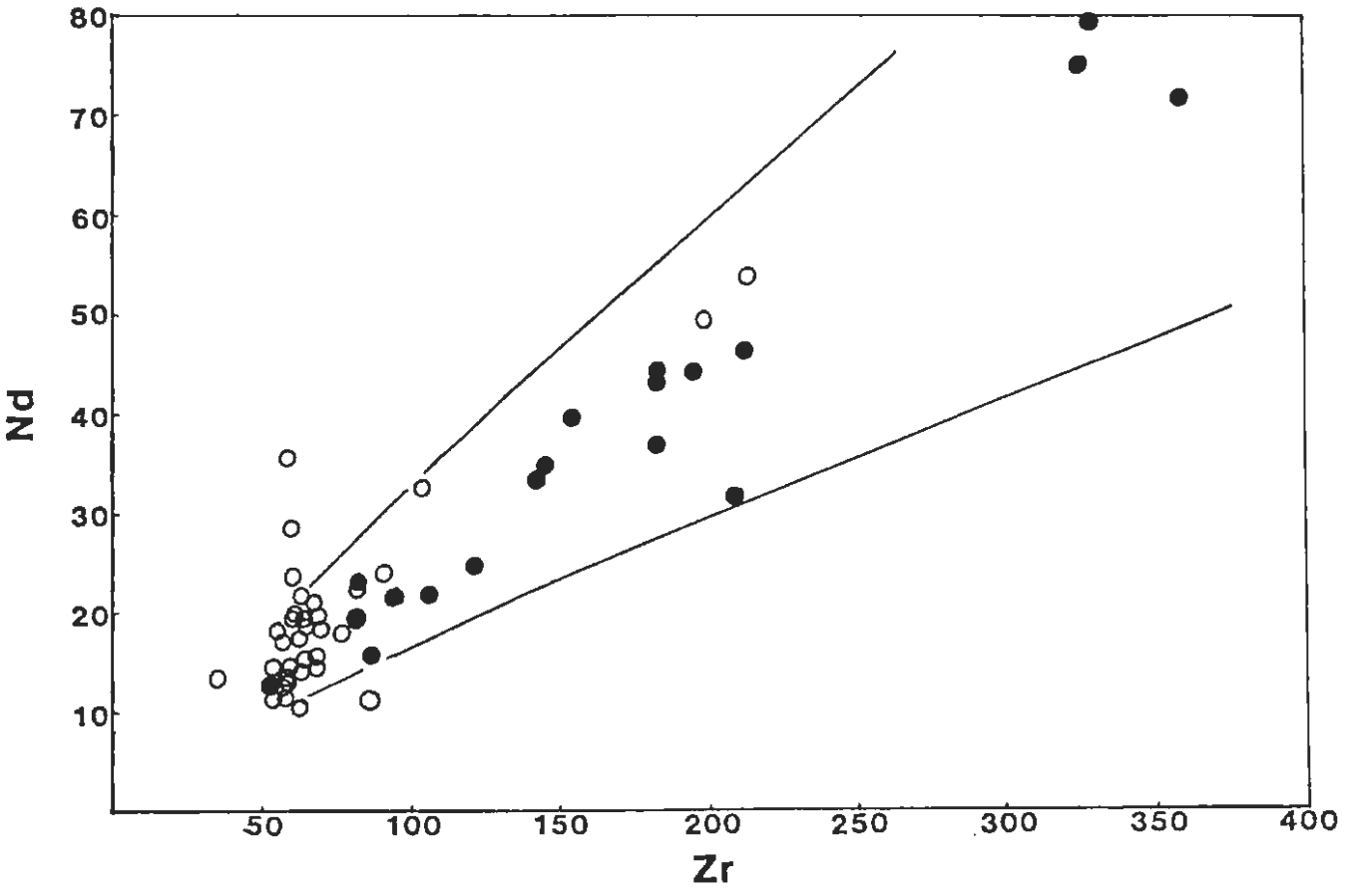

Figure 310

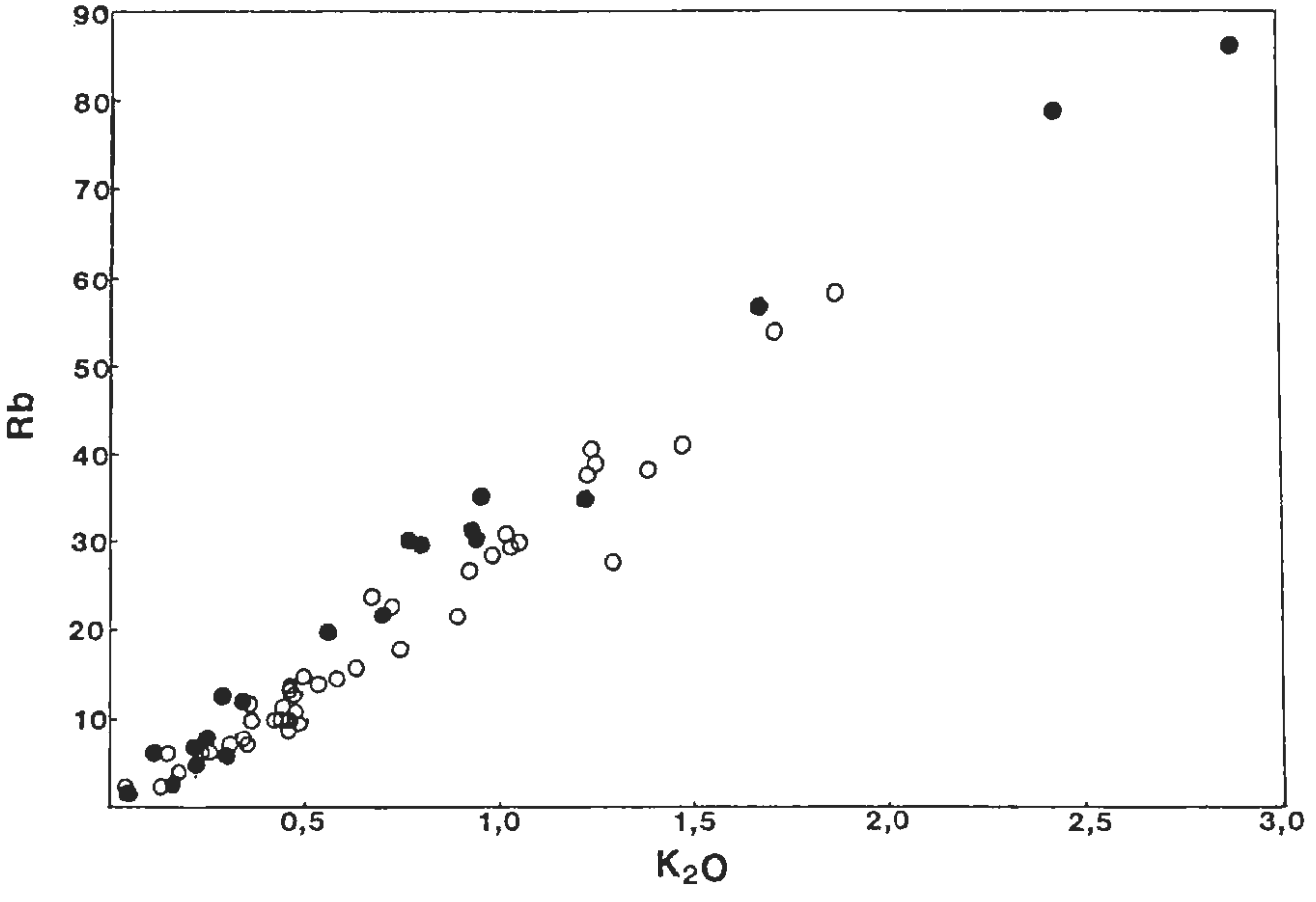

Figure 31P Trace element variation diagram (in parts per million) using K_2O as the abscissa

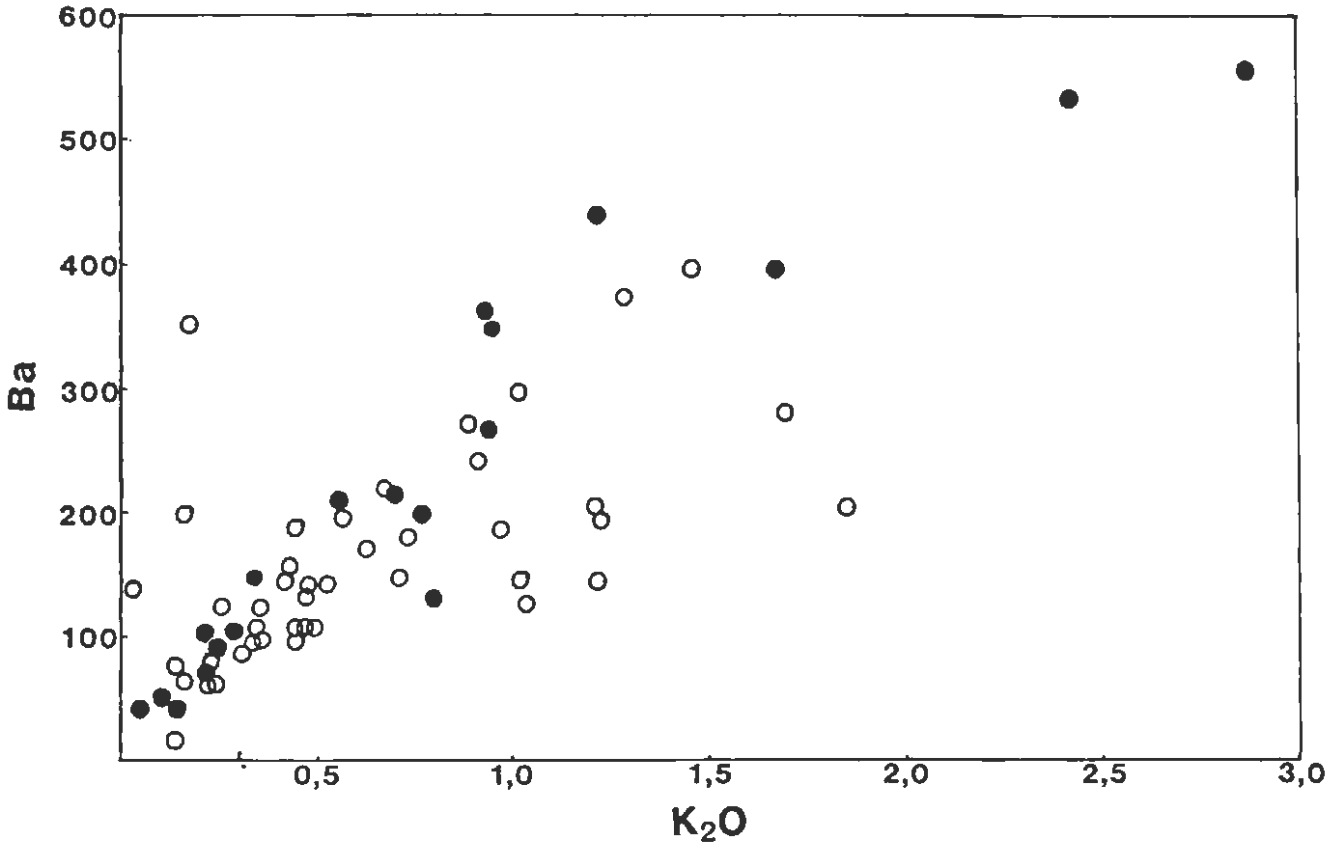

Figure 310 Trace element variation diagram (in parts per million) using K_2O as the abscissa

5.5 Trace Element Geochemistry

5.5.1 Introduction

Variations in sixteen trace elements are presented diagrammatically in Figures 31A to O, using Zr as an index of differentiation. Trace element variation diagrams, interelement ratios and spidergrams are discussed in this chapter to verify conclusions suggested by major element compositions and to form a realistic differentiation model that accounts for both major and trace element variation.

5.5.2 Theoretical background to trace element modelling

To account for the observed compositional variation in the suite of Dordabis Formation lavas, several processes, namely alteration, fractional crystallisation, melting of the upper mantle, mixing of magmas and crustal contamination, need to be evaluated. The effects of alteration and especially metamorphism on the chemistry of the lavas has already been discussed in section 5.2. In trace element modelling it is essential to be able to quantitatively measure the affinity of an element for a crystal or a melt phase. It is assumed that trace elements obey Henry's law for dilute solutions when partitioning between two phases in a silicate solution. This leads to the relationship:

$$\frac{[X]\ \text{crystal}}{[X]\ \text{liquid}} = K_D$$

where [X] is the concentration of the trace element X and K_D is the distribution or partition coefficient for a given crystal-liquid equilibrium.

When modelling the evolution of a magmatic liquid it is necessary to quantify its equilibrium with a number of mineral phases. The bulk distribution coefficient (D) is used. It is calculated from the weight proportions (W) of each mineral in the assemblage and can be represented by the expression:

$$D = \sum_{i=1}^{n} W_i\ K_{Di}$$

Equilibrium crystallisation and fractional crystallisation are two end members which best describe crystallisation models. The former assumes equilibrium between the whole of the crystallising solid and melt whereas the latter assumes equilibrium between the surface of the crystallising phases and the melt. For simplification, only fractional crystallisation is considered, because most natural systems cool relatively rapidly and hence only surface equilibrium exists. The equation for fractional crystallisation, as given by Greenland (1970) is:

$$C_l/C_i = F' (D_s-1)$$

where F' is the fraction of liquid remaining, C_i and C_l are the concentration of a given trace element in the initial melt and differentiated liquid respectively. D_s is the bulk distribution coefficient for crystallising solids.

Batch melting and fractional melting are two end member models for melting. Batch melting occurs when there is continuous equilibrium of the liquid phase with the residual solid until the liquid is removed from the solid. Fractional melting takes place when fractions of the melt are continuously removed from the residual solid. Batch melting is usually considered to be far more realistic than the physically unlikely fractional melting. The equation for batch melting, as given by Shaw (1970) is:

$$C_l/C_o = \frac{1}{D_o + F(1-D_o)}$$

where F is the weight fraction of the melt relative to the residual parent, C_o and C_l are initial trace element concentration of the solid and liquid respectively and D_o is the bulk distribution coefficient of the residual solid.

A problem with trace element modelling is selecting a suitable set of partition coefficients. The review of Irving (1978) and the work of Mysen (1978) have shown how varying temperatures, pressures, crystal growth rates, trace element diffusion, melt composition and structure effect distribution coefficients. Distribution coefficients therefore change continuously during fractionation. A set of partition coefficients appropriate to the Dordabis lava variation trends was selected from available literature and is provided in Table 6.

Table 6 Selected partition coefficients for trace elements in the tholeiitic basaltic assemblage

	Olivine	Clinopyroxene	Plagioclase
D_{Ti}	0,025 (1)	0,35 (1)	0,045 (1)
D_{Y}	0,01 (1)	0,5 (1)	0,03 (1)
D_{Zr}	0,01 (1)	0,1 (1)	0,01 (1)
D_{Nb}	0,01 (1)	0,1 (1)	0,01 (1)
D_{p}	0,043 (2)	0,009 (2)	0,024 (2)
D_{Zn}	1,80 (3)	0,5 (4)	0,13 (3)
D_{Cu}	0,02 (3)	0,18 (4)	0,004 (3)
D_{Ni}	$\frac{124,13}{MgO}$ - 0,897 (5)	1,42-2,11 (6)	0,08 (7)
D_{Co}	1-7 (8)	0,5-2,0 (9)	0,03 (3)
D_{Cr}	0,6 $\pm$ 0,2 (10)	4,72-11,43 (6)	0 (11)
D_{V}	0,05 (12)	0,06-3,4 (13)	0,05 (11)
D_{La}	0,0021 (14)	0,084 (14)	0,2 (15)
D_{Ce}	0,0005 (16)	0,098 (16)	0,2 (16)
D_{Nd}	0,001 (16)	0,21 (16)	0,14 (16)

(1) Pearce and Norry (1979) (2) Anderson and Greenland (1969)
(3) Paster et al. (1974) (4) Bougault and Hekinian (1974)
(5) Hart and Davis (1978) (6) Dale and Henderson (1972)
(7) Le Roex (1980) (8) Irving (1978)
(9) Lindstrom and Weill (1978) (10) Lindstrom (1976)
(11) Bender et al. (1984) (12) Duke (1976)
(13) Ringwood (1970) (14) Frey et al. (1974)
(15) Mann (1983) (16) Hanson (1980)

Crustal contamination is the bulk assimilation of crustal rocks by a magma and in a magma chamber contamination is usually associated with fractional crystallisation. DePaolo (1981) presented a general equation describing a coupled assimilation-fractional crystallisation model:

$$\frac{dCm}{dt} = \frac{M_a}{M_m}(C_a - C_m) - \frac{M_c}{M_m}(D - 1)\,C_m$$

where M_m is the mass of the magma body, M_a is the rate of assimilation of wallrock, M_c is the rate at which fractionating phases are separated from the magma, C_m is the concentration of the element in the magma, C_a is the concentration of the element in the assimilated wallrock and D is the bulk partition coefficient.

5.5.3 Systematic description

The partition of elements between a melt and cumulus phases depends on factors such as ionic radius, charge balance (Goldschmidt, 1954),

electronegativity and crystal field stabilisation energy (CFSE) (Williams, 1959). The CFSE of transition metals in a crystal site is of particular importance in determining the way in which these ions partition into various phases (Campbell and Borley, 1974).

A feature of the variation diagrams is that the partially mobile and immobile element concentrations of the Opdam lavas exhibit a wide range for incompatible elements, and a narrow range for compatible elements. Conversely, most Bitterwater lavas exhibit a restricted range for incompatible elements, but a wide range for compatible elements.

A. The mobile trace elements

The trace elements Ba, Sc, Co, Rb and Sr have been mobilised and therefore display no systematic trends when plotted against Zr (Figs. 31A to E). There is little difference in the concentrations of these elements when data for the Bitterwater Member are compared with those for more evolved Opdam Member. Within both members the ranges in concentration are as follows: 18 to 555ppm Ba; 25 to 52ppm Sc; 46 to 77ppm Co; 2 to 86ppm Rb and 56 to 447ppm Sr.

Despite their lack of correlation with Zr, the elements Rb and Ba are strongly correlated with K_2O (Fig. 31P and Q). The coherent behaviour of these elements in magmatic processes is well known (Goldschmidt, 1954) and data presented here indicates that this behaviour persists during both greenschist facies metamorphism and alteration processes described in section 5.2.5.

B. The partially mobile trace elements

(i) Zinc (Zn)

Zinc has zero octahedral site preference energy (OSPE) (Burns, 1970) and therefore discriminates against octahedral sites in ferromagnesian silicates. Zn^{2+} substitutes into tetrahedral co-ordinated sites (Burns, op. cit.) and therefore has high partition coefficients for magnetite and certain other sulphide phases that can occur in basaltic systems. The Zn content increases with differentiation in the Dordabis lavas (Fig. 31F), and concentrations vary from 83 to 161ppm in the Bitterwater lavas and from 99 to 228ppm in the Opdam lavas.

(ii) Copper (Cu)

Copper concentrations show a wide scatter in the Dordabis lavas, despite which there is a suggestion of a positive correlation with Zr indicating its incompatible nature (Fig. 31G). Copper has low partition coefficients (Table 6) and is generally rejected from common fractionating phases (olivine, clinopyroxene and plagioclase) in basaltic systems. Anomalous Cu concentrations are usually associated with malachite staining, which probably resulted from the oxidation of sulphide minerals. Although these lavas were avoided during sampling, enriched concentrations up to 926ppm in sample IWJ68 were encountered. As these samples plot off any possible variation trend, they were rejected for purposes of modelling. The Bitterwater lavas have Cu concentrations ranging from 24 to 204ppm, while concentrations vary between 73ppm and 533ppm in the more evolved Opdam lavas.

(iii) Nickel (Ni)

Nickel (Ni^{2+}) preferentially enters early-crystallising olivine and pyroxene and is therefore depleted in the residual liquid. It has high OSPE and can be expected to have high partition coefficients (Campbell and Borley, 1974) (see Table 6). Nickel is depleted in the Opdam basalts (Fig. 31H) which have concentrations between 86ppm and 187ppm Ni. The Ni contents in some of the more evolved basalts tend to be anomously high, indicating that sulphides may have been present in some of these basalts. The primitive Bitterwater Member lavas have concentrations ranging from 140 to 387ppm Ni. Sample IWJ78 has a high content of plagioclase phenocrysts and therefore an anomously low concentration of 108ppm Ni.

(iv) Chromium (Cr)

Chromium (Cr^{3+}) partitions strongly into early-fractionating pyroxenes and is therefore rapidly depleted in the residual liquid. It has the highest OSPE of any transition metal ion (Campbell and Borley, 1974). This accounts for its high pyroxene partition coefficient which ranges from 4,7 to 11,4. Chromium (Cr^{3+}) has higher OSPE than Ni^{2+} and is therefore more depleted in the residual liquid.

Chromium concentrations in the primitive Bitterwater lavas are tightly clustered between 300ppm and 400ppm, although the more fractionated lavas

have as little as 107ppm. The more evolved Opdam lavas are generally depleted in Cr, with concentrations varying between 52ppm and 321ppm (Fig. 31I).

(v) Vanadium (V)

Vanadium is present in the trivalent state in most magmatic rocks. In basaltic systems V^{3+} enters into Fe^{3+}, Fe^{2+}, Ti and Mn lattice sites. It is mainly accommodated in clinopyroxene and rarely olivine, as can be seen from its partition coefficients listed in Table 6. Burns (1970) predicted that V^{3+} ions will also be enriched in the distorted octahedral sites in the epidote structure. Although a large range exists, the V contents of the Dordabis lavas are positively correlated with their Zr contents (Fig. 31J). The Bitterwater lavas generally have concentrations of between 210ppm and 280ppm vanadium. However, concentrations as low as 172ppm and concentrations as high as 373ppm were also measured in this member. Vanadium concentrations in the Opdam lavas are evenly spread between 220ppm and 422ppm.

C. The immobile trace elements

(i) Niobium (Nb), Yttrium (Y) and Zirconium (Zr)

Niobium, Y and Zr are elements with high field strength (Pearce and Norry, 1979). As a result they are usually immobile during alteration. In common basaltic systems these three elements are incompatible, with Nb and Zr having partition coefficients approaching zero. Zirconium and Nb show extensive fractionation with a ten-fold enrichment in the Dordabis lavas. Concentrations of Zr vary from 35ppm in the primitive Bitterwater basalts to 359ppm in the more evolved Opdam basalts. Yttrium exhibits a well-defined variation trend with five-fold enrichment. Niobium and Y concentrations vary from a minimum of 2ppm and 14ppm respectively in the Bitterwater Member, to a maximum of 31ppm and 68ppm respectively in the Opdam Member (Figs. 31K and L). The enrichment factor of Y is less than that of Nb and Zr because of its higher partition coefficients for clinopyroxene and plagioclase (Table 6). As with the other incompatible trace elements discussed, Nb, Y and Zr concentrations are lower in the Bitterwater lavas than in the Opdam lavas.

(ii) The rare earth elements (REE)

The rare earth elements are particularly useful in petrogenetic studies. Lanthanum (La), Cerium (Ce) and Neodymium (Nd) are geochemically very similar and are trivalent under most geological conditions, although Ce may be tetravalent under highly oxidising conditions (Hanson, 1980). Lanthanum, Ce and Nd have the greatest abundance in minerals that accept cations with a radius of about 1,0 Angstron. Partition coefficients (Table 6) indicate that these elements are rejected by the common phases crystallising from basaltic magmas (plagioclase, olivine and clinopyroxene). The lower limits of determination for La and Ce are 8,1ppm and 12,5ppm respectively (see Appendix 2). In the more primitive Bitterwater lavas most of the La concentrations, and two of the Ce concentrations are below these limits. This is further discussed in section 5.5.5. Within the Dordabis basalts the ranges in concentration are as follows: 0 to 32ppm La; 11 to 131ppm Ce and 10 to 79ppm Nd (Figs. 31M, N and O).

D. Interelement ratios

Selected interelement ratios for the Opdam and Bitterwater metalavas are listed in Table 7 and diagrammatically presented in Figure 32 (A to G). They are interpreted together with trace element data in section 5.5.4.

The K/Rb ratios in the Dordabis basalts cover a wide range, their distribution being skewed towards higher values. These ratios average 270 in the Opdam lavas and 320 in the Bitterwater lavas (Fig. 32A).

Incompatible element ratios of Y/Nb, Zr/Y and Zr/Nb are presented in Figures 32B, C and D. The ratios provide a reasonable separation between the Opdam and Bitterwater lavas. Y/Nb ratios, discounting Nb values below determination limits, range from 2,1 to 7,0 in the Dordabis metalavas, with average values of about 3,5 and 5,5 in the Opdam and Bitterwater Members respectively. Zr/Y ratios are generally higher in the Opdam basalts (2,76 to 5,28) than in the Bitterwater basalts (2,25 to 4,13). Zr/Nb ratios are similar for lavas from both members which have values ranging from 11,4 to 20,0 in the Opdam basalts and from 12,2 to 22 in the Bitterwater basalts (ratios with Nb concentrations above determination limits).

TABLE 7 SELECTED INTERELEMENT RATIOS FOR THE DORDABIS METABASALTS

OPDAM MEMBER	$\frac{K}{Rb}$	$\frac{Y}{Nb}$	$\frac{Zr}{Y}$	$\frac{Zr}{Nb}$	$\frac{Ni}{Co}$	$\frac{Cr}{V}$	$\frac{Cr}{Ni}$
IWJ143	439	9,05*	2,76	25,0*	1,87	0,63	1,38
IWJ145	192	6,93	2,89	20,0	1,59	0,19	0,54
IWJ146	150	2,19	5,28	11,6	2,10	0,30	0,78
IWJ147	498	4,82	3,18	15,3	2,02	0,56	1,49
IWJ148	256	2,58	4,84	12,5	2,34	0,33	0,81
IWJ149	276	2,65	4,80	12,7	2,31	0,23	0,59
IWJ150	224	4,29	3,83	16,4	2,20	0,54	1,21
IWJ151	246	3,62	4,36	15,8	2,06	0,19	0,64
IWJ152	290	2,86	4,40	12,6	2,36	0,41	0,72
IWJ153	244	2,92	4,47	13,1	2,55	0,52	0,92
IWJ2	222	3,43	3,33	11,4	2,44	1,12	2,21
IWJ3	144	3,89	4,29	16,7	2,64	0,61	0,99
IWJ4	256	2,92	4,47	13,1	2,69	0,46	0,73
IWJ5	260	2,93	4,52	13,3	1,77	0,31	0,93
IWJ6	166	3,10	4,36	13,5	1,88	0,25	0,56
IWJ7	262	3,00	4,27	12,8	1,85	0,22	0,60
IWJ8	238	3,75	3,84	14,4	1,91	0,23	0,81
IWJ9	282	2,80	4,45	12,5	2,00	0,33	0,84
IWJ10	380	3,67	3,73	13,7	2,89	1,02	1,29
IWJ11	236	3,75	3,40	12,8	2,22	0,70	1,54
BITTERWATER MEMBER							
IWJ12	234	11,00*	2,77	30,5*	3,21	1,52	2,40
IWJ13	334	10,00*	3,25	32,5*	2,89	1,30	1,85
IWJ14	360	7,00	3,14	22,0	3,16	1,14	1,50
IWJ15	350	6,50*	2,54	16,5*	5,40	2,56	1,14
IWJ16	340	6,00	3,00	18,0	3,20	1,69	2,08
IWJ17	352	4,50	2,83	12,8	3,35	1,65	2,08
IWJ19	276	4,75	3,16	15,0	5,17	1,66	1,59
IWJ20	264	6,67	2,95	19,7	3,81	1,51	1,50
IWJ21	262	6,67	3,10	20,7	3,90	1,53	1,59
IWJ49	260	5,75	3,13	18,0	2,43	1,36	2,30
IWJ50	366	10,00*	3,05	30,5*	3,07	1,41	1,86

* Concentrations below lower limits of determination.

TABLE 7 (continued)

BITTERWATER MEMBER	K/Rb	Y/Nb	Zr/Y	Zr/Nb	Ni/Co	Cr/V	Cr/Ni
IWJ51	284	12,00*	3,62	43,5*	2,45	0,95	1,92
IWJ52	282	5,00	2,75	13,8	3,48	1,56	1,78
IWJ53	328	9,50*	2,90	27,5*	3,09	1,52	2,08
IWJ54	310	9,00*	3,22	29,0*	2,95	1,49	2,09
IWJ56	266	10,00*	3,20	32,0*	3,57	1,47	1,52
IWJ57	270	6,33	3,00	19,0	2,62	1,31	2,32
IWJ58	388	9,00*	2,83	25,5*	3,11	1,69	2,12
IWJ59	290	9.00*	3,06	27,5*	3,85	1,68	1,73
IWJ60	288	4,25	3,24	13,8	3,85	1,57	1,51
IWJ61	282	5,75	3,39	19,5	3,41	1,23	1,48
IWJ62	264	4,20	3,14	13,2	2,75	1,11	1,73
IWJ64	372	10,00*	2,55	25,5*	2,95	1,79	2,37
IWJ89	414	9,50*	3,11	29,5*	3,92	1,41	1,40
IWJ88	398	5,67	3,24	18,3	3,88	1,41	1,41
IWJ87	366	5,00	3,00	15,0	3,78	1,41	1,41
IWJ86	342	5,67	3,18	18,0	3,37	1,49	1,79
IWJ85	346	10,00*	2,75	27,5*	3,14	1,63	2,07
IWJ84	514	4,50	3,06	13,8	2,86	1,64	2,49
IWJ83	192	5,00	3,00	15,0	3,28	1,39	1,88
IWJ82	252	7,50*	3,67	27,5*	3,00	1,38	2,29
IWJ79	340	9,00*	2,94	26,5*	3,02	1,31	1,84
IWJ68	-	11,50*	2,61	30,0*	6,00	1,30	1,07
IWJ69	316	4,75	3,11	14,7	5,39	1,37	0,87
IWJ70	430	9,00*	3,00	27,0*	3,65	1,37	1,38
IWJ71	300	4,00	3,15	12,6	3,60	1,32	1,41
IWJ72	318	9,00*	3,22	29,0*	4,58	1,41	1,15
IWJ73	296	2,88	2,25	12,2	2,15	0,48	1,16
IWJ74	274	3,62	4,13	14,9	2,92	0,36	0,75
IWJ75	368	3,85	3,70	14,3	3,79	1,43	1,30
IWJ76	286	4,60	3,44	15,8	4,02	1,38	1,22
IWJ77	390	5,00	3,68	18,4	3,47	1,57	1,74
IWJ78	298	3,50	3,91	13,7	2,36	0,84	1,41

* Concentrations below lower limits of determination.

Figure 32(A-G) Selected inter-element ratio diagrams where each shaded square represents an Opdam sample and each unshaded square a Bitterwater sample.

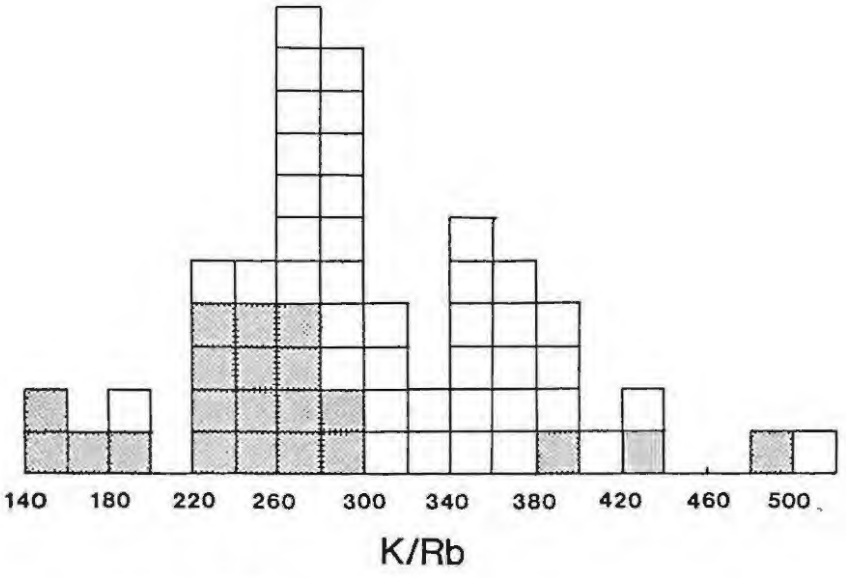

Figure 32A

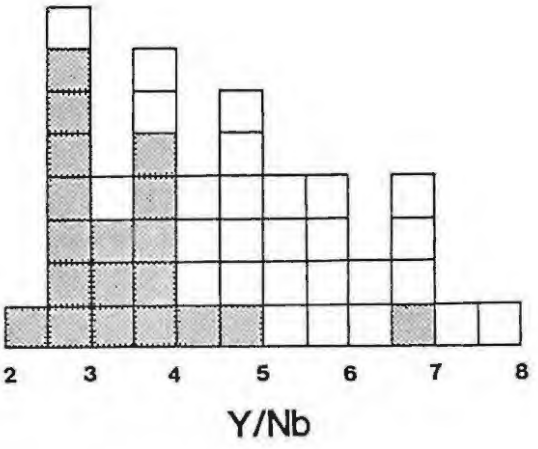

Figure 32B

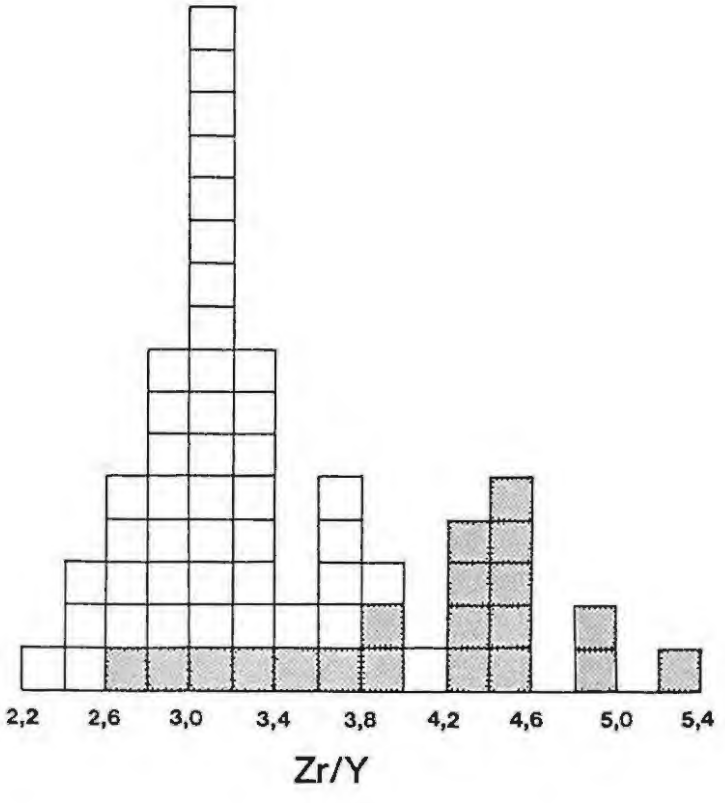

Figure 32C

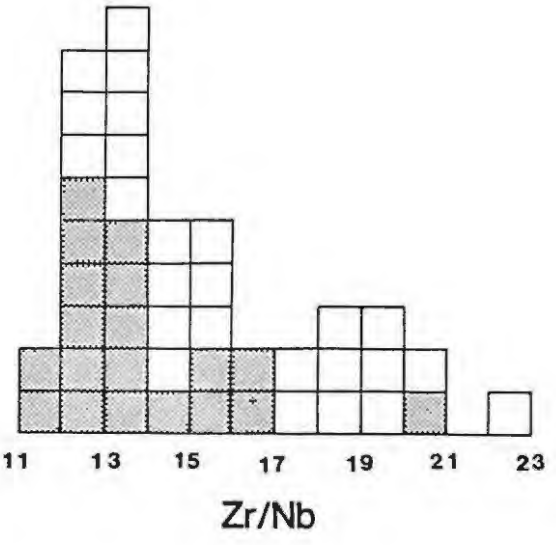

Figure 32D

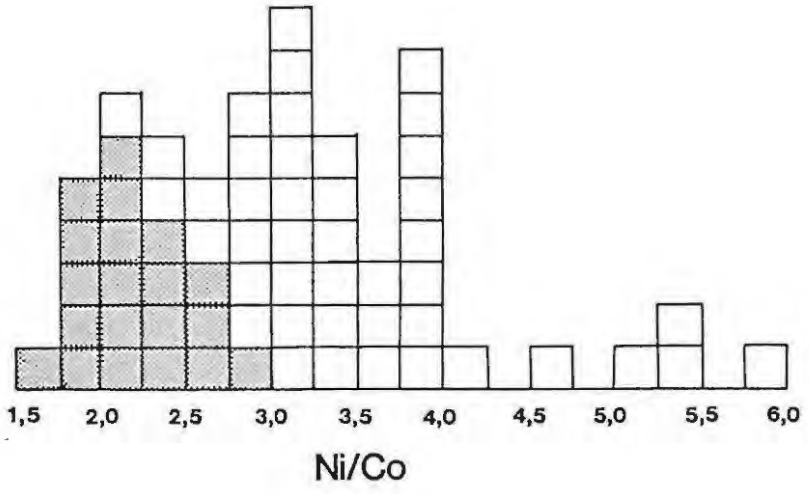

Figure 32E

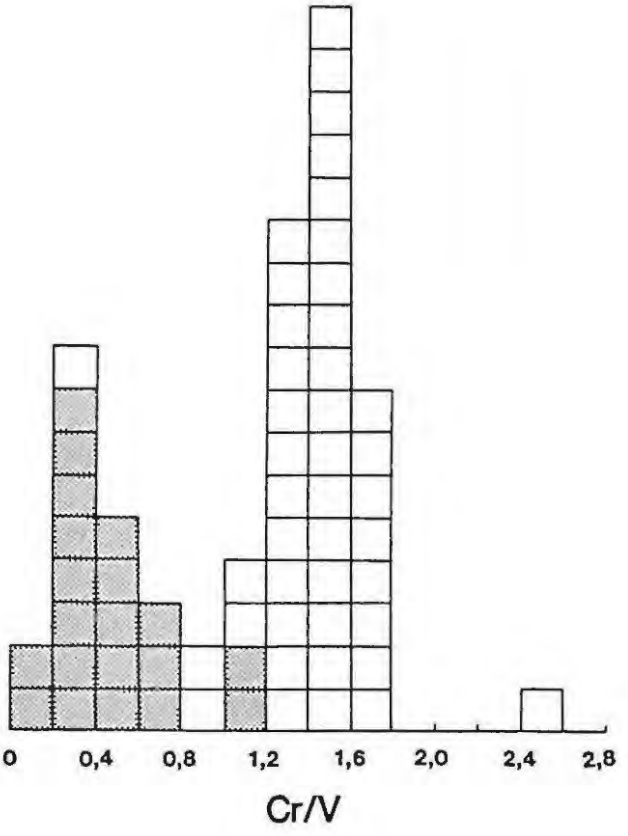

Figure 32F

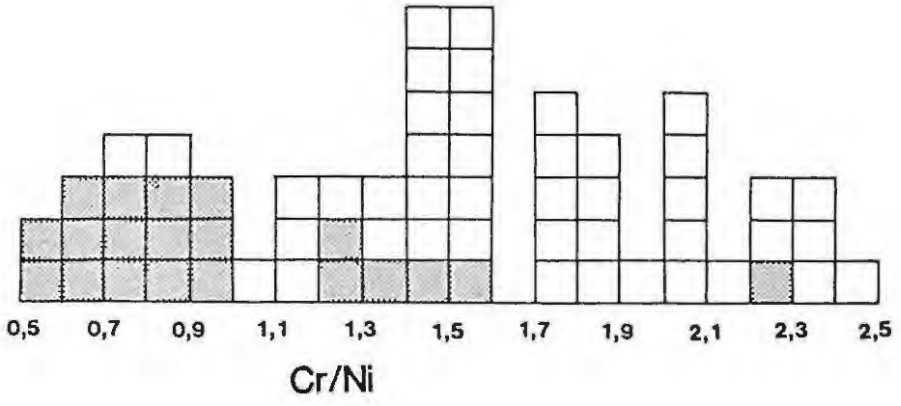

Figure 32G

Ratios involving trace elements of different compatibilities change during differentiation. Ni/Co and Cr/V ratios are generally lower in the more evolved Opdam basalts, which have values averaging about 2,2 and 0,4 respectively, than in the more primitive Bitterwater basalts, with average values of about 3,5 and 1,5 respectively (Figs. 32E and F). This separation is not as well defined by the compatible element ratio, Cr/Ni. The Opdam metalavas however generally have lower Cr/Ni ratios (0,5 to 1,6) than the Bitterwater metalavas which show a wide variation of values ranging from 0,75 to 2,49.

5.5.4 Petrogenesis of the Dordabis Formation lavas

In this section trace element variation data are used to construct the best feasible model for the genesis of the Dordabis metalavas. Trace element models including crustal contamination, magma mixing, source heterogeneity, fractional crystallisation and partial melting are evaluated before the applicable model is discussed in terms of the quantitative trace element theory summarised in section 5.5.2.

If either a two-component magma mixing model, or a crustal contamination model is used to describe the variation trends on Figures 30 and 31, the two components mixing must have compositions that fall at either end of the variation trends. One component clearly must have a composition similar to that of the least evolved basalt (sample IWJ15). The other component must have a more evolved composition with greater than 4,5% TiO_2, 19% Fe_2O_3, 0,28% MnO, 0,6% P_2O_5, 240ppm Zn, 430ppm V, 32ppm Nb, 70ppm Y, 25ppm Cu, 120ppm Ce and 80ppm Nd, and less than 14% Al_2O_3, 5% MgO, 5% CaO, 100ppm Ni and 100ppm Cr. This is an improbable crustal composition, and also an unlikely composition of a melt of the crust or a melt of the mantle. Crustal contamination and magma mixing are therefore unlikely to have caused the variation trends noted in the Dordabis lavas.

Immobile trace element data for the primitive Bitterwater and the more evolved Opdam lavas plot in well-defined overlapping variation trends (Figs. 31K to O) suggesting that these two members are cogenetically related by partial melting of a common source or fractional 93ystallisation of a common parent magma. Limited degrees of fractional crystallisation (up to 70%) result in extreme depletion of compatible elements in later liquids, but little variation in incompatible

element concentrations. Fractional crystallisation also results in parallel shifts of chondrite-normalised REE patterns for fractionated cogenetic lava suites. On the other hand variable degrees of partial melting may result in limited depletion of compatible elements in the melt. In deep continental crust partial melting can enrich incompatible elements (e.g. light REE), relative to the more compatible elements in the melt. This is because garnet and clinopyroxene are expected to be important residual phases during small degrees of melting, resulting in partition coefficients for heavy REE and Y approaching unity (Cox et al., 1979). Direct partial melts of the mantle generally also have Mg#$>$67 (Kesson, 1973).

The rapid depletion of the immobile elements Cr and Ni, the overall parallel nature of the REE patterns and a Mg# generally less than 67 indicate that the Dordabis lavas are probably related mainly by fractional crystallisation. Quantitative trace element models explained in section 5.5.2 have been used to develop a model of fractional crystallisation for the Dordabis lavas. A number of assumptions made in modelling variation trends are discussed below.

Partition coefficients listed in Table 6 show that, in contrast to olivine, pyroxenes accept more Cr than Ni. The Cr/Ni ratio should therefore decrease with increasing pyroxene-controlled fractionation and increase with fractionation dominated by olivine. The generally low Cr/Ni ratios in the Dordabis basalts, especially in the Opdam member, indicate that pyroxene dominates the mafic component of the fractionating assemblage.

The Dordabis lavas have been altered (see section 5.2) making estimations of primary mineral proportions difficult. Major element geochemistry illustrates that fractionating minerals included substantial amounts of plagioclase ($<$70%), clinopyroxene and olivine, while Cr/Ni ratios show that pyroxenes dominated the mafic component of the fractionating assemblage. However, exact proportions of fractionating phases are required to model variation trends.

Biggar (1983) illustrated that to produce a tholeiitic daughter liquid by fractional crystallisation of a mantle melt, augite, plagioclase and olivine can only crystallise in the limited range of 30:50:15 to 20:60:20. For quantitative modelling purposes, the primary melt which

resulted in the Dordabis lavas was assumed to have precipitated 30% augite, 50% plagioclase and 15% olivine and to have contained 55ppm Zr. Two limiting concentrations of other trace elements modelled were estimated for this original melt. Bulk distribution coefficients were calculated using selected partition coefficients listed in Table 6. Variation trends are modelled and plotted as lines on Figures 30B and J and on Figures 31F to O.

The compatible elements, Ni and Cr, although spread over a fairly wide range, fall reasonably within the limits of the modelled trace element concentrations (Fig. 31H to I). The incompatible immobile elements TiO_2, P_2O_5, Nb and Y are progressively enriched in the more evolved lavas of the Dordabis Formation. Concentrations of these elements plot almost exclusively within the modelled envelopes on Figures 30B and J, and Figures 31K and L). TiO_2 and P_2O_5 behave essentially as trace elements and have therefore been modelled as such. The slightly mobile incompatible elements Zn, Cu, V, La, Ce and Nd, although spread over a wider range, are progressively enriched in the more evolved lavas and plot to varying degrees within the modelled envelopes (Figs. 31F, G, J, M, N and O). An exception is sample IWJ78 which plots outside modelled envelopes on many diagrams, because of the large amounts of feldspar phenocrysts present.

Ratios of incompatible, immobile trace elements should remain nearly constant during fractional crystallisation in a basaltic system. However, the more evolved Opdam basalts have lower Y/Nb and higher Zr/Y ratios than the primitive Bitterwater basalts (Figs. 32B and C). This can be explained by the fact that Y is the least incompatible of the common immobile, incompatible trace elements Y, Zr, Nb (see Table 6). A slightly greater fractionation of ratios involving Y during fractional crystallisation would therefore be expected. This can be seen by the better separation of the Opdam lavas from the Bitterwater lavas on the Y/Nb and Zr/Y diagrams (Fig. 32B and C), than on the Zr/Nb diagram (Fig. 32D).

K/Rb ratios higher than 400 (K/Rb ratio for chondritic meteorites (Beswick, 1976)) are normally characteristic of basaltic rocks, with the exception of continental tholeiites. There is controversy as to why

continental tholeiitic basalts have low K/Rb ratios (Compston et al., 1968). It may reflect either conditions in the upper mantle or selective contamination processes affecting the magma as it ascends through the K- and Rb-rich environment in the continental crust . Spidergrams (section 5.5.6) indicate that in the Dordabis lavas, primordial normalised K and Rb values are enriched relative to Sr, P and Nb values. This suggests minor assimilation of granitic crust before the commencement of the fractionation or a mantle source that has been metasomatically enriched in K and/or Rb. It is therefore not possible to resolve the cause of the low K/Rb ratios in the Dordabis lavas. However, the ratios of less incompatible to more incompatible elements is low (average Zr/Nb ratio for the Opdam basalts is about 13). This probably reflects conditions in the source material rather than crustal assimilation.

Low-pressure fractional crystallisation models can explain variations in the trace element concentrations in the cogenetic Dordabis lavas. Before any final conclusions can be made anomalous REE behaviour should be examined.

5.5.5 Anomalous REE behaviour

An aspect of REE is that Y is assumed to behave coherently with dysprosium (Dy) (Herrmann, 1978). Chondrite-normalised Y and Dy abundances should be similar in the Dordabis lavas. Even if these abundances were to vary by a factor of two, the shape of th REE diagrams (Figs. 33A to C) would not change. However a difference as large as this would not be expected, and it can be assumed that heavy REE/chondrite abundances are depleted with respect to light REE in the Dordabis metalavas. The anomalously low La and Ce concentrations in some of the lavas must be accounted for. The problem arises of trying to establish whether this depletion is a result of analytical errors, alteration, or is a primary feature of the magmas.

In assessing analytical errors it is important to note that the technique used, X-ray fluorescence spectrometry (XRF), is not as precise in determining REE concentrations as methods involving spark source mass spectrometry, neutron activation and isotope dilution (Hanson, 1980). However, samples were analysed on two separate occasions to check the authenticity of this anomalous REE behaviour. The two sets of analyses showed good reproducibility with lower limits of determination for the Dordabis lavas averaging about 13ppm Ce, about 18ppm Nd and about 8ppm La. For the Bitterwater lavas a few of the Ce determinations and 90% of

the La determinations are below the lower limits of determination. The imprecise nature of the analytical method used may have caused slight errors in the absolute concentrations of the REE determined, but it is unlikely to have caused general depletions in La or Ce.

The mobility of light REE (La, Ce and Nd) during alteration processes is controversial. Frey et al. (1974), Hellman and Henderson (1977) and Haskin et al. (1966) claimed that REE can be mobile during alteration processes like spilitisation, while other authors (O'Nions and Pankhurst, 1974) claimed that REE are relatively immobile during alteration processes. The REE contents exhibit well defined correlation with the Zr concentrations in the Dordabis lavas (Figs. 31 M, N and O). As discussed in section 5.2.5 mobilisation of an element has usually resulted in the scattering of the plotted data points on such variation diagrams. Mobility of light REE concentrations could explain the occasional large deviations from trends on the REE versus Zr graphs, but the regularity of the overall REE trends probably represents an original igneous pattern.

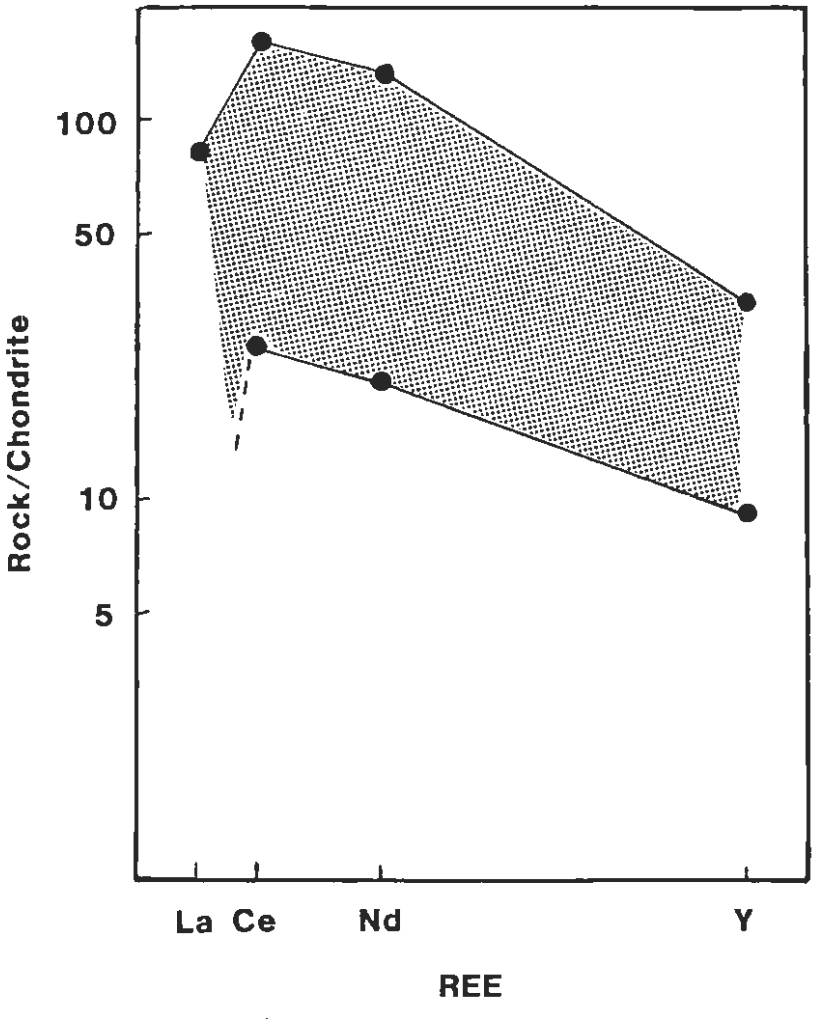

Figure 33A Chondrite-normalised REE variation in the Opdam metabasalts (Solid lines represent REE concentration limits)

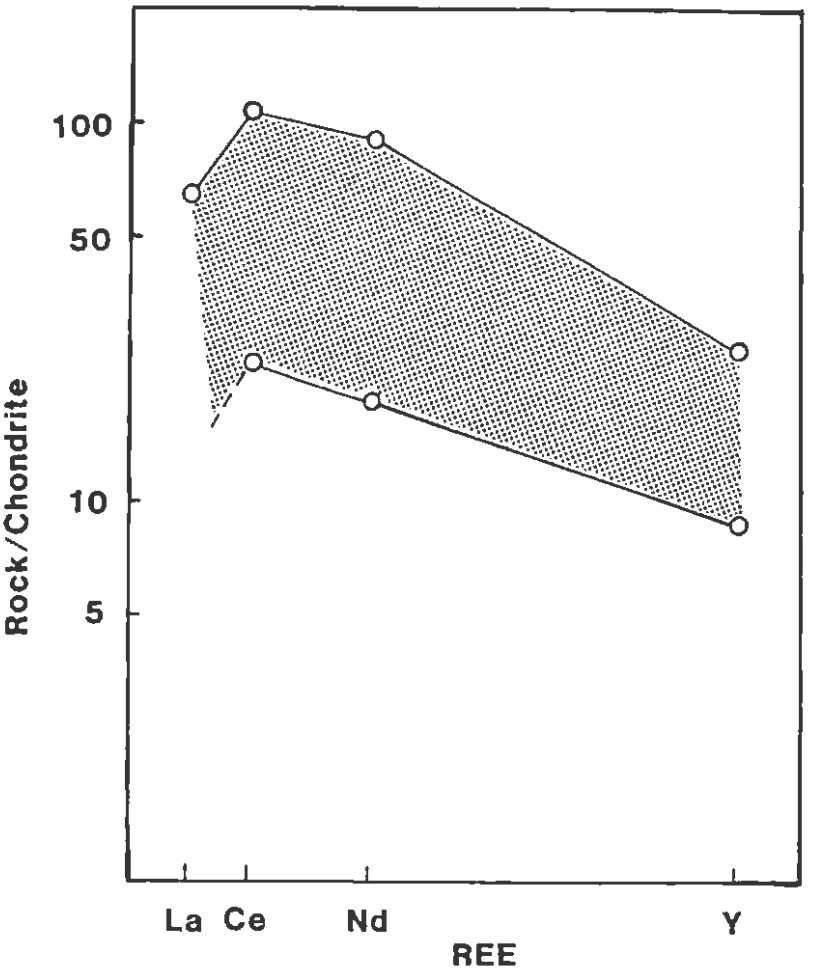

Figure 33B La-depleted chondrite-normalised REE variation in the Bitterwater metabasalts (solid lines represent REE concentration limits)

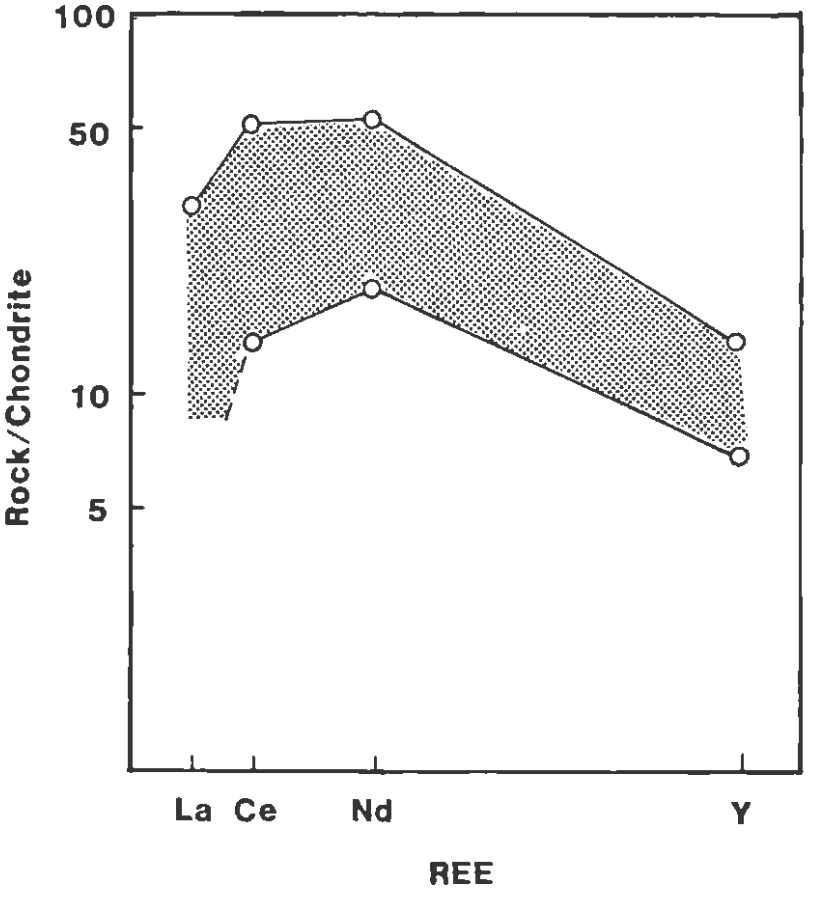

Figure 33C La- and Ce-depleted A chondrite-normalised REE variation in the Bitterwater Metabasalts (solid lines represent REE concentration limits).

Chondrite-normalised light REE depletion has been noted in a variety of locations such as ocean-ridge basalts and island arc tholeiites (Jahn et al., 1974). The more evolved Opdam lavas are however generally only depleted in La (Fig. 33A). The Bitterwater lavas can be grouped into those depleted only in La (Fig. 33B) and those depleted in both La and Ce (Fig. 33C). All three groups have light REE relatively enriched over Y, and hence presumably enriched over heavy REE contents. Although unusual, REE patterns similar to those of the Dordabis lavas, i.e. with anomalously low Ce and La, have been noted by Jahn et al., (1980) in the Kuhno continental tholeiitic basalts. The general parallel nature of the REE patterns, ranging from the primitive to the more evolved lavas of the Dordabis Formation is consistent with a fractional crystallisation model. La and Ce depletion has probably been inherited from the source material because it cannot be adequately explained by analytical error, alteration or fractionation. The problems discussed with the interpretations of the limited REE data available for the Dordabis volcanic rocks, make further discussion based on its quantitative nature futile.

5.5.6 Spidergrams

Spidergrams have recently become popular amongst geochemists. They are used to compare the compositions of groups of igneous rocks and to recognise diagnostic chemical characteristics of igneous suites. The abundances in the Dordabis lavas of the elements presented on the spidergram (Fig. 34) have been normalised to the primordial mantle values of Wood et al. (1979). Although alteration has caused considerable scatter in the concentrations of some of the more mobile elements in the Dordabis basalts, there is no evidence to suggest that there has been a nett loss or gain in the concentrations of these elements. The average composition of these lavas will therefore probably crudely represent their original composition.

A basalt originating from a primordial mantle source undergoing extensive melting would give a flat spidergram pattern, but if the melt fractions were small the resulting spidergram would slope smoothly downwards from Rb to Y, probably flattening between La and Ba (Thompson et al., 1983). Despite peaks and troughs, primordial normalised abundances for the Dordabis lavas generally decrease from Rb to Y, suggesting that they resulted from a mantle that had undergone small degrees of melting. This conclusion is only valid provided it is assumed that the mantle has

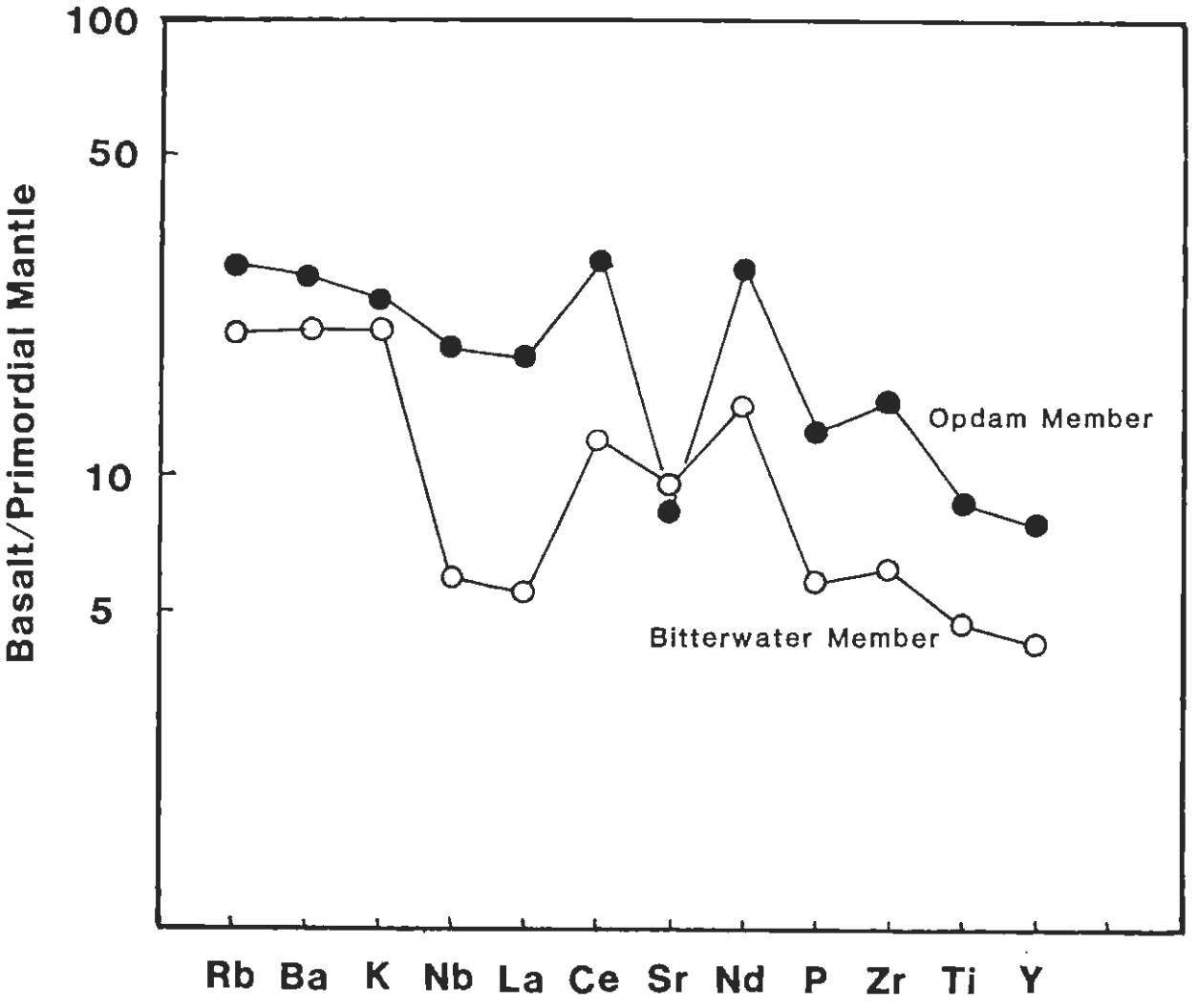

Figure 34 Spidergrams derived from average trace element concentrations of the Opdam and Bitterwater metalavas

primordial relative concentration of incompatible elements. Alternatively this relative depletion may reflect the primary patterns of the source. The Opdam and Bitterwater metalavas have similar patterns with negative anomalies at Nb, La and Sr and peaks at Nd and possibly Ce (Fig. 34). Anomalies can usually be ascribed to factors like source compositions, partial melting, fractional crystallisation or contamination by crustal materials. The negative anomaly at Sr probably resulted from fractional crystallisation of plagioclase from these basalts. The Sr anomaly is greater in the Opdam basalts than in the Bitterwater basalts, indicating that the Opdam lavas probably underwent a greater degree of plagioclase fractionation. This is in accordance with trace element data which indicates that the Opdam lavas are more evolved, and have undergone a greater degree of low-pressure fractional crystallisation than the Bitterwater lavas (see section 5.5.4).

The negative anomaly at Nb, especially in the primitive Bitterwater basalts, is common to most continental flood basalts and arc basalts

(Briqueu et al., 1984). Geochemists do not know the reason for this depletion, although Thompson et al. (1983) and Briqueu et al. (1984) suggested that it is widely accepted that Nb is retained in a stable phase in the mantle. In section 5.5.5 it was concluded that La depletions were probably caused by a natural heterogeneity of the source material of the Dordabis basalts, and not caused by analytical errors, alteration or fractionation.

Norry and Fitton (1983) offered two possible explanations for the enrichment of K and Rb relative to Sr, P and Nb, which is so common in continental basalts. Firstly this enrichment could be due to assimilation of granitic continental crust, since all granites tend to have high values for the ratios K/Sr and Rb/Nb. Alternatively this enrichment may have occurred if the basalt source (upper mantle) had been metasomatically enriched in elements such as K and Rb. However, this was discussed in section 5.5.4 where it was concluded that these enrichments probably reflect conditions in the source material, rather than assimilation.

6. A COMPARISON BETWEEN THE DORDABIS FORMATION AND POSSIBLE EQUIVALENTS

6.1 Introduction

S.A.C.S. (1980) correlated the Sinclair Sequence with the Koras Group and 'possible equivalents' in the Rehoboth area (Fig. 35). Isotopic age determination of igneous rocks from the three areas indicate that they are broadly coeval. S.A.C.S. (1980) reported that several radiometric age measurements of the Nückopf lavas in the Dordabis-Rehoboth area range between 1080Ma and 1232Ma. Kröner (1975) obtained an age of 1265 ±10Ma using a six-point Rb-Sr whole-rock isochron on lavas from the Barby Formation of the Sinclair Sequence. A seven-point Rb-Sr whole-rock isochron on lavas from the Lambrechtsdrif Formation of the Koras group gave an age of 1176Ma (Kröner et al., 1977). It is the aim in this chapter to compare the Dordabis Formation rocks with possible equivalent formations in the Sinclair Sequence and the Koras Group.

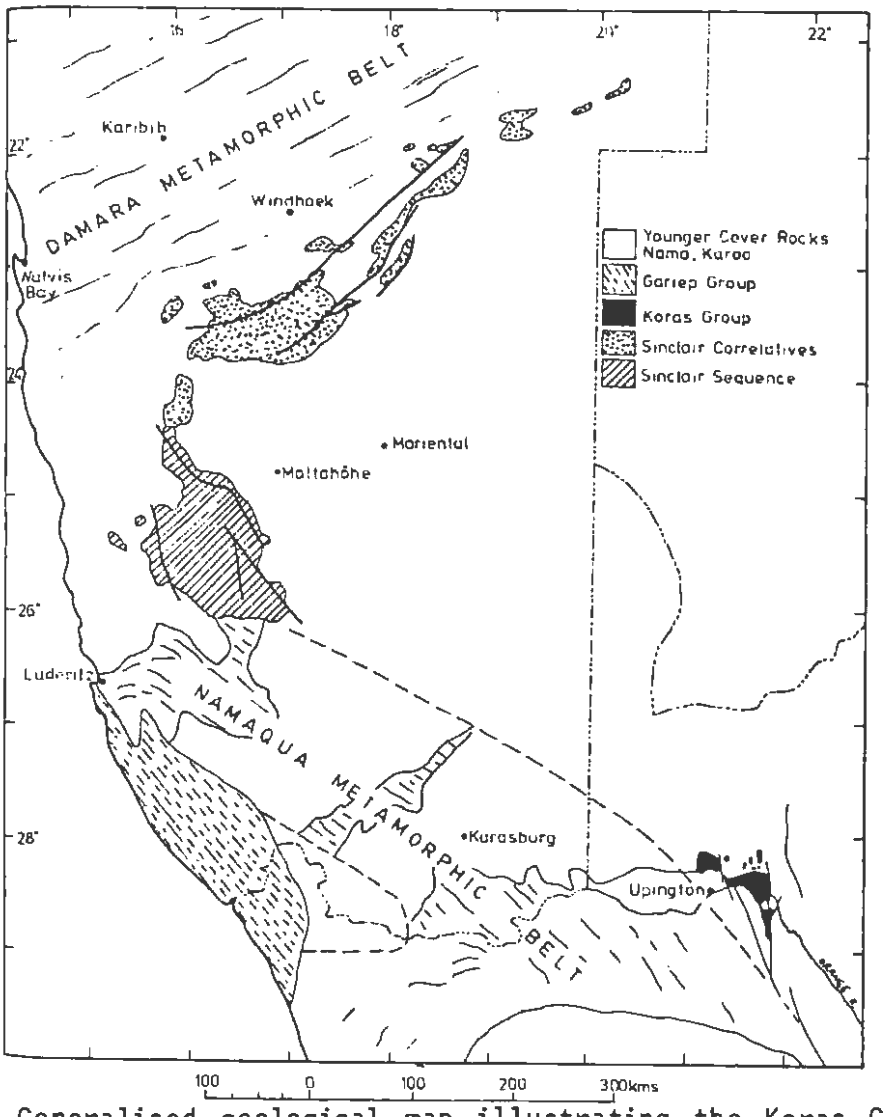

Figure 35 Generalised geological map illustrating the Koras Group, the Sinclair Sequence and its equivalents (after Sanderson-Damstra, 1982).

6.2 Comparison with the Sinclair Sequence

The Sinclair Sequence is located in southern SWA/Namibia (Fig. 35). It forms a major part of the presently exposed Irumide zones of volcanism, sedimentation and granite emplacement in SWA/Namibia. Both the Sinclair Sequence and the formations in the Dordabis area form part of the southern margin of the Damara Belt. Watters (1977) proposed that the Sinclair Sequence resulted from three evolutionary cycles of deposition (Fig. 36), each cycle consisting of basic and acid lavas interbedded with immature quartzites and greywackes.

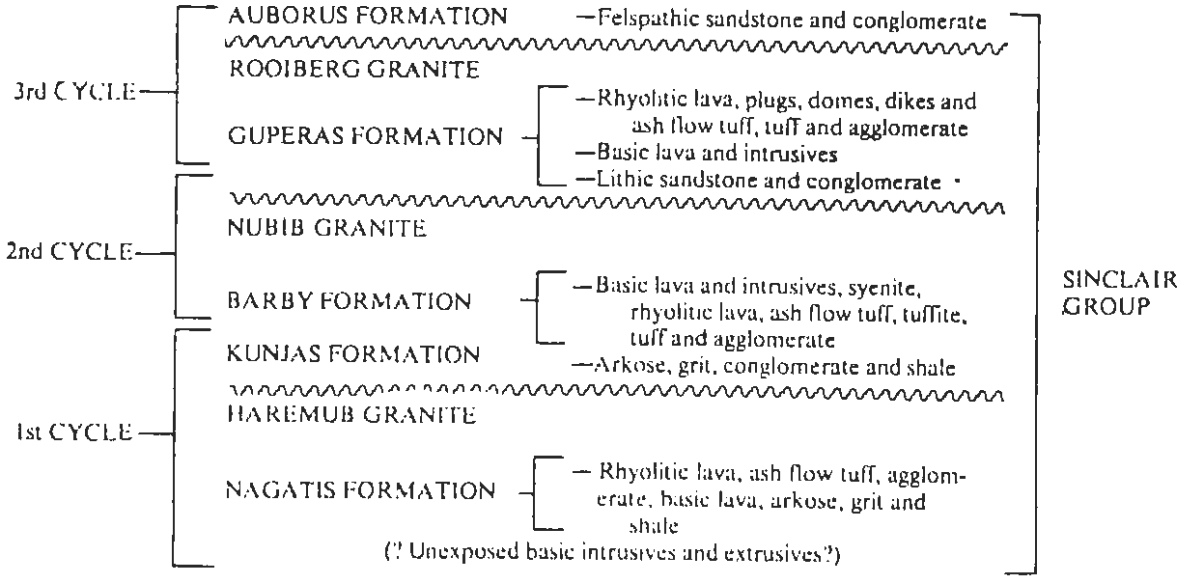

Figure 36 Geological succession and evolutionary cycles of the Sinclair Group (after Watters, 1977)

The Barby Formation is overlain by the Guperas and Auborus Formations, and the Dordabis Formation is overlain by the Doornpoort and Nückopf Formations. S.A.C.S. (1980) correlated the Auborus and Guperas Formations of the Sinclair Sequence with the Doornpoort and Nückopf Formations occuring in the Dordabis area. If this assumption is accepted it is possible that the Barby Formation could be correlated with the Dordabis Formation (Table 8). A comprehensive comparison between the two is therefore necessary.

Mapping and geochemical work is currently being carried out on the Barby Formation by G. Brown of Natal University, but unfortunately no detailed trace element geochemical data are presently available.

Table 8 Possible correlates of the Sinclair Sequence in the Dordabis area.

SINCLAIR SEQUENCE	POSSIBLE CORRELATES
Aubures Formation	Doornpoort Formation (S.A.C.S., 1980)
Guperas Formation	Nückopf Formation (S.A.C.S., 1980)
Barby Formation	Dordabis Formation

The Barby Formation consists of 8500m of interbedded sediments and intrusive and extrusive igneous rock-units (S.A.C.S., 1980). Immature extensively recrystallised greywackes and quartzites are indistinguishable, especially nearer the top of the formation, from those occurring in the Dordabis Formation. Near the base of the Barby Formation conglomeratic layers similar to those occurring at the base of the Opdam Member, are common (Brown, pers. comm.).

The major proportion of the extrusive succession of the Barby Formation is made up of basic lava, although felsic lava and ash-flow tuff constitute between 20% and 45% of the total thickness of extrusive lavas, and less than 5% of the total Barby Formation (Watters, 1974). The extrusive basic lavas are often plagioclase phyric in character (Watters, op. cit.). These volcanic rocks occur both as small- and large-feldspar phyric lavas, petrographically very similar, but less metamorphosed than those in the Bitterwater Member. Lavas which are petrographically similar to the aphanitic, massive, basic volcanic rocks of the Barby Formation are common in the Dordabis Formation. These aphanitic volcanic rocks tend to be tholeiitic in character and usually occur in the top 2000m of the Barby Formation, while the feldspar-phyric lavas tend to be calc-alkaline and occur mostly at the bottom of the formation, interbedded with high-Ca rhyolites (Brown, pers. comm.). Brown (pers. comm.) has not recognised any 'Dordabis-like' flow breccias or ophitic lavas in the Barby Formation.

A spidergram (Fig. 37) compares Watters' (1974) average trace element data for tholeiitic basalts from the Barby Formation with those of the Bitterwater Member. Unfortunately Watters only analysed for six trace elements, Ba, Rb, Sr, Zr, Y and Nb in the Barby tholeiites, of which Ba, Rb and Sr could be mobile. The general pattern on the spidergram is very similar to, and generally falls within the spectrum occupied by the

Bitterwater lavas (Fig. 37), although the Barby tholeiites are slightly enriched in Rb and K. The major element composition of the Barby tholeiites also correlates well with that of the Dordabis Formation (Table 9). The spidergrams are similar, but unfortunately, because of the lack of detailed geochemical data for the Barby Formation, no further conclusions can be drawn on the basis of chemistry. The lack of bimodal basalt-rhyolite lavas and calc-alkaline basalts in the Dordabis Formation detracts from the suggestion that it might be a direct correlate of the Barby Formation.

Table 9 Average whole-rock composition of basic volcanics of the Dordabis Formation (± one standard deviation), the Sinclair Sequence and the Koras Group

DORDABIS FORMATION			XSINCLAIR SEQUENCE	*KORAS GROUP	
	OPDAM MEMBER	BITTERWATER MEMBER	BARBY FORMATION THOLEIITES	LAMBRECHTS-DRIF MEMBER	ROUXVILLE MEMBER
SiO_2	46,90 ± 2,57	46,04 ± 1,30	49,17	54,23	50,79
TiO_2	2,24 ± 0,84	1,21 ± 0,36	1,05	1,08	2,09
Al_2O_3	14,19 ± 1,14	16,12 ± 0,98	17,59	14,59	14,36
Fe_2O_3	14,35 ± 1,98	11,26 ± 1,40	11,29	10,50	13,64
MnO	0,19 ± 0,03	0,15 ± 0,02	0,19	0,13	0,14
MgO	5,93 ± 1,23	7,83 ± 1,04	7,06	5,37	4,62
CaO	7,88 ± 2,00	10,28 ± 1,60	10,08	8,80	7,39
Na_2O	2,84 ± 1,38	2,35 ± 0,76	2,19	2,20	2,87
K_2O	0,74 ± 0,70	0,64 ± 0,43	1,25	1,19	1,24
P_2O_5	0,26 ± 0,12	0,12 ± 0,04	0,13	0,14	0,59
Ba	204 ±158	156 ± 83	218	-	-
Rb	24 ± 22	18 ± 14	62	53,2	34,1
Sr	194 ± 81	218 ± 76	257	279	310
Zr	162 ± 79	68 ± 32	70	144	296
Y	38 ± 13	21 ± 6	19	33	55
Nb	12,1 ± 7,0	3,7 ± 2,9	2,5	10,6	22,1
Cr	131 ± 62	324 ± 64	-	127	212
V	296 ± 54	235 ± 31	-	237	281
Co	61,1 ± 7	58 ± 5	-	50	52
Ni	133 ± 27	200 ± 54	-	64	90
Cu	208 ±138	78 ±135	-	84	32
Zn	144 ± 31	97 ± 15	-	85	111
Sc	38 ± 7	35 ± 4	-	-	-
La	13 ± 9	4 ± 4	-	17	49
Ce	56 ± 32	23 ± 16	-	45	112
Nd	37 ± 19	19 ± 9	-	24	58

X After Watters (1974). Average of BW1415 and BW811
* After Sanderson-Damstra (1982)

6.3 Comparison with the Koras Group

The Koras Group is located in the northern Cape near the town of Upington (Fig. 35). Sanderson-Damstra (1982) has proposed that the group consists mainly of two cycles of bimodal basaltic-rhyolitic volcanic rocks interbedded with immature conglomerates and lithic greywackes. The first volcanic cycle commenced with the Lambrechtsdrif basaltic andesites, followed by the Swartkopsleegte rhyodacites, while the second cycle comprises the contemporaneous Rouxville basalts and the Swartkop and Kenilworth rhyolites (Sanderson-Damastra, op. cit.). The basic lavas in the Lambrechtsdrif and Rouxville Members are subalkaline and tholeiitic in character. Volcanic breccias and interbedded metagreywackes, similar to, but more immature than those in the Dordabis Formation, are common both in the Lambrechtsdrif and Rouxville Members. Structural, lithological and age similarities have resulted in correlation of the Koras Group with the Sinclair Sequence by Du Toit (1965), Grobler et al. (1977), S.A.C.S. (1980) and Sanderon-Damastra (1982).

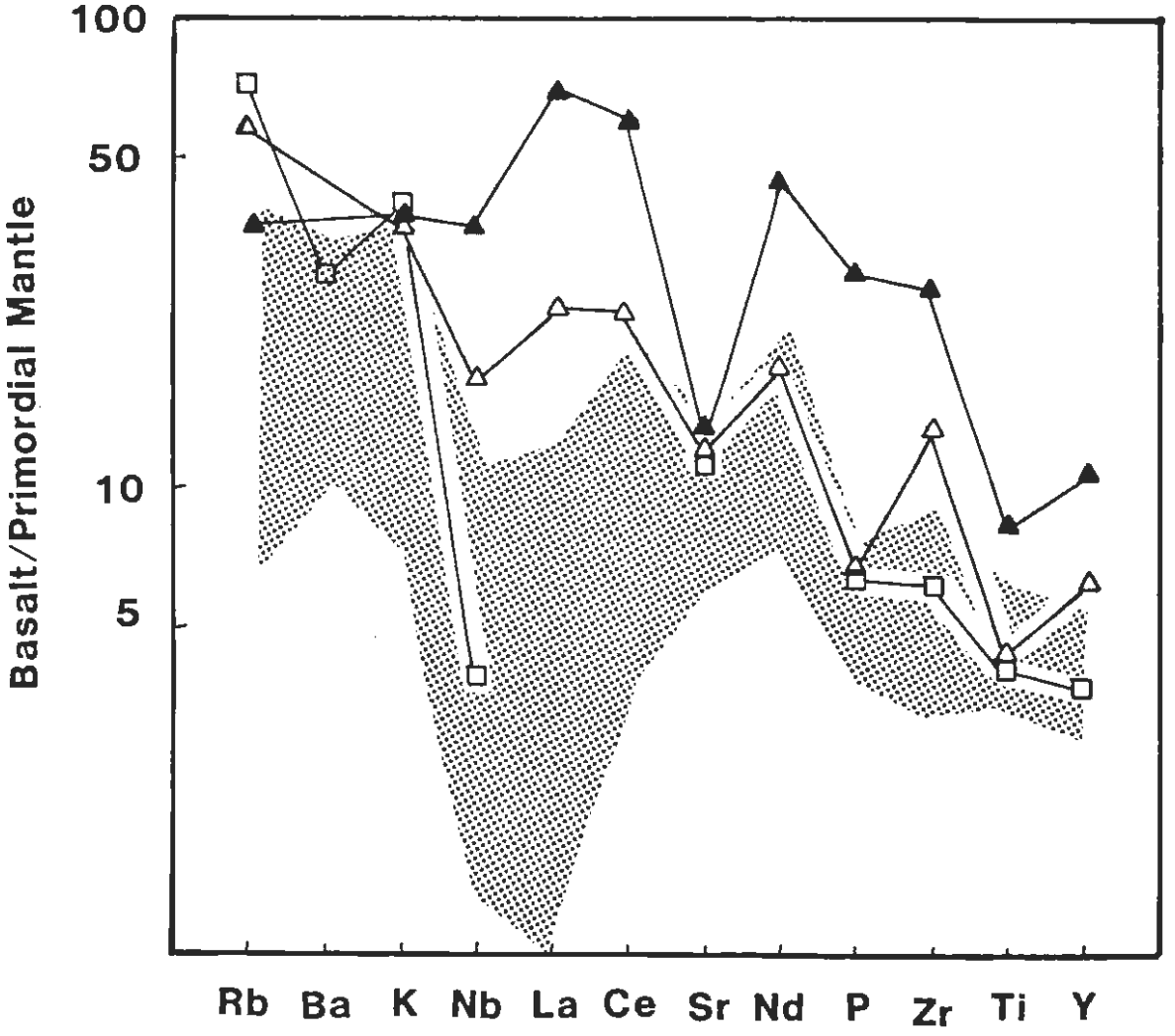

Figure 37 Spidergram comparing the range in concentrations for Bitterwater volcanics (shaded area), with the average concentrations for the Barby tholeiites (□), the Lambrechtsdrif basic volcanics (△) and the Rouxville basic volcanics (▲)

The Spidergram (Fig. 35) shows that the trace element patterns of the Lambrechtsdrif Member are similar to those of the Bitterwater Member, although absolute enrichments are generally higher in the former. The Rouxville Member however has a convex-upward shape with relative enrichments of Nb, La, Ce, Nd, P, Zr, Ti and Y compared to the downward sloping Bitterwater and Lambrechtsdrif Members.

6.4 General Comparison

The Dordabis Formation has many factors in common with parts of the Koras Group and Sinclair Sequence which are summarised by the following points.

1) Age measurements are similar for the three provinces and range from 1080 to 1265Ma.

2) The Dordabis Formation is petrographically and petrologically very similar to the tholeiitic Lambrechtsdrif Member of the Koras Group and the tholeiitic upper part of the Barby Formation of the Sinclair Sequence. However, Nb, La, Ce, Zr and Y are enriched in the Lambrechtsdrif basalts compared to the Dordabis basalts. The Dordabis metalavas exhibit a much more striking resemblance to the Barby tholeiites.

3) The associated sedimentary suites in the three provinces are similar.

4) The volcanics in the three provinces were primarily derived from fissure-type eruptions.

5) Structural trends are similar in the Sinclair Sequence and the Koras Group.

6) Bimodal basaltic and rhyolitic volcanics occur in both the Koras Group and the Sinclair Sequence.

7) The Dordabis Formation and the Sinclair sequence form part of the Irumide zone and are both situated on the southern margin of the Damara Belt.

These similarities suggest that the Dordabis Formation, the Sinclair Sequence and the Koras Group are possible coeval equivalents that formed in similar fault-bounded locations.

7. SUMMARY AND CONCLUSIONS

Petrography, petrology, field and age relationships have resulted in the proposal of a revised geological succession in the Dordabis area. This late-Proterozoic volcano-sedimentary succession is renamed the Dordabis Formation and consists of the Opdam and Bitterwater Members. It forms part of an Irumide zone of volcanism and sedimentation and is, together with Sinclair Sequence, situated on the southern margin of the Damara Sequence. The lower Opdam Member consists of a basal conglomerate overlain by interbedded immature sublitharenites, phyllites, flow breccias and basic volcanics metamorphosed to typical greenschist facies mineral assemblages. The overlying Bitterwater Member consists of interbedded and generally thicker immature sublitharenites, flow breccias and basic volcanics. Although both the Bitterwater Member and the Opdam Member have been metamorphosed to greenschist facies, recrystallisation of the former is incomplete. This suggests that either dryer metamorphic conditions, or lower pressures and temperatures prevailed in the Bitterwater Member.

Shearing, metasomatism and metamorphism of the Dordabis lavas has generally resulted in a scattering of the data points defining geochemical trends for certain elements. Evaluation of compositional data for the lavas indicates that Na_2O, K_2O, CaO, Ba, Rb, Sr, Co and Sc are mobile; SiO_2, Al_2O_3, Fe_2O_3, MnO, MgO, Zn, Cu, Ni, Cr and V are partially mobile and TiO_2, P_2O_5, Nb, Y, Zr, La, Ce and Nd are relatively immobile during these processes.

The Dordabis Formation metalavas are geochemically classified as sub-alkaline, tholeiitic continental basalts. The Opdam lavas are generally more evolved high-iron tholeiites, while the Bitterwater basalts are invariably more primitive magnesium tholeiites. Major and trace element variation trends for the Opdam metalavas overlap those for the Bitterwater lavas, indicating that these two members are cogenetic. Major and trace element variations in the Dordabis basic lavas are consistent with modelled low-pressure fractional crystallisation trends although the presence of feldspar phenocrysts, the mobilisation of elements, the uncertainties in bulk distribution coefficients and the uncertainties in the determination of original melt composition all place limitations on their quantitative use in trace element modelling. Light REE enrichment, decreasing primordial normalised abundances from Rb to Y

on the spidergrams and low K/Rb ratios can either be ascribed to crustal contamination, or primary patterns in the source, or a mantle source with primordial concentrations of incompatible elements that had undergone little previous partial melting. However, low ratios of less incompatible elements to more incompatible elements (average Zr/Nb ratio for the Opdam basalts is about 13) probably reflect conditions in the source material, rather than assimilation. Clearly the initial production of the primary basaltic magma was the result of a partial melting process. This primary basaltic magma underwent further modification en route to and nearer to the earth's surface by fractional crystallisation of about 30:50:15 weight percent augite : plagioclase : olivine.

One of the features of the Dordabis Formation basalts is the occurrence of alternating evolved and primitive lavas at the base of the sequence. Such alternations have frequently been problematical to explain, but recent research has resulted in a better understanding of the plumbing systems of modern volcanoes. This feature of the Dordabis lavas can possibly be explained by a model similar to that of the Socorro magma body in New Mexico. Geophysical studies in the Rio Grande Rift near Socorro indicate the presence of a molten, multilayered intrusive complex at midcrustal depths (Brocher, 1981). If a similar complex existed in the Dordabis area during Irumide times, 'separate layers' or sills of cogenetic magma could have undergone different degrees of crystal fractionation. Over a period of time the filter-pressed interstitial liquids from these partially crystallised sills may have been tapped by taphrogenic faults, resulting in the chemical variations now evident in the Dordabis volcanic pile.

A comparison of the Dordabis Formation with the Sinclair Sequence and the Koras Group indicates that they are possible coeval equivalents. However the lack of geochemical data on the Sinclair Sequence and its 'so-called' equivalents make detailed investigations of the correlations difficult. A detailed study and correlation between all the rocks associated with the Irumide cycle, and in particular the geochemistry of the related igneous rocks, would greatly enhance our understanding of late Proterozoic and hence Damaran cycles in central SWA/Namibia.

APPENDICES

APPENDIX 1 : ELECTRON MICROPROBE ANALYSES

Microprobe analyses were carried out on selected pyroxenes, feldspars and epidotes on a Cambridge Microscan V instrument. Polished sections were coated with carbon to a maximum thickness of 25nm. Ten second counts were performed up to seven times for each element analysed. The data were reduced using the H.V.E. Mark IV program which applies the Bence and Albee (1968) correction and also corrects for dead-time counting losses. Analytical conditions and standards employed are provided in Table A.

Table A Microprobe analytical conditions

.1 Pyroxene

ELEMENT	ACCELERATING POTENTIAL	SPECIMEN CURRENT	COUNTER	CRYSTAL	STANDARD	AV. STANDARD COUNTS (per 10 secs)
Si	20kV	30nA	Flow	RAP	Jadeite	27 844
Ti	20kV	30nA	Flow	LIF	Ilmenite	28 688
Al	20kV	30nA	Flow	RAP	Jadeite	15 159
Fe	20kV	30nA	Flow	LIF	St. J.Is. 01.	6 885
Mn	20kV	30nA	Flow	LIF	Rhodonite	29 941
Mg	20kV	30nA	Flow	RAP	St J.Is. 01.	15 904
Ca	20kV	30nA	Flow	LIF	Px.1	14 230
Na	20kV	30nA	Flow	RAP	Jadeite	1 259
Cr	20kV	30nA	Flow	LIF	Chromite	34 615

.2 Plagioclase

ELEMENT	ACCELERATING POTENTIAL	SPECIMEN CURRENT	COUNTER	CRYSTAL	STANDARD	AV. STANDARD COUNTS
Si	20kV	30nA	Flow	KAP	Px.1	36 379
Al	20kV	30nA	Flow	KAP	Sp. (UCT)	35 872
Fe	20kV	30nA	Flow	Quartz	Ilm,	15 592
Ca	20kV	30nA	Flow	Quartz	Px.1	12 874
Na	20kV	30nA	Flow	KAP	Jadeite	987
K	20kV	30nA	Flow	Quartz	Orth. (1A)	7 222

.3 Epidote

ELEMENT	ACCELERATING POTENTIAL	SPECIMEN CURRENT	COUNTER	CRYSTAL	STANDARD	AV. STANDARD COUNTS
Si	20kV	30nA	Flow	RAP	St. J.Is 01	18 273
Al	20kV	30nA	Flow	RAP	Jadeite	15 470
Fe	20kV	30nA	Flow	RAP	St. J.Is 01	6 843
Mn	20kV	30nA	Flow	LIF(220)	Rhodonite	30 333
Ca	20kV	30nA	Flow	LIF(220)	Px.1	14 583

APPENDIX 2 : X-RAY FLUORESCENCE SPECTROMETRY

Whole-rock analyses were carried out by XRF wavelength dispersive techniques using a Phillips 1410 X-ray spectrometer. The major elements, apart from sodium, were determined using duplicate fusion discs, prepared according to the method of Norrish and Hutton (1969). All iron was determined as Fe_2O_3. Sodium and trace elements were determined on pressed powder pellets. Mass absorption coefficients used in the processing of trace element data were derived from major element data using Heinrich's (1966) values.

H_2O^- and loss on ignition (LOI) were determined gravimetrically by heating samples for eight hours at 110°C and 950°C respectively. Standard departmental computer programs were used to process data. Corrections were made for deadtime, background, instrumental drift, spectral line interference and position factors. Details of analytical conditions for major and trace element runs are given in Table B and lower limits of determination (LLD) and absolute errors for trace element runs are provided in Table C. Working curves were calculated using the international and in-house rock standards presented in Table D.

Table B X-ray fluorescence analytical conditions

ELEMENT	EMISSION LINE	TUBE	kV	mA	CRYSTAL	TIME (SECS)	COUNTER	COLLIMATOR	SPECIMEN
Si	K_α	Cr	55	40	PET	40	FLOW	COARSE	FUSION DISC
Ti	K_α	Cr	55	40	LIF(200)	10	FLOW	FINE	FUSION DISC
Al	K_α	Cr	55	40	PET	40	FLOW	COARSE	FUSION DISC
Fe	K_α	Cr	55	40	LIF(200)	20	FLOW	FINE	FUSION DISC
Mn	K_α	Cr	55	40	LIF(200)	20	FLOW	COARSE	FUSION DISC
Mg	K_α	Cr	55	40	TLAP	100	FLOW	FINE	FUSION DISC
Ca	K_α	Cr	55	40	LIF(200)	10	FLOW	FINE	FUSION DISC
Na	K_α	Cr	55	40	TLAP	100	FLOW	FINE	POWDER PELLET
K	K_α	Cr	55	40	LIF(200)	10	FLOW	FINE	FUSION DISC
P	K_α	Cr	55	40	Ge	20	FLOW	COARSE	FUSION DISC
Ba	L_β	Cr	55	40	LIF(220)	200	FLOW	FINE	POWDER PELLET
Rb	K_α	W	55	40	LIF(220)	200	SCINT	FINE	POWDER PELLET
Sr	K_α	W	55	40	LIF(220)	200	SCINT	FINE	POWDER PELLET
Y	K_α	W	55	40	LIF(220)	200	SCINT	FINE	POWDER PELLET
Zr	K_α	W	55	40	LIF(220)	200	SCINT	FINE	POWDER PELLET
Nb	K_α	W	55	40	LIF(220)	200	SCINT	FINE	POWDER PELLET
Zn	K_α	Mo	55	40	LIF(220)	200	FLOW/ SCINT.	FINE	POWDER PELLET
Cu	K_α	Mo	55	40	LIF(220)	200	FLOW/ SCINT.	FINE	POWDER PELLET
Ni	K_α	Mo	55	40	LIF(220)	200	FLOW/ SCINT.	FINE	POWDER PELLET
Co	K_α	W	55	40	LIF(220)	200	FLOW	FINE	POWDER PELLET
Cr	K_α	W	55	40	LIF(220)	200	FLOW	FINE	POWDER PELLET
V	K_α	W	55	40	LIF(220)	200	FLOW	FINE	POWDER PELLET
Sc	K_α	Cr	55	40	LIF(200)	200	FLOW	FINE	POWDER PELLET
La	L_α	W	55	40	LIF(220)	200	FLOW	FINE	POWDER PELLET
Ce	L_β	W	55	40	LIF(220)	200	FLOW	FINE	POWDER PELLET
Nd	L_α	W	55	40	LIF(220)	200	FLOW	FINE	POWDER PELLET

Table C Average lower limits of determination (L.L.D.) and errors of determination for trace element analyses by X-ray fluorescence spectrometry

ELEMENT	L.L.D. (ppm)	ABSOLUTE ERRORS (ppm)
Ba	13,0	4,8
Rb	2,4	0,8
Sr	2,3	1,1
Y	2,5	0,8
Zr	2,1	0,8
Nb	2,8	0,8
Zn	1,7	0,9
Cu	1,7	1,0
Ni	2,4	1,3
Co	2,6	0,7
Cr	2,6	1,1
V	1,2	3,3
Sc	1,2	0,3
La	8,1	2,0
Ce	12,5	3,4
Nd	8,2	2,1

Table D International and in-house rock standards used

Major Elements:	GSP-1, AGV-1, PCC-1, DTS-1, NIM-N, JG-1
Na:	BCR-1, G-2, GSP-1, AGV-1, NIM-N, PCC-1
Ba:	CAR-08, KRF-13, BCR-1, S-12
Rb, Sr, Nb, Zr, Y:	CAR-08, KRF-13, S-09, S-12
Co, Cr, V:	BHVO, SDC-1, QLO-1, PCC-1, BCR-1
Zn, Cu, Ni:	S-9, S-12, S-15
Sc:	GSP-1, NIM-N, AGV-1, BCR-1
La, Ce, Nd:	BCR-1, AGV-1, G-2

APPENDIX 3 MAJOR ELEMENT ANALYSES (H_2O^- AND L.O.I. INCLUDED) AND C.I.P.W. WEIGHT PERCENT NORM

Opdam Member

	IWJ143	IWJ145	IWJ146	IWJ147	IWJ148	IWJ149	IWJ150	IWJ151	IWJ152	IWJ153	IWJ2	IWJ3	IWJ4	IWJ5	IWJ6	IWJ7
SiO_2	52,22	47,20	45,97	48,72	42,30	40,05	46,50	45,84	47,34	45,29	49,09	46,37	47,05	47,11	46,69	47,57
TiO_2	0,85	1,89	4,23	1,50	3,78	3,76	1,92	2,45	2,12	2,09	1,67	2,01	2,36	2,78	1,82	1,88
Al_2O_3	13,67	14,13	12,64	14,06	12,89	12,90	13,26	14,32	13,93	13,40	14,48	14,63	15,01	14,82	16,29	17,15
Fe_2O_3	10,57	13,44	17,43	12,48	16,54	17,22	14,72	16,61	14,65	14,73	11,59	14,57	15,33	14,30	12,05	12,70
MnO	0,17	0,20	0,19	0,19	0,25	0,22	0,19	0,23	0,18	0,18	0,16	0,20	0,16	0,22	0,16	0,18
MgO	6,80	7,35	5,21	6,74	4,57	4,97	6,58	5,55	5,75	4,72	7,65	6,28	6,45	8,05	3,83	3,62
CaO	8,46	10,35	9,89	9,44	8,16	7,79	7,18	8,21	8,41	8,77	10,73	8,12	5,65	4,30	8,65	10,21
Na_2O	3,03	2,54	0,00	3,47	0,37	0,31	3,10	2,23	2,56	2,61	2,39	2,95	4,53	3,53	4,16	2,95
K_2O	0,29	0,28	0,11	0,15	2,21	2,59	0,75	0,90	1,18	0,88	0,76	1,62	0,92	0,05	0,66	0,24
P_2O_5	0,07	0,12	0,55	0,12	0,45	0,47	0,19	0,29	0,27	0,30	0,12	0,24	0,29	0,29	0,23	0,27
L.O.I.	2,20	2,60	3,63	3,35	7,56	8,72	4,68	2,90	2,42	6,62	2,45	2,54	2,69	3,99	4,41	3,64
H_2O^-	0,20	0,17	0,44	0,94	0,27	0,26	0,12	0,24	0,18	0,18	0,20	0,18	0,13	0,16	0,17	0,15
TOTAL	98,53	100,25	99,30	100,15	99,34	100,25	99,20	99,77	98,97	99,76	101,28	99,71	100,56	99,60	99,14	100,57

C.I.P.W. WEIGHT PERCENT NORM ($Fe_2O_3/FeO = 0,2$)

Ap	0,17	0,28	1,31	0,29	1,06	1,11	0,45	0,69	0,65	0,71	0,27	0,56	0,68	0,69	0,55	0,64
Il	1,64	3,64	8,14	2,88	7,27	7,23	3,69	4,71	4,07	4,02	3,21	3,86	4,55	5,35	3,51	3,62
Or	1,70	1,65	0,63	0,86	13,07	15,33	4,45	5,29	6,96	5,19	4,51	9,59	5,41	0,28	3,90	1,42
Ab	25,59	21,48	0,00	29,33	3,14	2,65	26,26	18,87	21,67	22,11	20,23	24,60	34,72	29,88	31,38	24,99
An	22,87	26,32	34,17	22,38	26,97	26,14	20,04	26,43	23,03	22,24	26,54	21,87	17,91	19,41	23,83	32,82
C	0,00	0,00	0,00	0,00	0,00	0,00	0,00	0,00	0,00	0,00	0,00	0,00	0,00	1,84	0,00	0,00
Mt	2,34	2,97	3,86	2,76	3,66	3,81	3,26	3,67	3,24	3,26	2,56	3,22	3,39	3,16	2,67	2,81
DiEn	4,29	5,48	2,13	5,25	1,89	1,71	2,97	2,28	3,34	3,46	6,27	3,46	1,70	0,00	3,16	2,72
DiFs	3,20	4,30	2,56	4,31	2,54	2,23	2,89	2,89	3,62	4,60	4,05	3,46	1,68	0,00	4,18	4,04
DiWo	7,78	10,12	4,72	9,87	4,42	3,93	5,98	5,18	7,05	8,06	10,83	7,05	3,45	0,00	7,34	6,71
HyEn	12,66	7,09	10,84	5,17	9,50	10,67	7,16	9,98	8,61	6,29	8,73	0,00	0,00	19,20	0,00	6,30
HyFs	9,44	5,56	13,03	4,24	12,76	13,92	6,97	12,67	9,32	8,37	5,64	0,00	0,00	13,45	0,00	9,37
Q	3,72	0,00	13,50	0,00	3,96	0,22	0,00	0,00	0,00	0,00	0,00	0,00	0,00	0,00	0,00	0,32
Fo	0,00	4,03	0,00	4,47	0,00	0,00	4,39	1,10	1,65	1,41	2,84	8,54	10,07	0,60	4,48	0,00
Fa	0,00	3,48	0,00	4,05	0,00	0,00	4,70	1,54	1,97	2,07	2,02	9,40	11,01	0,46	6,54	0,00
Ne	0,00	0,00	0,00	0,00	0,00	0,00	0,00	0,00	0,00	0,00	0,00	0,21	1,95	0,00	2,07	0,00
TOTAL	95,41	96,40	94,89	95,84	90,22	88,94	93,21	95,30	95,21	91,79	97,70	95,82	96,52	94,32	93,60	95,77
Mg#	0,60	0,56	0,41	0,56	0,39	0,40	0,51	0,44	0,48	0,43	0,61	0,50	0,50	0,57	0,43	0,40

APPENDIX 3 (continued)

	Opdam Member				Bitterwater Member											
	IWJ8	IWJ9	IWJ10	IWJ11	IWJ12	IWJ13	IWJ14	IWJ15	IWJ16	IWJ17	IWJ19	IWJ20	IWJ21	IWJ49	IWJ50	IWJ51
SiO_2	49,13	49,16	48,74	45,70	45,28	46,64	46,10	44,39	46,71	47,59	46,50	46,87	46,38	48,36	45,97	47,59
TiO_2	2,07	2,60	1,64	1,48	1,11	1,14	1,67	0,66	1,07	1,82	1,07	1,37	1,05	1,24	1,11	1,41
Al_2O_3	13,48	13,27	14,13	15,37	14,86	16,83	15,99	15,90	16,80	15,95	16,16	15,92	16,38	15,24	16,31	15,12
Fe_2O_3	13,71	16,00	12,24	16,24	16,06	10,88	11,62	10,15	10,76	10,77	10,81	10,79	10,85	11,06	11,05	12,01
MnO	0,19	0,17	0,17	0,15	0,15	0,17	0,17	0,15	0,16	0,13	0,14	0,15	0,14	0,17	0,15	0,19
MgO	5,02	6,12	7,19	6,19	7,02	7,78	7,33	10,94	7,61	7,19	7,98	8,85	8,33	8,41	7,95	7,09
CaO	6,08	3,09	7,96	6,11	7,24	9,87	10,77	10,48	11,09	11,38	10,64	10,44	9,47	6,08	10,35	8,76
Na_2O	4,57	4,96	2,47	4,01	3,67	3,02	2,40	1,77	2,07	1,88	2,09	2,65	2,21	4,05	2,40	3,14
K_2O	0,32	0,21	0,20	0,54	0,63	0,60	0,41	0,23	0,23	0,40	0,21	0,69	1,65	0,34	0,28	0,88
P_2O_5	0,24	0,28	0,15	0,17	0,10	0,12	0,11	0,06	0,09	0,10	0,08	0,09	0,10	0,12	0,12	0,15
L.O.I.	3,61	2,52	4,24	2,72	2,78	3,09	3,60	4,44	3,42	3,37	3,73	3,31	3,42	3,65	3,89	2,80
H_2O^-	0,17	0,17	0,21	0,16	0,22	0,14	0,12	0,16	0,01	0,12	0,16	0,10	0,13	0,26	0,21	0,23
TOTAL	98,58	98,53	99,35	98,84	99,11	100,28	99,79	99,34	100,03	100,07	99,57	101,24	100,11	98,97	99,78	99,37
C.I.P.W. WEIGHT PERCENT NORM (Fe_2O_3/FeO = 0,2)																
Ap	0,56	0,65	0,35	0,41	0,24	0,28	0,18	0,15	0,22	0,24	0,20	0,21	0,24	0,28	0,27	0,36
Il	3,99	5,00	3,16	2,86	2,13	2,19	2,27	1,27	2,06	2,27	2,05	2,63	2,03	2,39	2,14	2,72
Or	1,89	1,25	1,18	3,17	3,73	3,55	2,39	1,37	1,33	2,37	1,24	4,10	9,73	1,99	1,67	5,19
Ab	38,64	41,92	20,93	32,64	27,07	23,94	20,32	14,99	17,55	15,89	17,72	21,87	18,66	34,24	20,29	26,54
An	15,33	13,35	26,87	22,35	22,24	30,59	31,61	34,75	35,88	33,90	34,09	29,51	29,93	22,41	32,89	24,57
C	0,00	0,00	0,00	0,00	0,00	0,00	0,00	0,00	0,00	0,00	0,00	0,00	0,00	0,00	0,00	0,00
Mt	3,03	3,54	2,71	3,59	3,62	2,41	2,56	2,25	2,38	2,38	2,39	2,39	2,40	2,45	2,45	2,67
DiEn	2,61	0,04	2,70	1,26	2,58	4,28	5,03	4,54	4,48	5,23	4,45	5,57	4,07	1,74	4,31	4,09
DiFs	2,87	0,04	1,99	1,58	2,79	2,72	3,63	2,02	2,89	3,51	2,75	2,97	2,42	1,03	2,73	3,10
DiWo	5,55	0,07	4,87	2,85	5,44	7,34	9,02	7,03	7,73	9,15	7,57	9,06	6,83	2,92	7,39	7,46
HyEn	6,44	9,94	15,22	0,00	0,00	0,00	3,64	4,53	8,58	11,71	9,49	0,00	0,00	5,78	4,99	2,63
HyFs	7,09	10,70	11,20	0,00	0,00	0,00	2,63	2,01	5,54	7,85	5,86	0,00	0,00	3,41	3,16	1,99
Q	0,00	0,00	2,74	0,00	0,00	0,00	0,00	0,00	0,00	0,00	0,00	0,00	0,00	0,00	0,00	0,00
Fo	2,42	3,69	0,00	9,93	10,44	10,59	6,62	12,75	4,14	0,69	4,16	11,55	11,69	9,41	7,36	7,67
Fa	2,93	4,39	0,00	13,79	12,41	7,40	5,27	6,25	2,94	0,51	2,83	6,79	7,67	6,12	5,13	6,41
Ne	0,00	0,00	0,00	0,70	2,14	0,87	0,00	0,00	0,00	0,00	0,00	0,30	0,01	0,00	0,00	0,00
TOTAL	93,36	94,57	93,91	95,13	94,83	96,16	95,15	93,91	95,72	95,70	94,79	96,95	95,67	94,16	94,79	95,42
Mg#	0,47	0,47	0,58	0,46	0,51	0,63	0,60	0,72	0,62	0,61	0,63	0,66	0,64	0,64	0,63	0,58

APPENDIX 3 (continued)

Bitterwater Member

	IWJ84	IWJ83	IWJ82	IWJ79	IWJ68	IWJ69	IWJ70	IWJ71	IWJ72	IWJ73	IWJ74	IWJ75	IWJ76	IWJ77	IWJ78
SiO_2	46,45	43,50	43,16	46,69	42,67	46,37	46,49	45,39	47,00	47,02	47,39	46,48	44,85	45,09	46,44
TiO_2	1,12	1,04	1,04	1,07	1,09	1,11	1,05	1,07	1,02	2,84	2,47	1,56	1,38	1,45	1,17
Al_2O_3	16,31	15,27	15,69	16,55	16,60	16,05	16,05	16,60	16,13	13,48	14,17	15,97	15,90	15,36	20,17
Fe_2O_3	10,42	9,81	10,41	10,51	11,83	11,00	10,78	11,09	10,62	15,78	15,75	11,76	11,90	12,24	8,81
MnO	0,13	0,12	0,11	0,15	0,16	0,15	0,15	0,14	0,14	0,21	0,19	0,16	0,16	0,17	0,13
MgO	7,08	6,62	8,19	7,92	7,18	8,87	8,31	8,13	8,33	5,70	5,36	7,83	8,28	8,60	4,65
CaO	11,30	10,67	7,66	11,08	16,41	10,65	10,82	11,29	11,23	8,96	8,85	10,59	12,05	10,77	9,93
Na_2O	0,99	1,68	0,83	2,46	0,03	2,03	1,92	2,07	1,80	2,22	2,49	2,35	1,85	2,27	3,11
K_2O	0,12	0,12	1,08	0,40	0,02	0,50	0,42	0,33	0,42	1,43	0,99	0,45	0,43	0,15	1,32
P_2O_5	0,11	0,10	0,10	0,11	0,12	0,11	0,11	0,11	0,11	0,24	0,29	0,19	0,15	0,16	0,15
L.O.I.	5,83	10,88	11,05	3,12	3,66	3,14	3,37	3,86	3,04	2,18	1,68	2,55	2,55	3,14	3,58
H_2O^-	0,17	0,17	0,30	0,21	0,24	0,18	0,18	0,17	0,16	0,15	0,13	0,12	0,16	0,17	0,12
TOTAL	100,03	99,98	99,62	100,26	100,00	100,16	99,66	100,24	100,00	100,19	99,75	100,00	99,65	99,56	99,58

C.I.P.W. WEIGHT PERCENT NORM (Fe_2O_3/FeO = 0,2)

Ap	0,26	0,24	0,24	0,25	0,28	0,27	0,25	0,26	0,26	0,57	0,69	0,44	0,36	0,37	0,35
Il	2,15	2,01	1,99	2,06	2,09	2,14	2,02	2,05	1,97	5,46	4,76	3,01	2,65	2,80	2,24
Or	0,70	0,70	6,37	2,33	0,12	2,95	2,49	1,97	2,49	8,44	5,83	2,63	2,56	0,91	7,79
Ab	8,34	14,18	7,05	20,78	0,25	17,19	16,21	17,51	15,22	18,82	21,05	19,84	15,63	19,19	21,94
An	39,73	33,80	35,90	32,96	45,11	33,19	33,96	35,02	34,69	22,58	24,57	31,74	33,82	31,29	37,17
C	0,00	0,00	0,00	0,00	0,00	0,00	0,00	0,00	0,00	0,00	0,00	0,00	0,00	0,00	0,00
Mt	2,31	2,17	2,30	2,32	2,62	2,43	2,39	2,45	2,35	3,49	3,48	2,60	2,63	2,71	1,95
DiEn	3,75	4,42	0,36	5,27	8,12	4,77	4,72	4,95	5,08	3,96	3,26	4,73	6,06	5,15	2,47
DiFs	2,48	2,95	0,21	3,18	6,17	2,69	2,80	3,09	2,96	4,42	3,98	3,08	3,88	3,25	2,03
DiWo	6,52	7,71	0,60	8,90	14,83	7,89	7,93	8,46	8,48	8,48	7,28	8,18	10,42	8,82	4,65
HyEn	13,90	11,69	20,04	2,62	6,32	6,39	9,01	3,32	10,17	8,02	8,94	5,25	1,31	3,31	0,00
HyFs	9,20	7,81	11,56	1,58	4,81	3,60	5,35	2,07	5,93	8,94	10,92	3,42	0,84	2,09	0,00
Q	3,85	0,00	0,81	0,00	0,00	0,00	0,00	0,00	0,00	0,00	0,00	0,00	0,00	0,00	0,00
Fo	0,00	0,26	0,00	8,29	2,41	7,67	4,89	8,39	3,87	1,54	0,82	6,68	9,29	9,08	6,39
Fa	0,00	0,19	0,00	5,51	2,02	4,77	3,20	5,77	2,48	1,90	1,10	4,80	6,55	6,31	5,79
Ne	0,00	0,00	0,00	0,00	0,00	0,00	0,00	0,00	0,00	0,00	0,00	0,00	0,00	0,00	2,38
TOTAL	93,18	88,13	87,42	96,07	95,14	95,94	95,22	95,31	95,94	96,61	96,68	96,39	95,98	95,27	95,16
Mg#	0,61	0,61	0,65	0,64	0,59	0,65	0,64	0,63	0,65	0,46	0,44	0,61	0,62	0,62	0,55

APPENDIX 3 (continued)

Bitterwater Member

	IWJ52	IWJ53	IWJ54	IWJ56	IWJ57	IWJ58	IWJ59	IWJ60	IWJ61	IWJ62	IWJ64	IWJ89	IWJ88	IWJ87	IWJ86	IWJ85
SiO_2	43,85	46,02	45,21	43,95	47,28	47,62	46,50	46,71	46,03	46,05	48,52	45,65	46,27	45,59	45,76	45,49
TiO_2	1,19	1,24	1,14	1,13	1,12	1,02	1,07	1,11	1,27	1,25	1,09	1,17	0,99	1,10	1,05	1,67
Al_2O_3	16,27	16,28	16,63	16,93	16,93	16,69	16,29	16,42	15,77	16,17	14,68	16,57	15,50	16,64	16,82	16,87
Fe_2O_3	10,96	11,31	10,88	11,34	10,62	10,35	11,13	10,89	11,14	11,22	10,70	11,29	10,41	11,22	10,65	10,85
MnO	0,16	0,16	0,16	0,15	0,16	0,15	0,14	0,16	0,16	0,18	0,16	0,15	0,13	0,15	0,16	0,15
MgO	8,21	6,62	8,38	8,81	7,03	7,68	7,85	8,46	8,57	7,71	8,07	8,61	8,10	8,40	8,17	8,42
CaO	12,00	11,50	11,38	7,62	9,26	10,19	8,95	10,05	8,99	9,61	10,18	10,75	10,49	11,17	10,35	10,72
Na_2O	3,03	3,38	2,06	2,71	3,28	2,70	3,25	2,44	3,08	2,65	3,34	2,07	1,78	1,53	2,25	1,92
K_2O	0,47	0,55	0,44	1,76	1,18	1,26	0,98	1,01	0,93	1,18	0,21	0,45	0,32	0,32	0,84	0,70
P_2O_5	0,10	0,09	0,08	0,10	0,12	0,10	0,12	0,11	0,15	0,13	0,11	0,12	0,11	0,12	0,10	0,11
L.O.I.	3,28	3,30	3,08	3,95	2,88	1,56	2,91	3,21	3,08	2,88	2,56	3,03	3,46	3,42	3,30	3,56
H_2O^-	0,17	0,13	0,15	0,24	0,18	0,17	0,15	0,18	0,21	0,18	0,18	0,18	2,11	0,15	0,19	0,17
TOTAL	99,68	100,40	99,60	98,69	100,03	99,47	99,33	100,73	99,38	99,22	99,80	100,04	99,67	99,82	99,65	100,13

C.I.P.W. WEIGHT PERCENT NORM (Fe_2O_3/FeO = 0,2)

Ap	0,23	0,21	0,20	0,25	0,27	0,24	0,28	0,26	0,35	0,30	0,25	0,27	0,26	0,29	0,25	0,26
Il	2,28	2,39	2,20	2,17	2,15	1,96	2,05	2,13	2,45	2,41	2,09	2,24	1,91	2,12	2,03	2,24
Or	2,75	3,24	2,62	10,41	6,97	7,43	5,79	5,97	5,52	6,98	1,24	2,67	1,90	1,88	4,98	4,15
Ab	10,93	18,15	17,40	15,93	20,36	21,38	23,28	20,60	22,46	20,73	28,24	17,55	15,06	12,95	19,00	16,24
An	29,44	27,65	34,84	28,83	27,98	29,72	26,98	30,89	26,48	28,73	24,46	34,56	33,36	37,60	33,34	35,36
C	0,00	0,00	0,00	0,00	0,00	0,00	0,00	0,00	0,00	0,00	0,00	0,00	0,00	0,00	0,00	0,00
Mt	2,42	2,46	2,41	2,51	3,44	2,29	2,46	2,41	2,46	2,48	2,37	2,50	2,30	2,48	2,36	2,40
DiEn	7,30	6,62	5,25	2,07	3,46	4,95	4,02	4,55	4,29	4,37	6,27	4,48	4,48	4,20	4,31	4,29
DiFs	4,39	4,99	3,09	1,22	3,62	3,05	2,61	2,67	2,49	2,85	3,78	2,66	2,63	2,56	2,57	2,49
DiWo	12,31	12,05	8,79	3,47	7,19	8,42	6,94	7,61	7,16	7,56	10,59	7,52	7,50	7,11	7,25	7,15
HyEn	0,00	0,00	1,47	0,00	0,00	0,00	0,00	0,74	0,00	0,00	1,70	4,08	13,21	10,38	1,37	4,09
HyFs	0,00	0,00	0,87	0,00	0,00	0,00	0,00	0,43	0,00	0,00	1,03	2,42	7,77	6,33	0,82	2,37
Q	0,00	0,00	0,00	0,00	0,00	0,00	0,00	0,00	0,00	0,00	0,00	0,00	0,00	0,00	0,00	0,00
Fo	9,22	6,92	9,92	13,92	9,85	9,94	10,89	11,06	11,95	10,41	8,51	9,04	1,74	4,44	10,28	8,83
Fa	6,11	5,75	6,44	8,99	11,34	6,74	7,78	7,14	7,64	7,50	5,66	5,92	1,13	2,99	6,75	5,65
Ne	7,96	5,65	0,00	3,80	4,01	0,78	2,28	0,00	1,93	0,93	0,00	0,00	0,00	0,00	0,00	0,00
TOTAL	95,34	96,07	95,49	93,58	100,65	96,90	95,36	96,45	95,18	95,25	96,19	95,91	93,26	95,33	95,29	95,52
Mg#	0,64	0,58	0,64	0,64	0,51	0,63	0,62	0,64	0,64	0,62	0,64	0,64	0,65	0,64	0,64	0,64

ACKNOWLEDGEMENTS

I would like to sincerely thank the following organisation and people for their help and time during the course of this thesis:

1. The Geological Survey of SWA/Namibia for financial help, and its staff, particularly Dr K.E.L. Schalk, for his assistance during the field work and the initiation of this project.

2. My supervisor, Dr J.S. Marsh for his guidance and advice, as well as other members of the geological staff at Rhodes University, in particular Professor R.E. Jacob.

3. The technical staff of the Geology Department for their able assistance.

4. The farmers in my field area, particularly Mr & Mrs Kroft whose hospitality was greatly appreciated.

5. My fellow students, in particular David Phillips, whose resolute nature helped overcome many problems and Andrew Mitchell for help with computing.

6. G. Brown for information on the Barby Formation.

7. Teral Bowen for kindly helping correct the final draft of this thesis.

8. My family and girlfriend for their constant support and encouragement.

9. Angela Stuurman for deciphering and typing this thesis.

REFERENCES

ANDERSON, A.T. AND GREENLAND, L.P. (1969) : Phosphorus fractionation diagram as a quantitative indicator of crystallization differentiation of basaltic liquids. Geochim. Cosmochim. Acta, 33, 493-505.

BENCE, A.E. AND ALBEE, A.L. (1968) : Empirical correction factors for the electron microanalysis of silicates and oxides. J. Geology, 76, 382-403.

BENDER, J.F., LANGMUIR, C.H. AND HANSON, G.N. (1984) : Petrogenesis of basalts glasses from the Tamayor Region, East Pacific Rise. J. Petrol., 25, 213-254.

BESWICK, A.E. (1976) : K and Rb relations in basalts and other mantle derived materials. Is phlogopite the key? Geochim. et Cosmochim., 44, 1176-1183.

BESWICK, A.E. AND SOUCIE, G. (1978) : A correction procedure for metasomatism in a Archaean Greenstone Belt. Precambr. Res., 6, 235-248.

BIGGAR, G.M. (1983) : Crystallization of plagioclase, augite, and olivine in synthetic systems and in tholeiites. Mineralog. Mag., 47, 161-176.

BOTHA, M.J. (1980) : Comparative geochemistry of the Witwatersrand triad lavas. Unpubl. Honours Project, Rhodes University.

BOUGAULT, H. AND HEKINIAN, R. (1974) : Rift valley in the Atlantic Ocean near 36°50'N: Petrology and geochemistry of basaltic rocks. Earth Planet. Sc. Lett., 24, 249-261.

BRIQUEU, L., BOUGAULT, H. AND JARON, J.L. (1984) : Quantification of Nb, Ta, Ti and V anomalies in magmas associated with subduction zones: petrogenetic implication. Earth Planet. Sc. Lett., 68, 297-308.

BROCHER, T.M. (1981) : Geometry and physical properties of the Socorro, New Mexico, magma bodies. J. Geophys. Res., 86, 9420-9432.

BROOKS, C.J. (1976) : The Fe_2O_3/FeO ratio of basalt analyses. An appeal for a standardized procedure. Bull. Geol. Soc. Denmark, 25, 117-120.

BURNS, R.G. (1970) : Mineralogical applications of Crystal Field Theory. Cambridge University Pres, 224pp.

CAHEN, L., HELHAL, J. AND LAVREAU, J. (1976) : The Archaean of Equatorial Africa, a review. In: B.F. Windley (ed.). The early history of the earth. Wiley, London, 489-498.

CAMPBELL, I.H. AND BORLEY, G.D. (1974) : The geochemistry of pyroxenes from the lower layered series of the Jimberlana Intrusion, Western Australia. Contr. Miner. Petrol., 47, 281-297.

CAMERON, M. AND PAPIKE, J.J. (1981) : Structural and chemical variations in pyroxenes. Am. Miner., 66, 1-50.

CANN, J.R. (1970) : Rb, Sr, Y, Zr and Nb in some ocean floor basalt rocks. Earth Planet. Sc. Lett., 10, 7-16.

COISH, R.A. (1977) : Ocean floor metamorphism in the Betts Cove Ophiolite, Newfoundland. Contr. Miner. Petrol., 60, 255-270.

COMPSTON, W., McDOUGALL, I. AND HEIER, H.S. (1968) : Geochemical comparison of the Mesozoic basaltic rocks of Antarctica, South Africa, South America and Tasmania. Geochim. et Cosmochim., 32, 129-149.

COX, K.G., BELL, J.D. AND PANKHURST, R.J. (1979) : The interpretation of igneous rocks. George Allen & Unwin, London, 450pp.

DALE, I.M. AND HENDERSON, P. (1972) : The partition of transition elements in phenocryst-bearing basalts and the implications about melt structure. Int. Geol. Congr., 24th session, 10, 105-111.

DAVIES, J.F., GRANT, R.W.E. AND WHITEHEAD, R.E.S. (1979) : Immobile trace elements and Archaean volcanic stratigraphy in the Timmins mining area, Ontario. Can. J. Earth Sci., 16, 305-311.

DEER, W.A., HOWIE, R.A. AND ZUSSMAN, J. (1962) : Rock-forming minerals. Vol. 1, Ortho- and Ring Silicates. John Wiley and Sons Inc., N.Y., p183-210.

DEER, W.A., HOWIE, R.A. AND ZUSSMAN, J. (1978) : Rock-forming minerals. Vol. 2A, Single-Chain Silicates. Second edition, Longman Group Limited, London, pp668.

DEPAOLO, D.J. (1981) : Trace elements and isotopic effects of combined wallrock assimilation and fractional crystallization. Earth Planet. Sc. Lett., 53, 189-202.

DUKE, J.M. (1976) : Distribution of the period four transition elements among olivine, calcic pyroxene and mafic silicate liquid: Experimental results. J. Petrol., 17, 499-521.

DU TOIT, M.C. (1965) : A geological investigation and correlation of rocks belonging to the Koras Formation in the Gordonia and Kenhardt districts, Northern Cape Province. Unpubl. M.Sc. Thesis, Univ. O.F.S..

FLOYD, P.A. (1976) : Geochemical variation in the greenstones of S.W. England. J. Petrol., 17, 522-545.

FLOYD, P.A. AND WINCHESTER, J.A. (1975) : Magma type and tectonic setting discrimination using immobile elements. Earth Planet. Sc. Lett., 27, 211-218.

FREY, F.A., BRYAN, W.B. AND THOMPSON, G. (1974) : Atlantic ocean floor: geochemistry and petrology of basalts from legs 2 and 3 of the deep-sea drilling project. J. Geophys. Res., 79, 5507-5527.

FRYE, K. (1981) : The encyclopedia of mineralogy, volume IVB. Hutchinson Ross Publishing Company, Stroudsburg, Pennsylvania, 794pp, p153-157.

GAMBLE, R.P. AND TAYLOR, L.A. (1980) : Crystal/liquid partitioning in augite: effects of cooling rate. Earth Planet. Sc. Lett., 47, 21-33.

GEVERS, T.W. (1934) : The geology of the Windhoek district in South West Africa. Trans. Geol. Soc. S. Afr., 37, 221-251.

GOLDSCHMIDT, V.M. (1954) : Geochemistry. Muir, A. (ed.), Clarendon Press, Oxford, 730pp.

GREENLAND, L.P. (1970) : An equation for trace element distribution during magmatic crystallization. Am. Miner., 55, 455-465.

GROBLER, N.J., BOTHA, B.J.V. AND SMIT, C.A. (1977) : The tectonic setting of the Koras Group. Trans. Geol. Soc. S. Afr., 80, 167-175.

HANSON, G.N. (1980) : Rare earth elements in petrogenetic studies of igneous suites. Ann. Rev. Earth Planet. Sc., 8, 371-406.

HART, S.R. AND DAVIS, K.E. (1978) : Nickel partitioning between olivine and silicate melt. Earth Planet. Sc. Lett., 40, 203-219.

HASKIN, L.A., FEY, F.A., SCHMITT, R.A. AND SMITH, R.H. (1966) : Meteoritic, solar and terrestial rare-earth distributions. Phys. Chem. Earth, 7, 167-321.

HEINRICH, K.F.J. (1966) : X-ray absorption uncertainty. In McKinley, T.D., Heinrich, K.F.J. and Whittry, D.B., (Eds.), The Electron Microprobe.

HELLMAN, P.L. AND HENDERSON, P. (1977) : Are rare-earth elements mobile during spilitisation? Nature, 267, 38-40.

HERRMANN, A.G. (1978) : Yttrium and Lanthanides. In K.H. Wedepohl (ed.). Handbook of Geochemistry. Vol. II-5, Springer-Verlag, Berlin.

HUNTER, D.R. AND PRETORIUS, D.A. (1981) : Structural framework of southern Africa. In: D.R. Hunter (ed.) Precambrian of the Southern Hemisphere. Elsevier, Amsterdam, pp.397-422.

IRVING, A.J. (1978) : A review of experimental studies of crystal/liquid trace element partitioning. Geochim. et. Cosmochim, 42, 743-770.

IRVINE, T.N. AND BARAGAR, W.R.A. (1971) : A guide to the chemical classification of the common volcanic rocks. Can. J. Earth Sc., 8, 523-548.

JAHN, B.-M., AUVROY, B., BLAIS, S., CAPDEVILA, R., CORNICHET, J., VIDAL, F. AND HAMEURT, J. (1980) : Trace element geochemistry and petrogenesis of Finnish Greenstone Belts. J. Petrol., 21, 201-244.

JAHN, B.-M., SHIN, C.-Y. AND MURTHY, V.R. (1974) : Trace element geochemistry of Archaean volcanic rocks. Geochim. et Cosmochim., 38, 611-627.

JENSEN, L.S. (1976) : A new cation plot for classifying subalkalic volcanic rocks. Ontario Div. Mines, Ministry of Nat. Resources, Misc. Pap., 66.

JOLLY, W.T. (1972) : Degradation (hydration) - aggradation (dehydration) and low-rank metamorphism of mafic volcanic sequences. 24th Int. Geol. Cong., 2, 11-18.

KASCH, K.W. (1981) : The structural geology, metamorphic petrology and tectonothermal evolution of the southern Damara belt around Omitara S.W.A./Namibia. Bull. Precamb. Res. Unit, Univ. Cape Town, 27, 333p.

KERRICH, D.M. (1970) : Contact metamorphism in some areas of the Sierra Nevada, California. Bull. geol. Soc. Am., 81, 2913-2938.

KESSON, S.E. (1973) : The primary geochemistry of the Monaro alkaline volcanics, southeastern Australia - Evidence for upper mantle heterogeneity. Contr. Miner. Petrol., 42, 93-108.

KRÖNER, A. (1975) : Geochronology: 13a. Rep. Precambr. Res. Unit, Univ. Cape Town, 139-143.

KRÖNER, A. (1977) : The Precambrian geotectonic evolution of Africa : Plate accretion versus plate destruction. Precambr. Res., 4, 163-213.

KRÖNER, A., VAJNER, V. AND BURGER, A.J. (1977) : Geotectonic significance of radiometric age data from the late-Proterozoic Koras Group, Northern Cape Province, South Africa. 9th Collogium on African Geology, Univ. Gottingen, West Germany, 80-81.

KUSHIRO, I. (1960) : Si-Al relation in clinopyroxene from igneous rocks. Am. J. Sc., 258, 548-554.

LE BAS, M.J. (1962) : The role of aluminium in igneous rocks. Am. J. Sc., 260, 267-288.

LE MAITRE, R.W. (1976) : Some problems of the projection of chemical data into mineralogical classifications. Contr. Miner. Petrol., 56,, 181-189.

LE ROEX, A.P. (1980) : Geochemistry and mineralogy of selected Atlantic Ocean basalts. Unpubl. Ph.D. Thesis, University of Cape Town.

LINDSTROM, D.J. (1976) : Experimental study of the partitioning of transition metals between clinopyroxene and coexisting silicate liquid. Unpubl. Ph.D. Thesis, Univ. of Oregon.

LINDSTROM, D.J. AND WEILL, D.F. (1978) : Partitioning of transition metals between diopside and coexisting silicate liquids - 1. Nickel, cobalt, and manganese. Geochim. et Cosmochim., 42, 817-832.

LIOU, J.G. (1973) : Synthesis and stability relations of epidote, $Ca_2Al_2\ FeSi_3O_{12}$ (OH). J. Petrol., 14, 381-413.

Mac DONALD, G.A. (1968) : Composition and origin of Hawaiian lavas. Geol. Soc. Am. Mem., 116, 477-522.

MANN, A.C. (1983) : Trace element geochemistry of high alumina basalt-andesite-dacite-rhyodacite lavas of the main volcanic series of Santorini Volcano, Greece. Contr. Miner. Petrol., 84, 43-57.

MARTIN, H. AND PORADA, H. (1977) : The intracratonic branch of the Damara orogen in South West Africa. 1. Discussion of geodynamic models. Precambr. Res., 5, 311-338.

MASON, R. (1981) : The Damara Mobile Belt in South West Africa/Namibia. In: D.R. Hunter (ed.) Precambrian of the Southern Hemisphere. Elsevier, Amsterdam, pp.754-788.

MITCHELL, A.A. (1980) : The extrusive and intrusive rocks of the Molteno-Jamestown area, Cape Province. Unpubl. M.Sc. Thesis, Rhodes University.

MIYASHIRO, A., SHIDO, F. AND EWING, M. (1969) : Diversity and origin of abyssal tholeiite from the Mid-Atlantic Ridge near 24° and 30° north latitude. Contr. Miner. Petrol., 23, 38-52.

MORRISON, M.A. (1978) : The use of "immobile" trace elements to distinguish the palaeotectonic affinities of metabasalts: Applications to the Palaeocene basalts of Mull and Sky, Northwest Scotland. Earth Planet. Sc. Lett., 39, 407-416.

MYSEN, B.O. (1978) : Limits of solution of trace elements in minerals according to Henry's Law: Review of experimental data. Geochim. et Cosmochim., 42, 871-886.

NISBET, E.G. AND PEARCE, J.A. (1977) : Clinopyroxene composition in mafic lavas. Contr. Miner. Petrol. 63, 149-160.

NORRISH, K. AND HUTTON, J.T. (1969) : An accurate X-ray spectrographic method for the analysis of a wide range of geologic samples. Geochim. et Cosmochim., 33, 431-453.

NORRY, M.J. AND FITTON, J.G. (1983) : Oceanic and continental basic lavas, 5-19. In Hawkesworth, C.J. and Norry, M.J., (Eds.), Continental basalts and mantle xenoliths, 272pp.

O'NIONS, R.K. AND PANKHURST, R.J. (1974) : Rare-earth element distribution in Archeaen gneisses and anorthosites, Gothob area, West Greenland. Earth Planet. Sc. Lett., 22, 328-338.

PARSONS, W.H. (1968) : Criteria for the recognition of volcanic breccias: Review. In Larson, L; Manson, V. and Pring, M., (Eds.), Igneous and Metamorphic Geology. The Geol. Soc. of Am. Mensoir 115, 263-304.

PASTER, T.P., SCHAUWECHER, D.S. AND HASKIN, L.A. (1974) : The behaviour of some trace elements during solidification of the Skaergaard Layered Series. Geochim. Cosmochim. Acta., 38, 1549-1577.

PEARCE, J.A. AND CANN, J.R. (1971) : Ophiolite origin investigated by discriminant analyses using Ti, Zr and Y. Earth Planet. Sc. Lett., 12, 339-349.

PEARCE, J.A. AND NORRY, M.J. (1979) : Petrogenetic implications of Ti, Zr, Y and Nb variations in volcanic rocks. Contr. Miner. Petrol., 69, 33-47.

PETTIJOHN, F.J., POTTER, P.E. AND SIEVER, R. (1972) : Sand and sandstone. Springer-Verlag, Berlin, 618pp.

RINGWOOD, A.E. (1970) : Petrogenesis of Apollo 11 basalts and implications for lunar origin. J. Geophys. Res., 75, 6453-6479.

SANDERSON-DAMSTRA, C.G. (1982) : Geology of the Central and Southern Domains of the Koras Group, Northern Cape Province. Unpubl. M.Sc. Thesis, Rhodes University.

SCHALK, K.E.L. (1961) : The geology of the country around Dordabis. Unpubl. Rep. Geol. Surv. S.Afr.

SCHWEITZER, E.L., PAPIKE, J.J. AND BENCE, A.E. (1979) : Statistical analysis of clinopyroxenes from deep-sea basalts. Am. Miner., 64, 501-513.

SHAW, D.M. (1970) : Trace element fractionation during anatexis. Geochim. et Cosmochim., 34, 237-248.

SOUTH AFRICAN COMMITTEE FOR STRATIGRAPHY, (S.A.C.S., 1980) : Stratigraphy of South Africa. Part 1 (comp. L.E. Kent). Lithostratigraphy of the Republic of South Africa, South West Africa/Namibia, and the Republic of Bophutatswana, Transkei, Venda and Ciskei. Handb. Geol. Surv. S.Afr., 8, 690pp.

TANKARD, A.J., JACKSON, M.P.A., ERIKSSON, K.A., HOBDAY, D.K., HUNTER, D.R. AND MINTER, W.E.L. (1982) : Crustal evolution of Southern Africa. 3.8 billion years of earth history. Springer-Verlag, New York, 314-328.

THOMPSON, R.N., MORRISON, M.A., DICKIN, A.P. AND HENDRY, G.L. (1983) : Continental flood basalts... arachnids rule OK? 158-185. In Hawkesworth, C.J. and Norry, N.J., (Eds.), Continental basalts and mantle xenoliths, 272pp.

WATTERS, B.R. (1974) : Stratigraphy, igneous petrology and evolution of the Sinclair Group in southern South West Africa. Bull. Precambr. Res. Unit, Univ. Cape Town, 16, 235pp.

WATTERS, B.R. (1977) : The Sinclair Group : Definition and regional correlation. Trans. Geol. Soc. S. Afr., 80, 9-16.

WILLIAMS, R.J.P. (1959) : Deposition of trace elements in basic magma. Nature, 184, 44.

WINCHESTER, J.A. AND FLOYD, P.A. (1977) : Geochemical discrimination of different magma series and their differentiation products using immobile elements. Chem. Geol., 22, 325-343.

WINKLER, H.G.F. (1979) : Petrogenesis of metamorphic rocks. Springer-Verlag, New York, 348pp (fifth edition).

WOOD, D.A., GIBSON, I. AND THOMPSON, R.N. (1976) : Elemental mobility during zeolite facies metamorphism of the Tertiary basalts of eastern Iceland. Contr. Miner. Petrol., 55, 241-254.

WOOD, D.A., JORON, J.-L., TREUIL, M., NORRY, M. AND TARNEY, J. (1979) : Elemental and Sr isotope variations in basic lavas from Iceland and the surrounding ocean floor. The nature of mantle source inhomogeneities. Contr. Miner. Petrol., 70, 319-339.

YODER, H.S. AND TILLEY, C.E. (1962) : Origin of basalt magmas: an experimental study of natural and synthetic rock systems. J. Petrol., 3, 345-532.